The Dissertation Committee for Aishwarya Ravindran certifies that this is the approved version of the following dissertation:

THE STRUCTURAL BASIS OF CHEMOKINE BINDING AFFINITY AND RECEPTOR SELECTIVITY: ROLE OF RECEPTOR N-TERMINAL DOMAIN

Committee:

Krishna Rajarathnam, Ph.D. Supervisor

Wlodek Bujalowski, Ph.D.

Werner Braun, Ph.D.

Scott Gilbertson, Ph.D.

Andrew Hinck, Ph.D.

_____

Dean, Graduate School

THE STRUCTURAL BASIS OF CHEMOKINE BINDING AFFINITY AND RECEPTOR SELECTIVITY: ROLE OF RECEPTOR N-TERMINAL DOMAIN

by

Aishwarya Ravindran, B.Tech.

Dissertation

Presented to the Faculty of the Graduate School of
The University of Texas Medical Branch
in Partial Fulfillment
of the Requirements
for the Degree of

Doctor of Philosophy

Approved by the Supervisory Committee
Krishna Rajarathnam, Ph.D.
Wlodek Bujalowski, Ph.D.
Werner Braun, Ph.D.
Scott Gilbertson, Ph.D.
Andrew Hinck, Ph.D.

December, 2010
Galveston, Texas

Keywords: Chemokine-Receptor Interaction, Molecular Mechanisms and Structural Basis, Specificity and Affinity

To my mother, Dr. Padma Ravindran, for her unceasing love and encouragement in letting me pursue my dreams, and for teaching me the value of perseverance in overcoming obstacles.

ACKNOWLEDGEMENTS

The work presented in this dissertation could not have been accomplished without the support of several people, who have made my tenure in graduate school an enjoyable experience.

I owe a debt of sincerest thanks to my mentor, Dr. Krishna Rajarathnam for his unceasing support and guidance. I am very grateful to him for shaping me as a scientist and for providing me opportunities to realize my potential. His constructive criticisms and advice will always continue to linger in my mind throughout my professional life. I am eternally grateful to him for showing me the importance of being critical when it comes to interpreting scientific data. I will always cherish my interactions with him, which in turn has developed in me a passion for science that will continue to last forever.

I would like to thank past and present members of the Rajarathnam lab for being very supportive and for making my years of stay in the lab an enjoyable experience.

I am very thankful to Dr. Prem Raj Joseph for his guidance with NMR experiments, and Dr. Lavanya Rajagopalan for help with ITC experiments and for taking personal interest in my graduate training. The scientific discussions I had with them has always been enriching and rewarding.

I would like to thank all the members of my supervisory committee, Drs. Wlodek Bujalowski, Werner Braun, Scott Gilbertson and Andrew Hinck for their involvement and guidance in my research progress.

My special thanks goes to Dr. Wlodek Bujalowski for being always approachable and for his guidance. My interactions with him has made a great impact on my professional development as a scientist and has showed me the importance of being objective when it comes to taking important career decisions.

I am very thankful to Dr. Amar Natarajan for help with HTS experiments and Dr. Jeorg Roesgen for his guidance and support.

I am very grateful and thankful to Dr. Junji Iwahara for his expert advice and guidance and for being always approachable with respect to understanding NMR concepts.

I would like to thank Dr. Lillian Chan, former Program Director of the Biochemistry and Molecular Biology (BMB) program, for her support and encouragement towards the BMB student community. I would like to thank Dr. Andres Oberhauser for taking personal attention in my graduate training.

I extend my thanks to the Sealy Center for Structural Biology and the John S. Dunn Gulf Course Consortium for Magnetic Resonance for providing me with instrumentation access that have been essential for my research work. I also thank members of Drs. Wayne Bolen and Vince Hilser labs for providing me a great working environment

during these years. I would like to extend my thanks to all members of the BMB journal club for their support and involvement in promoting a forum for scientific discussions.

I owe a debt of thanks to the American Heart Association for providing me financial support that was key towards completing my graduate research.

I thank Ms. Angelina Johnson, Debora Botting and Rhoda Thompson for help with administrative support. I would like to thank Ms. Lisa Pipper for help with computational support.

I am thankful to all of my wonderful teachers both at school and in college, who have always been a source of inspiration. My special thanks goes to all of my dear friends for moral support towards overcoming difficulties and challenges in my graduate life.

Finally, I am deeply indebted to my parents and my brother for believing in my potential. I am truly grateful to my parents for all their sacrifices, love and inspiration that have enabled me to overcome life's hurdles.

THE STRUCTURAL BASIS OF CHEMOKINE BINDING AFFINITY AND RECEPTOR SELECTIVITY: ROLE OF RECEPTOR N-TERMINAL DOMAIN

Publication No._____

Aishwarya Ravindran, Ph.D.
The University of Texas Medical Branch, 2010

Supervisor: Krishna Rajarathnam

Chemokines recruit leukocytes by binding and activating 7-transmembrane G-protein coupled receptors present on the cell surface. Ligand-receptor interaction is complex and involves a broad range of affinities and selectivities. Furthermore, receptor binding involves interaction of both monomeric and dimeric ligands. Interactions between the ligand N-loop and the receptor N-domain (site-I), and between the ligand N-terminus and the receptor extracellular loops (site-II) mediate binding affinity, receptor selectivity and activation. However, the structural basis of how these interactions mediate affinity and selectivity is not known. Therefore studies in this dissertation are focused on the structural basis of interaction of chemokines, IL-8 and MGSA monomers and dimers with their receptors CXCR1 and CXCR2. CXCR1 is specific and binds IL-8 alone with high affinity, whereas CXCR2 is promiscuous and binds both ligands with high affinity. The receptor structures are not known, and also due to the intrinsic difficulties of working with receptors, structural studies were carried out to describe site-I interactions using the isolated receptor N-domains.

Chapter I provides an introduction to the chemokine-receptor system. Chapter II of the dissertation focuses on characterizing the structural basis of differential binding of IL-8 monomers and dimers to the CXCR1 N-domain. Using binding induced NMR chemical shift perturbations and line broadening changes, it was shown that a network of extensive direct and indirect coupled interactions mediate site-I binding of the IL-8 monomer and dimer and that these interactions play a fundamental role in determining binding affinity. Chapter III describes the characterization of the structural basis of CXCR2 receptor N-domain binding of IL-8 and MGSA monomers and dimers, and how coupled interactions between site-I and site-II play a key role in determining receptor affinity and selectivity. Chapter IV describes the structural studies and mechanistic description of how the steric bulk of Ile10, a solvent exposed hydrophobe in the IL-8 N-loop, mediates CXCR1 binding affinity. It was observed that mutating Ile10 to Ala does not affect site-I binding affinity, but negatively regulates site-II binding, resulting in reduced overall receptor

binding affinity and activity. Finally, Chapter V describes attempts and progress towards designing inhibitors that target site-I interaction, and how this data could be used for future inhibitor design against chemokine-mediated inflammatory and autoimmune diseases.

TABLE OF CONTENTS

LIST OF TABLES

LIST OF FIGURES

CHAPTER I

INTRODUCTION

The Chemokine System

Chemokines or 'chemotactic cytokines' are small secretory proteins that belong to the cytokine family, and play key regulatory roles in such diverse processes as organ development, homeostasis, host defense against infection and inflammation, and leukocyte trafficking (1, 2). During host defense against infection, chemokines recruit leukocytes to the site of infection by binding and activating 7-transmembrane (TM) G-protein coupled receptors (GPCR) on the cell surface (3). To date, more than 40 chemokines and 19 receptors have been identified (4). Chemokines are mainly classified into CXC, CC, C or CX_3C based on the presence of conserved cysteine residues (5). The receptors are classified according to the ligands they bind. The majority of chemokines fall into the CXC and CC subclass. The CXC chemokines are further classified into 'ELR' and 'non-ELR', based on the presence or absence of this motif before the first cysteine at the N-terminus.

Under normal circumstances, chemokines play beneficial roles such as cell trafficking and modulating immune response; however, they can potentially cause significant damage when they function as pathologically dysregulated molecules. Indeed, chemokines and their receptors are intimately involved in the onset and progression of numerous inflammatory and autoimmune diseases such as atherosclerosis, rheumatoid arthritis, and as well as cancer and HIV infection, and so are extremely attractive drug targets (6-10).

Chemokine-mediated leukocyte recruitment is a fine tuned process and involves the following steps (1, 11) **(Figure 1.1)**. During conditions of infection or injury, there is a local upregulation of proinflammatory chemokines in response to signaling molecules such as tumor necrosis factor-α (TNF-α) and interferon-gamma (IFN-γ). Chemokines bind and activate receptors present on the leukocyte cell

surface, resulting in leukocyte rolling, adhesion, shape change and extravasation through the endothelial cell surface. Leukocytes migrate towards the site of infection or injury following the chemokine gradient in the extracellular matrix. Each of these processes plays a key role in fine-tuning of chemokine regulation and can be exploited for drug design against inflammation (10, 12). For my doctoral work, I have focused exclusively on structure-function studies of ligand-receptor interactions using the pro-inflammatory chemokines IL-8 and MGSA and their receptors.

Chemokine-receptor system: Structure-function

Chemokine-receptor interaction is complex, involving a broad range of affinities, and selectivities with individual ligands binding multiple receptors, and individual receptors binding multiple ligands (13). There is also a subset of receptors that stringently bind a single ligand with high specificity. Understanding this complex nature of chemokine-receptor interaction is extremely challenging, and requires information on the structures of the ligands and the receptors, as well as knowledge of the structural basis of their interaction. Even though chemokines show large differences in sequence identity, the structures indicate that all chemokines share a common tertiary fold consisting of a short N-terminus, followed by an extended N-loop, three antiparallel β-strands and a C-terminal α-helix (14-29).

Structural and functional characteristics of the ligands have been extensively studied, but very little is known about the structural basis of receptor function. This is mainly because the structures of the receptors are not known. Solving their structures has been a challenging task because they are membrane bound proteins, and therefore one has to overcome roadblocks such as protein expression, purification, reconstitution and limitations in current NMR and X-ray methods. However, a few GPCR structures are now available including those of bovine rhodopsin, and human β_2-adrenergic receptor (30-35). These studies have laid the foundation for understanding the molecular mechanisms involved in GPCR activation and function but have not provided any insights into how chemokines bind their receptors.

Chemokine monomers and dimers

A shared feature of all chemokines is their ability to exist as monomers and dimers and in some cases, higher order oligomers (36) **(Figure 1.2)**. The dimerization potency varies among different chemokines with some forming strong dimers (K_d ~nM), and some forming very weak dimers (K_d ~mM). Furthermore, dimer formation is also sensitive to solution conditions such as ionic strength and pH (37-39). Using trapped monomers, monomeric mutants and trapped dimers, it has been shown that both monomers and dimers can activate the receptor (40-46). Together these observations indicate that the equilibrium between monomers and dimers that are free in solution, bound to GAGs, and at the leukocyte cell surface is likely to play a key role in regulating chemokine function. Therefore, knowledge of the structural basis of how chemokine monomers and dimers bind and activate their receptors is essential for understanding function.

Chemokine-receptor interaction: Dissecting the complexity

On the basis of structure-function data, a general two-site mechanism of receptor binding has been proposed for all chemokines. This involves binding of the ligand N-loop to the receptor N-domain (site-I) and binding of the ligand N-terminus to one or more receptor exoloops (site-II) (13, 14, 16, 38, 40, 44, 47-75) **(Figure 1.3)**. However, nothing is known regarding the molecular mechanisms of these interactions and how they mediate ligand binding affinity and selectivity. Towards this, I have investigated the structural basis of interaction of IL-8 and MGSA with its receptors CXCR1 and CXCR2.

IL-8 and MGSA belong to the 'ELR-CXC' subfamily of chemokines. Among all 'ELR-CXC' chemokines, IL-8 alone binds both receptors with high nM affinity; all others including MGSA bind CXCR2 with high affinity and CXCR1 with low affinity (67, 75-78). IL-8 and MGSA structures show that the conformationally flexible N-loop and N-terminal regions are tethered to the structural scaffold through the conserved disulfides (15, 18, 26). Sequences of all 'ELR-CXC' chemokines show

that the N-terminal 'ELR' residues are conserved, whereas the N-loop residues are moderately conserved **(Figure 1.4)**. Numerous site directed mutagenesis and domain-swapping studies of IL-8 and MGSA have shown that the N-terminal and the N-loop residues play a key role in binding affinity, selectivity and activation (49, 53, 56, 59, 62, 64-68, 74, 76, 79, 80). For instance, using IL-8 and MGSA N-terminal 'ELR' mutants, it was demonstrated that site-II binding is a low affinity, yet highly specific interaction that is important for receptor activation.

IL-8 and MGSA sequences show that the N-loop is longer in IL-8 due to the insertion of a Lys **(Figure 1.4)**. IL-8 and MGSA structures show the largest conformational difference for the N-loop residues (15, 18, 42) **(Figure 1.5)**. These observations suggest that the N-loop residues play a key role in binding affinity and specificity. Structure-function data for other chemokines also indicate that the N-terminus and N-loop plays a key role in binding affinity, specificity and activity (16, 54, 57, 63, 81). These studies together indicate that the β-strands and the helix act as a structural scaffold, and the N-loop and the N-terminus are tethered to the protein core through the disulfides for optimal receptor binding and function. Together, these observations suggest that site-I and site-II interactions differentially influence receptor binding affinity, selectivity and activity.

Characteristics of CXCR1 and CXCR2 receptors

Studies pertaining to CXCR1 and CXCR2 receptors show that both receptors exhibit distinct differences in functional regulation. For instance, both receptors mediate different cellular responses and differ in their internalization rates (45, 77, 82-85). Receptor binding studies have shown that CXCR2 is promiscuous and binds all ELRCXC chemokines with high affinity, whereas CXCR1 is specific and binds only IL-8 with high affinity (58, 75). CXCR1 and CXCR2 receptor sequences show that they share an overall similarity of 77%, but the lowest sequence homology is observed for residues in the N-domain (involved in site-I interaction), and the C-domain (involved in signaling) **(Figure 1.6)**.

Mutagenesis studies and generation of CXCR1 and CXCR2 chimeras indicate that the receptor N-domain plays a key role in binding affinity and specificity (58, 86-88). A characteristic feature of the receptor N-domains is that they contain negatively charged Asp/Glu residues that could play a role in electrostatic interactions with their cognate ligands. However, mutagenesis studies of these residues have provided conflicting results. It was shown that mutating the Asp/Glu residues in the CXCR1 N-domain in the context of the intact receptor did not affect binding affinities, and that the N-domain residues that play key role in the binding are mostly hydrophobic (61, 89). However, another mutagenesis study using isolated CXCR1 N-domain peptides showed that some of the negatively charged residues are important for binding to neutrophil receptors (90). Differences could be due to higher sensitivity in measuring the binding affinities using the isolated N-domain. Similar studies on the mutagenesis of negatively charged residues in the CXCR2 N-domain showed that mutating Asp8 and Glu12 resulted in as much as 20 fold reduced binding affinity of IL-8 (59). However these residues are not conserved between the two receptors suggesting that electrostatic interactions play distinctly different roles between the two receptors **(Figure 1.6)**.

Mutagenesis studies of the isolated CXCR1 N-domain as well as of the CXCR1 N-domain in the intact receptor have shown that hydrophobic residues play an important role in receptor binding (61, 89, 90). These residues are Pro21, Pro22 and Tyr27. However, nothing is known regarding the molecular basis of how these N-domain residues mediate ligand binding. Therefore, knowledge of the structure of the complex is essential to describe the structural basis of interaction of the CXCR1 and CXCR2 receptor N-domain residues that mediate ligand binding affinity and specificity.

For my doctoral research, I have focused on obtaining insights into the structural basis of receptor binding affinity and specificity at site-I using the IL-8/MGSA/CXCR1/CXCR2 system. Insights gained from these studies will provide a

good starting point towards dissecting the intricate complexity of the entire chemokine-receptor system.

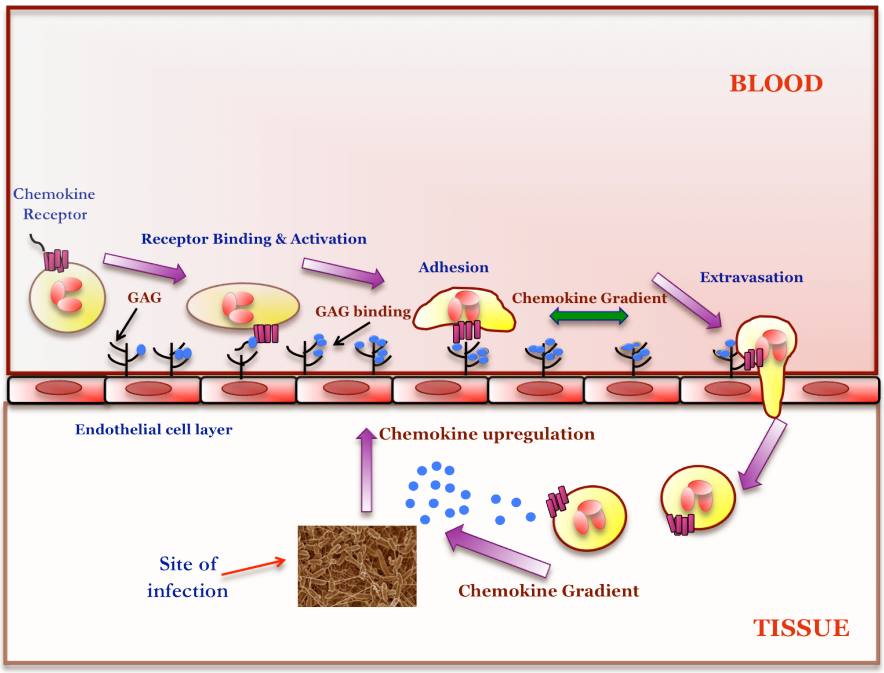

Figure 1.1 A schematic representation of the chemokine-mediated leukocyte recruitment process. Chemokine ligands are shown in blue circles, and the receptors corresponding to the 7 transmembrane helices on the leukocyte cell surface are shown in pink. Each step plays a key role in the fine-tuning of chemokine regulation.

Figure 1.2 Structures of a characteristic chemokine dimer and a monomer.

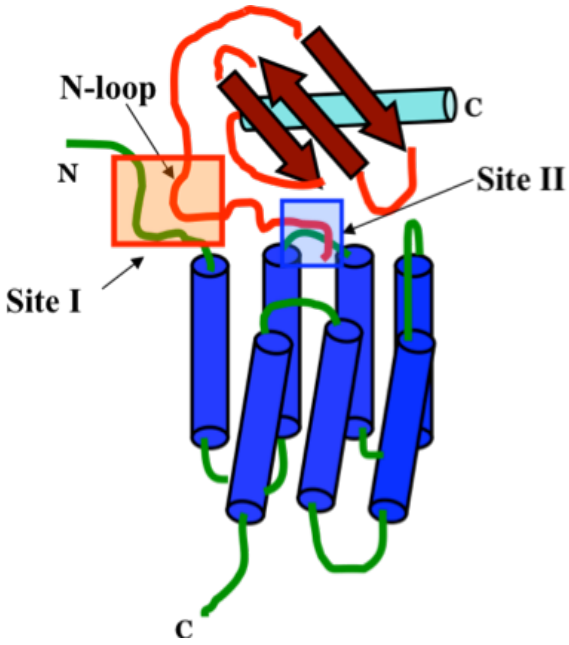

Figure 1.3 A schematic representation of chemokine-receptor interaction. The interaction between ligand N-loop and the receptor N-domain (site-I) is highlighted in red, and that between ligand N-terminus and receptor exoloop (site-II) is highlighted in blue. *(Figure adapted from ref. 91).*

```
IL-8          SAKELRCQCIKTYSKPFHPKFIKELRVIESGPHC---
MGSA        ASVATELRCQCLQTLQ-GIHPKNIQSVNVKSPGPHC---
GROβ        APLATELRCQCLQTLQ-GIHLKNIQSVKVKSPGPHC---
GROγ        ASVVTELRCQCLQTLQ-GIHLKNIQSVNVRSPGPHC---
NAP-2         AELRCMCIKTTS-GIHPKNIQSLEVIGKGTHC---
ENA-78  AGPAAAVLRELRCVCLQTTQ-GVHPKMISNLQVFAIGPQC---
GCP-2    GPVSAVLTELRCTCLRVTLR-VNPKTIGKLQVFPAGPQC---
```

Figure 1.4 Sequence alignment of the 'ELRCXC' chemokines. The conserved 'ELR' residues in the N-terminus are shown in blue and the N-loop residues are shown in red. For simplicity, residues up to the third conserved cysteine are shown.

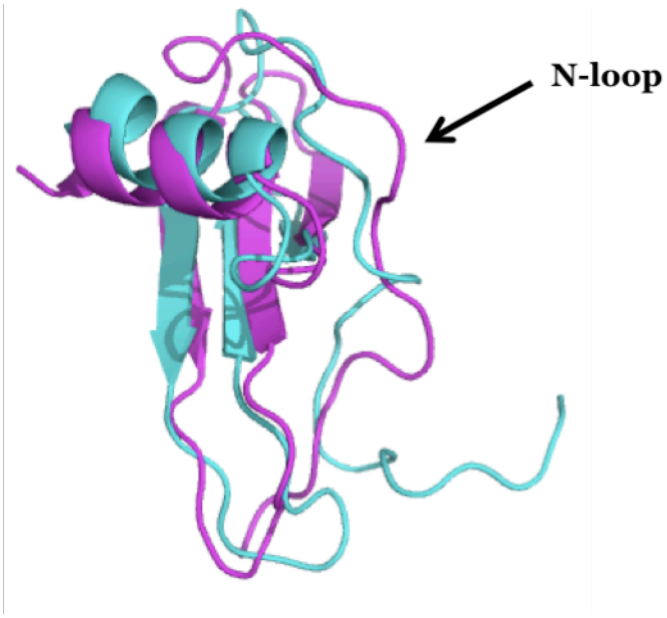

Figure 1.5 Structural alignment of IL-8 and MGSA. Best-fit superimposition of a single subunit of IL-8 (shown in pink) and MGSA (shown in cyan) solution structures are shown to highlight the conformational difference in the N-loop. The alignment was done using PyMOL (96).

Strategy to study site-I interaction

Understanding the structural basis of receptor interactions of IL-8 and MGSA becomes challenging without the receptor structures. Our strategy to circumvent this bottleneck involves studying site-I interaction using the isolated N-domains. The receptor N-domains are unstructured in solution, and N-domain peptides bind IL-8 and MGSA with micromolar (μM) affinity. Also, eliminating site-II by deleting the 'ELR' residues results in μM binding to the intact receptor (56, 65, 79, 88, 90-93). These results together indicate that studying ligand binding to the isolated N-domain mimics binding to the N-domain in the intact receptor. Indeed, several studies with other chemokines have used isolated N-domain peptides to study site-I interaction and observe μM binding affinity (14, 23, 24, 48, 94, 95). Based on the knowledge gained from these studies, and from the structure-function studies on other chemokines, we have proposed a model for the two-site chemokine-receptor interaction, which takes into account that site-I and site-II interactions are not independent, but rather are coupled (13). However, nothing is known regarding the structural basis of how coupled interactions play a role in mediating binding affinity and receptor selectivity.

On the basis of all the structure-function studies on ligand-receptor interaction, I hypothesize that the binding of the chemokine to site-I results in structural/dynamic changes in the ligand and/or the receptor, which mediates site-II binding, and that the coupling between the two sites is responsible for optimal receptor interaction and function.

To address this hypothesis, I have used isolated CXCR1 and CXCR2 N-domain peptides to study the structural basis of site-I binding of IL-8 and MGSA monomers and dimers. Binding induced NMR chemical shift and line broadening changes show that the structural and/or dynamic changes that occur on site-I interaction play a key role in mediating coupling between the two sites. Studies pertaining to this dissertation emphasize the 'big picture' of how studying site-I

binding using the isolated N-domains provides novel insights into the role of coupled interactions in the molecular basis of ligand binding affinity and receptor selectivity.

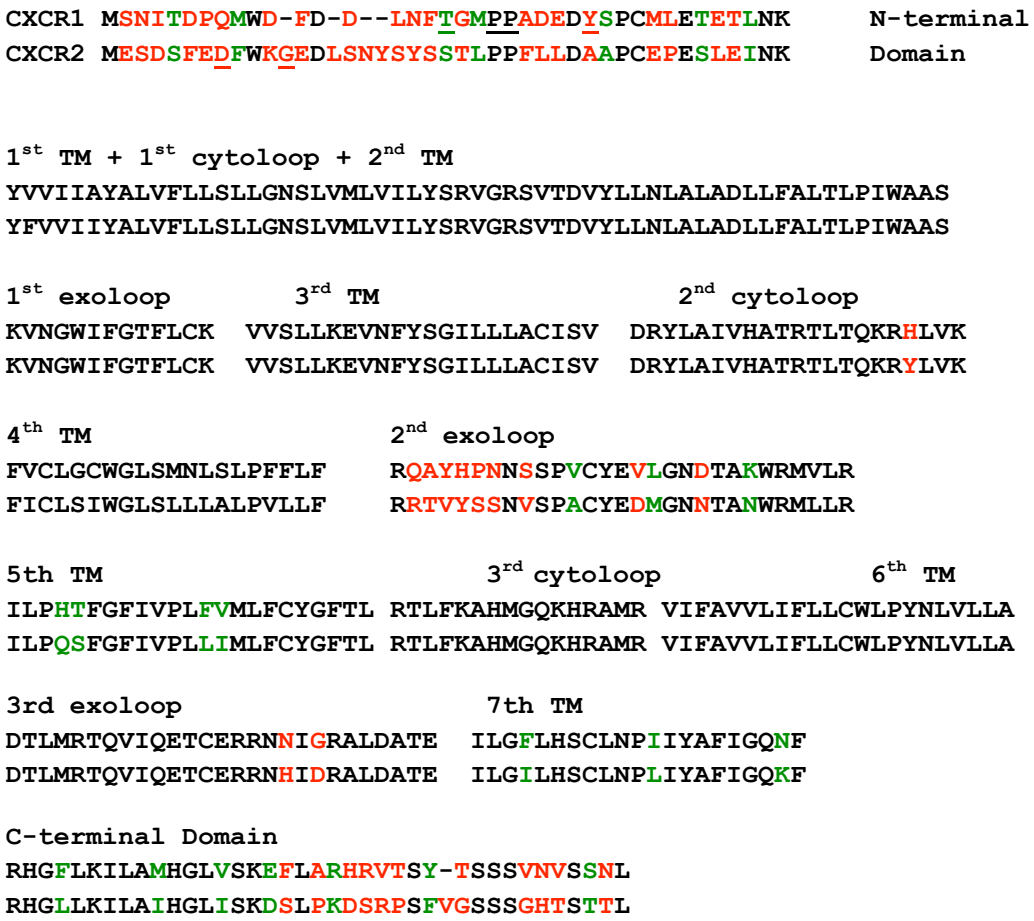

Figure 1.6 Sequence alignment of CXCR1 and CXCR2 sequences. The residues that are not conserved are shown in red, the residues that are conserved are shown in black and the residues in green indicate a conservative substitution. Residues in the N-domain that have been shown to be important from mutagenesis studies are underlined.

CHAPTER II

STRUCTURAL BASIS FOR DIFFERENTIAL BINDING OF THE INTERLEUKIN-8 MONOMER AND DIMER TO THE CXCR1 N-DOMAIN: ROLE OF COUPLED INTERACTIONS AND DYNAMICS

INTRODUCTION

Chemokines constitute the largest subfamily of cytokines and mediate various biological processes from organogenesis and homeostasis to recruitment and activation of leukocytes during host defense against infection (1, 2). Chemokines exert their function by binding and activating 7-TM GPCRs on the cell surface. An imbalance in chemokine function can be detrimental and has been attributed to the pathophysiology of several inflammatory and autoimmune diseases (7, 9, 10). All chemokines share the fundamental property of reversibly existing as monomer and dimer, and therefore knowledge of the structural and molecular basis of receptor binding of both monomeric and dimeric species is essential to understand how chemokines mediate function.

Interleukin-8 (IL-8, also known as CXCL8), one of the best studied chemokines, plays a critical role in host immune response by binding and activating the CXCR1 receptor on neutrophils. Structures of a trapped IL-8 monomer and WT dimer are known (15, 26). The structure of the monomer is similar to that of the monomeric subunit in the dimer, except the C-terminal helical residues that are structured in the dimer are unstructured in the monomer. Using trapped monomeric and trapped dimeric IL-8 variants, it has been shown that both forms can bind the CXCR1 receptor, but the monomer is the high-affinity ligand (41). Site-specific mutagenesis and generation of chimeric chemokines by swapping similar domains between IL-8 and other chemokines have shown that IL-8 N-terminal and N-loop residues play a critical role in mediating affinity, activity, and specificity (49, 65, 66, 68, 76, 80). On the basis of these data and similar studies with other chemokines, it has been proposed that IL-8 receptor binding

involves two interactions: between the IL-8 N-loop and the receptor N-domain residues (site-I) and between the IL-8 N-terminal and the receptor extracellular loop residues (site -II) (13, 16, 49, 51, 58, 76, 80, 88, 89).

In this study, the structural basis of CXCR1 N-domain binding of three different IL-8 variants, a designed monomer, a trapped dimer, and WT dimer, have been characterized using NMR spectroscopy. We used an IL-8(1–66) deletion mutant which is a monomer at millimolar concentrations and an IL-8(1–72) R26C mutant which is a trapped dimer that contains a disulfide across the dimer interface at the 2 fold symmetry. Binding-induced NMR chemical shift perturbation and peak intensity changes in the HSQC spectra of the monomer indicate global structural changes and suggest that direct and indirect interactions mediate the binding process. In particular, these data show that nonsequential residues dispersed through the entire span of the N-loop are involved in docking to the receptor N-domain. Most interestingly, NMR data of the WT dimer show binding-induced dissociation of the dimer–receptor N-domain complex. NMR data including ^{15}N-relaxation measurements for the trapped dimer show evidence of increased conformational flexibility in the bound form providing a structural rationale for the binding-induced dissociation of the WT dimer. These results together indicate that binding is not a localized event, but a global event, and is mediated by extensive coupled interactions within the monomer and across the dimer interface and that these interactions play a fundamental role in determining binding affinity.

EXPERIMENTAL PROCEDURES

Design, Expression, and Purification of IL-8 Variants

WT IL-8 dimerizes at micromolar concentrations, and therefore is a dimer at millimolar concentrations used in NMR studies (37, 38, 97). We observe from NMR structural and relaxation studies that the IL-8(1–66) deletion mutant is a monomer at millimolar concentrations (P. R. B. Joseph and K. Rajarathnam, unpublished results). The

trapped R26C dimer was designed by substituting a disulfide across the dimer interface at the site of 2-fold symmetry. This mutation does not perturb the dimer interface, and the structure of this trapped dimer is similar to that of the WT dimer (41).

The recombinant IL-8(1–66) monomer, trapped R26C dimer, and the WT were generated as described previously (91). All IL-8 variants were expressed in *Escherichia coli* strain BL21(DE3), and ^{15}N-labeled proteins were produced by growing cells in minimal medium containing $^{15}NH_4Cl$ as the nitrogen source. Transformed *E. coli* BL21(DE3) cells were grown in minimal medium containing ampicillin to an A_{600} of 0.8 and induced with 1 mM isopropyl β-D-thiogalactopyranoside (IPTG) for 8 h at 37 °C. Purity and molecular weight of the proteins were confirmed using analytical high-pressure liquid chromatography (HPLC) and matrix-assisted laser desorption/ionization mass spectrometry (MALDI MS), respectively. The CXCR1 N-domain 24-mer (LWTWFEDEFANATGMPPVEKDYSP) is the same as that used in our previous studies and was synthesized using solid-phase peptide synthesis (91).

NMR Spectroscopy

For titration experiments, ^{15}N-labeled WT, trapped R26C dimer, and IL-8(1–66) monomer were prepared in 50 mM sodium acetate buffer, pH 6.0, containing 1 mM 2,2-dimethyl-2-silapentanesulfonic acid (DSS), 1 mM sodium azide, and 10% ^2H_2O (v/v). Chemical shifts were referenced to DSS (98). All H-^{15}NHSQC spectra were acquired at 30°C using Varian Unity Plus 600 or INOVA 800 MHz spectrometers equipped with field gradient accessories. A stock solution of the CXCR1 N-domain peptide prepared in the same buffer was used for titration experiments, and NMR spectra of all IL-8 variants were collected until essentially no change in chemical shifts was observed. The final molar ratios for monomer, trapped R26C dimer, and WT dimer are 3.4, 17.8, and 11.2, respectively. Two-dimensional ^{1}H–^{15}N HSQC spectra were acquired with 2048 complex points for direct ^{1}H and 128 complex points for indirect ^{15}N dimensions. The spectra were processed using NMRPipe and analyzed using NMRView (99, 100). The chemical shifts of the WT dimer and the trapped R26C dimer were assigned using previously available

assignments (41, 51), and the chemical shifts of the IL-8(1–66) monomer were assigned using ^{15}N-edited NOESY and TOCSY, CBCANH, and CBCA-(CO)NH experiments (P. R. B. Joseph and K. Rajarathnam, unpublished results).

The NMR ^{15}N-T_2 relaxation experiments were carried out using the gradient 2D ^{1}H–^{15}N correlation pulse sequences on both the free and the receptor-peptide-bound trapped R26C dimer at 30°C on the Varian Unity Plus 600 spectrometer (101). The data were acquired at delays of τ = 10, 30, 50, 70, 90, 110, 130, 150, and 170 ms, and the delays were scrambled to avoid any systematic errors. We used 16 transients per increment for the free form and 128 transients per increment for the bound form due to the relatively weak and broadened signals. The T_2 values were calculated by weighted nonlinear least-squares fits of the peak heights in the 2D spectra to a two-parameter exponential decay using the Mathematica suite of programs (102). The uncertainties in T_2 values were taken to be the standard error of the fitted parameters.

Calculation of Binding Constants

Apparent dissociation constants (K_d) were determined by fitting the binding-induced chemical shift changes ($\Delta\delta$) to the following set of equations (103):

$$C = C_{IL\text{-}8}(\Delta\delta/\Delta\delta_{max}) \qquad (2.1)$$

where $\Delta\delta_{max}$ is the maximum chemical shift change between bound and free IL-8, $C_{IL\text{-}8}$ is the total concentration of IL-8, and C is the concentration of bound IL-8.

$\Delta\delta$ is the observed chemical shift deviation, given by the equation:

$$\Delta\delta = \sqrt{(\Delta\delta_H)^2 + (\Delta\delta_N/8)^2} \qquad (2.2)$$

where $\Delta\delta_H$ and $\Delta\delta_N$ are the ^{1}H and ^{15}N chemical shift changes (in parts per million). C is also defined by the equation:

$$C = 0.5 \times [(K_d + C_{IL-8} + C_{pep}) - \sqrt{((K_d + C_{IL-8} + C_{pep})^2 - 4 \times C_{IL-8} \times C_{pep})}] \qquad (2.3)$$

where C_{pep} is the total concentration of the peptide. Substituting eq 2.3 in eq 2.1 allows estimation of K_d.

RESULTS

Binding of the IL-8 Monomer

For all NMR experiments, unlabeled CXCR1 N-domain peptide was titrated into ^{15}N-labeled IL-8 variants, and binding was followed by changes in 2D ^{15}N–^{1}H HSQC spectral characteristics. Binding-induced changes in chemical shifts are excellent probes for mapping binding surfaces involved in protein–protein interactions (104). Line broadening of resonances during titration could occur as a consequence of chemical shift differences between the free and bound forms and when the binding is in the intermediate to fast exchange regime on NMR time scale (105).

We will first describe the results of the binding of IL-8 monomer and then compare and contrast the binding of the trapped dimer and WT dimer. In the monomer, peaks corresponding to the N-loop, third β-strand, and the C-terminal helical residues showed the largest chemical shift perturbations and also substantial line broadening, indicating that these regions play a key role in the binding process **(Figure 2.1)**.

Role of the N-Loop Residues : Large chemical shift perturbations were observed for N-loop residues Ile10, Thr12, and Tyr13 and to a lesser extent for residues Ser14, Lys20, and Phe21, and peaks corresponding to Lys15 and His18 completely disappear. These residues also show the largest decrease in intensity due to line broadening **(Figure 2.2)**. The IL-8 structure reveals that these residues span the entire N-loop and that electrostatic and hydrophobic/packing interactions mediate binding of IL-8 to the receptor N-domain **(Figure 2.3, panel A)**.

Ile10, Ser14, Lys15, and Lys20 are solvent exposed (ASA ~ 0.8) and so exert their influence by making direct contact with the receptor residues. On the other hand, residues Thr12, Tyr13, His18, and Phe21 are partially buried in the structure (ASA ~ 0.3–0.6); therefore, describing their role in binding on the basis of a static structure is less straightforward **(Figure 2.3, panel B)**. For instance, the structure reveals that one face of the aromatic ring side chain of His18 and Phe21 is solvent exposed, while the other face is buried in the structure and is probably involved in some form of favorable packing/aromatic interactions **(Figure 2.3, panel A)**. However, as the N-loop is conformationally flexible, the side chain could become completely exposed and engage in binding. It is also possible that these residues indirectly influence the binding of Ile10, Lys15, and Lys20 through packing interactions. NMR studies of binding-induced structural changes of these N-loop mutants are essential to provide a more definite answer as to how these residues mediate binding affinity.

Our NMR data showing that the entire N-loop is involved in receptor binding is inconsistent with a structural model proposed by Williams et al. and Hammond et al. (49, 64). On the basis of mutagenesis, these authors propose a binding site as that formed by residues Phe17, Phe21, and Ile22 (49, 64). Our data show only minimal perturbation for residues Phe17 and Ile22, discounting any major role for these residues in direct binding. Phe17 is largely buried (ASA ~ 0.2) and Ile22 is completely buried, and they are involved in extensive packing interactions with each other and with residues Phe21 and Leu43. Further, mutation of Phe17 to Ala resulted in an unfolded protein, indicating that Phe17 is essential for maintaining the integrity of the structural scaffold and so is involved in the presentation of the N-loop residues for receptor binding (49). Similarly, we propose that Ile22 is part of the structural scaffold and plays a role in function by indirectly influencing the binding of N-loop residues.

The solution structure of a CXCR1 N-domain peptidomimetic bound to dimeric IL-8 has been solved using NMR spectroscopy (51). The structure was determined on the basis of intermolecular NOEs between ^{13}C- and ^{15}N-labeled IL-8 and unlabeled CXCR1

peptide and reveals that the binding interface predominantly involves the N-loop residues, including hydrophobic residues Ile10, Tyr13, Phe17, and Phe21 and charged residues Lys11 and Lys15. Our data are largely consistent with the structure, though it is very unlikely that Phe17 is involved in direct binding interactions (vide supra).

Other studies have shown that mutating His18, Lys15, and Lys20 results in significant loss of binding, whereas mutating residues Thr12 and Ser14 had only a modest effect (53, 64, 66, 76, 80). Our NMR data show that Lys15 and His18 broaden out, whereas Thr12 shows large binding-induced perturbation and remains significantly weak, indicating that these residues are conformationally flexible in the bound form **(Figures 2.1 and 2.2)**. The structure of the complex also fails to reveal specific interactions for residues Thr12 and Ser14, suggesting a more subtle role for these residues (51). The dynamic nature of these residues in the receptor-bound form suggests that such a property could play a more prominent role for receptor activities such as chemotaxis and Ca^{2+} release than for binding affinity.

Role of the Third β-Strand Residues: The third β-strand residues that are significantly perturbed are Glu48, Leu49, Cys50, Leu51, and Asp52 **(Figure 2.1, panel C)**. The ASA indicates that Glu48 alone is exposed while others are largely buried. Interestingly, Asp52 shows the largest perturbation of all amino acids, which is unexpected considering that the CXCR1 N-domain is highly negatively charged. The CXCR1 N-domain sequence has only one Lys, and it can be argued that Asp52 interacts with this Lys. However, IL-8 also binds CXCR2 receptor with similar high affinity, and the corresponding residue in the CXCR2N-domain is a Leu. Asp52 is also significantly perturbed on binding to the CXCR2 N-domain (Ravindran et al., unpublished results), indicating that the perturbation of Asp52 should be due to indirect interactions.

The NMR structure of the monomer reveals that both Leu51 andAsp52 interact with the N-loop residues, Thr12 and Tyr13 (26), and so binding-induced changes in Thr12 and Tyr13 are most likely propagated to Leu51 and Asp52 through packing interactions **(Figure 2.4, panel A)**. The structure also reveals that Leu49 is largely buried

but nevertheless shows side chain packing interactions with Tyr13, suggesting binding-induced conformational changes in Tyr13 could be propagated through packing interactions to Leu49 **(Figure 2.4, panel A)**. Another mechanism by which conformational changes could be propagated is through the Cys9–Cys50 disulfide bridge, which tethers the conformationally flexible N-loop to the third β-strand. Chemical shift data show that both Cys9 and Cys50 are significantly perturbed and also broaden out during the titration **(Figures 2.1)**. These data together indicate that the changes observed in the third β-strand are not due to direct binding, but due to indirect coupling interactions propagated through the N-loop.

Structure–function studies of conservatively mutating Asp52 to Asn had no effect on binding affinity, indicating that the carboxylate side chain is not important for function (64). This is consistent with our conclusion that Asp52 is involved in packing interactions and not in direct binding. Mutating Leu49 and Leu51 to Ala results in reduced binding, and Glu48 to Lys had no effect on binding (49, 64, 76). We have previously shown that it is possible to substitute cysteines with a non-natural cysteine analogue in a disulfide without breaking the disulfide and that Cys50 plays a role in receptor binding (106). Cys50 like Leu49 and Leu51 is largely buried, and we propose that these residues form a part of the hydrophobic core, which functions as a scaffold, and indirectly influence the binding of the N-loop residues by coupled interactions.

Role of the C-Terminal Helix Residues : Significant chemical shift perturbations and line broadening are observed for the C-terminal helical residues Val58, Arg60, Val61, Val62, and Phe65 **(Figures 2.1)**. ASA data indicate that except Arg60 all other residues are buried (ASA < 0.2). We observe a periodicity in chemical shift perturbation with residues Val58, Val61, and Phe65 showing the largest change **(Figure 2.1)**. The side chains of these residues are oriented in the same direction and are packed against hydrophobic residues of the β-strand **(Figure 2.4, panel B)**. Except for Arg60, the remaining solvent-exposed helical residues Gln59, Glu63, and Lys64 are relatively less perturbed **(Figure 2.1)**. The side chains of Arg60 and Lys64 are located on the surface of the helix and

pointed away from the N-loop **(Figure 2.4, panel B)**. Therefore, the perturbation of the C-terminal helical residues cannot be due to direct interaction with the N-domain.

The role of C-terminal helix for receptor binding and function has been investigated using C-terminal deletion mutants and IL-8 chimera containing helices of IP-10 or PF-4 (65, 66). The chimeras are as active as the WT IL-8, but successive deletion of helical residues in WT IL-8 results in progressive loss of binding affinity (68). On the other hand, mutagenesis studies have shown that positively charged residues Arg60 and Lys64 bind to negatively charged glycosaminoglycans, and such binding has been shown to be essential in the neutrophil recruitment process (107). Our NMR studies and the structure–function data together indicate that the helical residues are part of the structural scaffold and are not involved in direct receptor binding, but indirectly influence the binding of the N-loop residues through long-range coupling interactions.

Role of the First and Second β-Strand Residues: Chemical shift perturbations are also observed for residues in the first and second β-strand and in the 40s turn which link the second and third β-strands. The extent of perturbation is lower compared to that observed for the N-loop, third β-strand, and the C-terminal helix **(Figure 2.1)**. However, perturbation is differential, involving relatively large as well as small chemical shift changes. For instance, relatively large perturbations are observed for Lys23 and Leu25 in the first β-strand, Ile39 and Val41 in the second β-strand, and Leu43 and Ser44 in the 40s turn, and in contrast, minimal perturbations are observed for Arg26 in the first β-strand and Ile40 in the second β-strand. The monomer structure reveals packing interactions between Lys23 and Ser44, between Leu25 and Val41, and between Ile39 and Leu51, suggesting indirect coupling interactions as the cause for the observed perturbations (26).

Hammond et al. have proposed, on the basis of mutagenesis, that Val41 and Leu43 play a direct role in receptor binding and that these and N-loop residues Tyr13, Phe17, and Ile22 together form a receptor-binding site (64). Williams et al. have characterized the function of a wide variety of mutants including those of the 40s residues and also studied the consequence of mutation on the tertiary structure using NMR

spectroscopy. On the basis of their results, the authors propose that N-loop residues Phe17, Phe21, Ile22, and Leu43 form the receptor-binding pocket (49). Skelton et al. also propose that Leu43 is involved in binding on the basis of the structure of the complex (51).

Leu43 is largely buried (ASA ~0.2), and the monomer structure reveals that the side chain is packed against residues Phe17, Tyr21, and Ile22 (26). Though mutating Leu43 to Ala resulted in ~15 fold lower affinity, mutating to Asp had no effect, indicating that the large hydrophobic side chain is not critical for binding but important for packing interactions (49). Val41 is completely buried and is packed against Leu25 and Phe17, and mutating it to Ala results only in marginal loss of binding (2-fold), suggesting that it cannot be involved in direct binding interactions (49). Though chemical shifts of Ile40 are only minimally perturbed, mutating Ile40 to Ala results in substantial loss of binding and also in perturbation of the structure, indicating that loss of function is due to indirect interactions (49). Our NMR and the mutagenesis data together indicate that the 40s residues, if any, play a minimal role in direct binding and, like the C-terminal helical and third β-strand residues, are part of the structural scaffold and indirectly influence the binding of the N-loop residues by coupling interactions.

Role of the N-Terminal and 30s Loop Residues: Our NMR data show minimal chemical shift and intensity changes in the N-terminal and the 30s loop regions **(Figure 2.1)**. The 30s loop residues link the first and second β-strands. The N-terminal region binds to the receptor extracellular residues (site-II) and is linked to the 30s loop region via the Cys7–Cys34 disulfide bridge. Mutating the 30s loop residues and the cysteines of the 7–34 disulfide results in significant loss of binding, indicating a role for coupled interactions in site-II binding (66). Minimal chemical shift changes indicate that these regions are not directly involved in site-I binding. Perturbation of these residues nevertheless indicates that site-I binding could influence site-II binding.

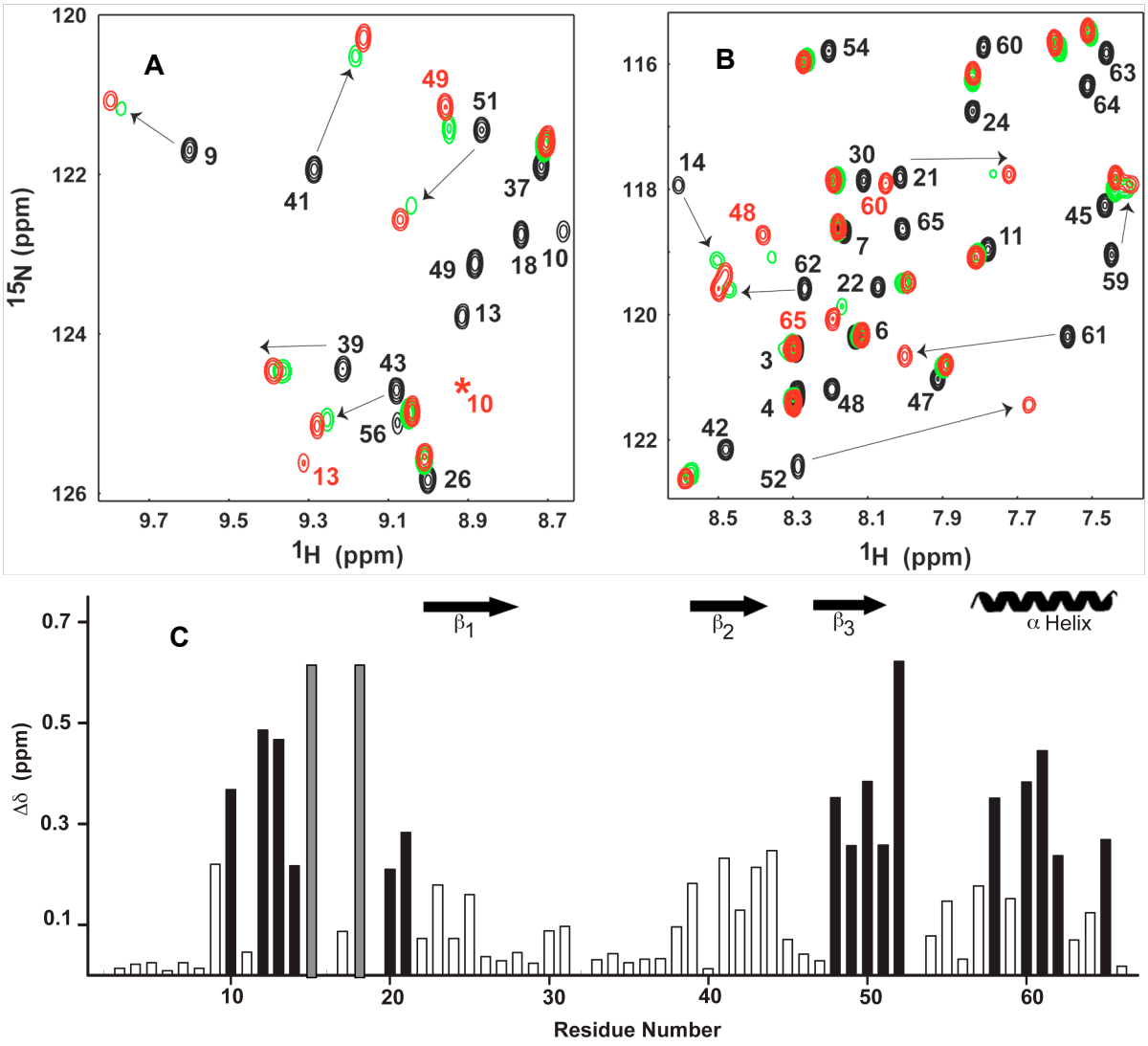

FIGURE 2.1 Binding of the IL-8 monomer to the CXCR1 N-domain. Sections of the ^{15}N–^{1}H HSQC spectra showing binding-induced chemical shift changes of the IL-8 monomer residues **(panels A and B)**. Arrows indicate the direction of peak movement, and for some residues (Ile10, Tyr13, Glu48, Leu49, Arg60, Phe65) showing large chemical shift changes, the final bound peaks are labeled in red. The peaks are color coded according to peptide: protein molar ratios of 0 (black), 1.2 (green), and 3.4 (red). The peak for the bound form of residue Ile10 is not visible at the contour level shown and is marked by an asterisk. Histogram showing the binding-induced chemical shift change ($\Delta\delta$) of the IL-8 monomer **(panel C)**. The residues showing significant perturbation in the N-loop, third β-strand, and the C-terminal helix are highlighted in black. Chemical shift for Lys15 and His18 are represented by a grey bars as they disappear during titration. The grey bar is shown at the same height as that of Asp52, which shows the maximum chemical shift change to indicate that the perturbation of these residues should be similar or higher than that of Asp52. Residues 16, 19, 32, and 53 are prolines.

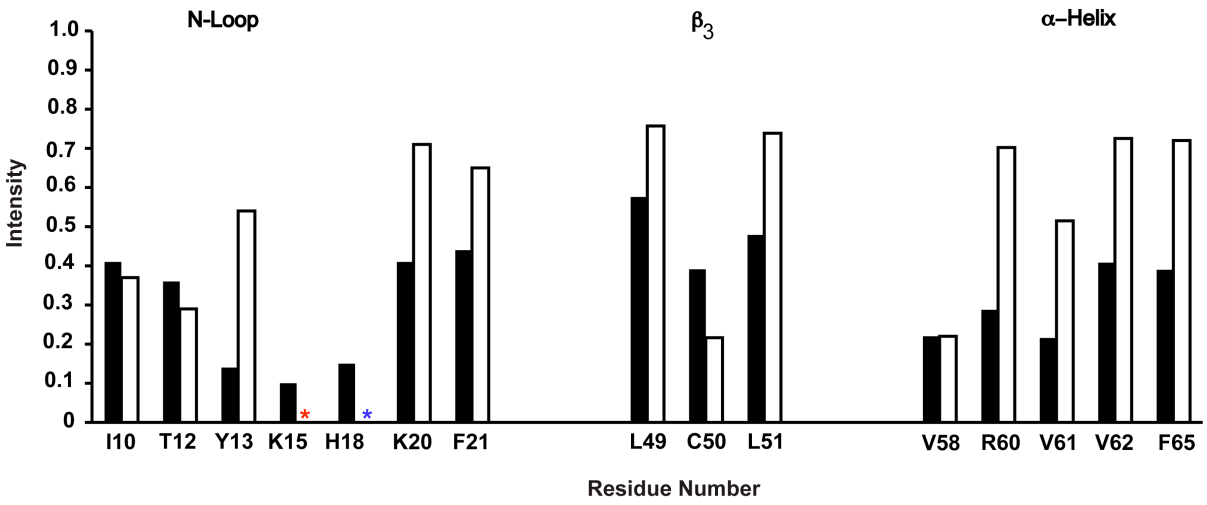

FIGURE 2.2 Binding-induced line broadening of the IL-8 monomer residues. A plot showing binding-induced loss of peak intensity for the N-loop, third β-strand, and the C-terminal helical residues. The unbound intensities are normalized to 1. The intensities are shown for peptide protein molar ratios of 0.07 (black) and 3.4 (open). Lys15 is broadened out and is indicated by a red asterisk. The intensity change for His18 is not available due to peak overlap and is denoted by a blue asterisk.

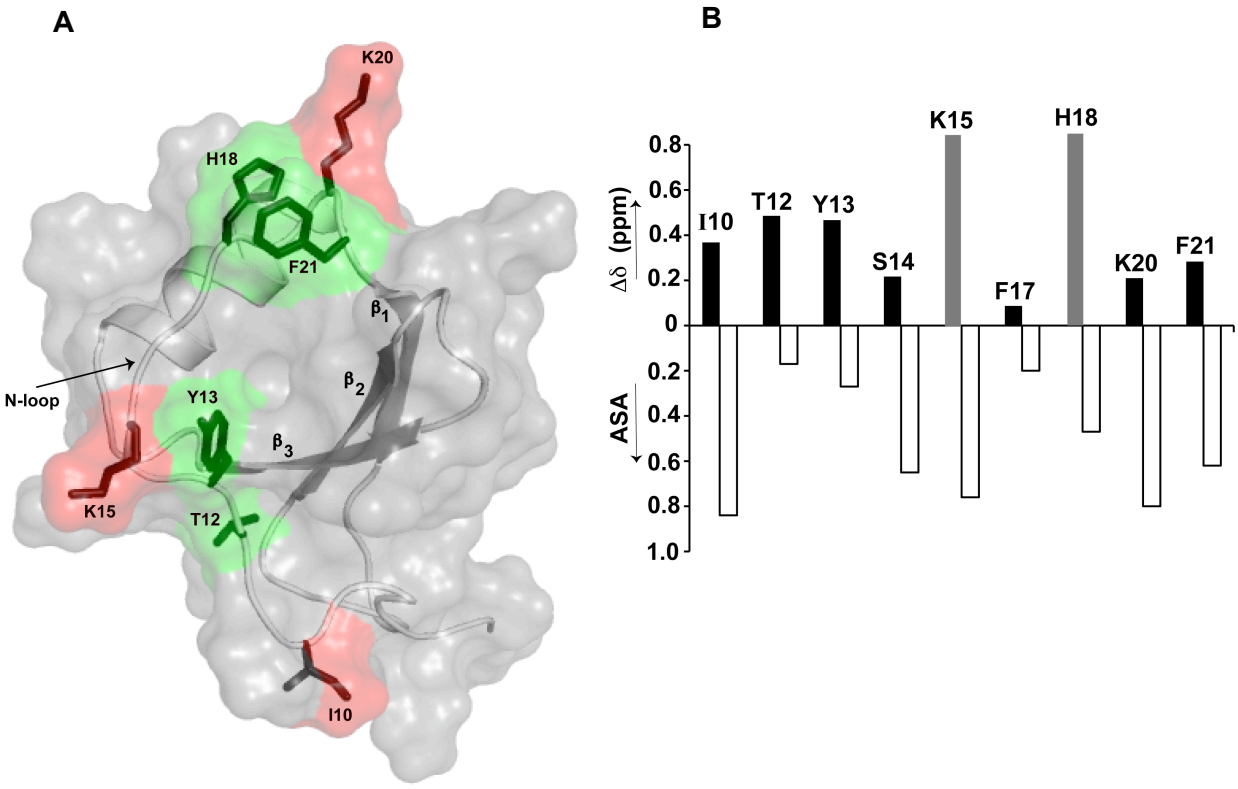

FIGURE 2.3 A molecular plot of the IL-8 monomer (PDB id 1IKM(26)) showing the N-loop residues involved in CXCR1 N-domain binding (panel A). The solvent-exposed residues, Ile10, Lys15, and Lys20, are highlighted in red, and partially buried residues, Thr12, Try13, His18, and Phe21, are highlighted in green. The plot was rendered using PyMOL (96). Chemical shift changes and ASA **(panel B)**. A plot of the chemical shift change (top y-axis) and the side chain ASA (bottom y-axis) of the IL-8 monomer N-loop residues shows that they are not necessarily correlated. Chemical shift changes for Lys15 and His18 are not available due to line broadening and represented as grey bars. The ASA of the IL-8 monomer (PDB id 1IKM) was calculated using the program VADAR (116).

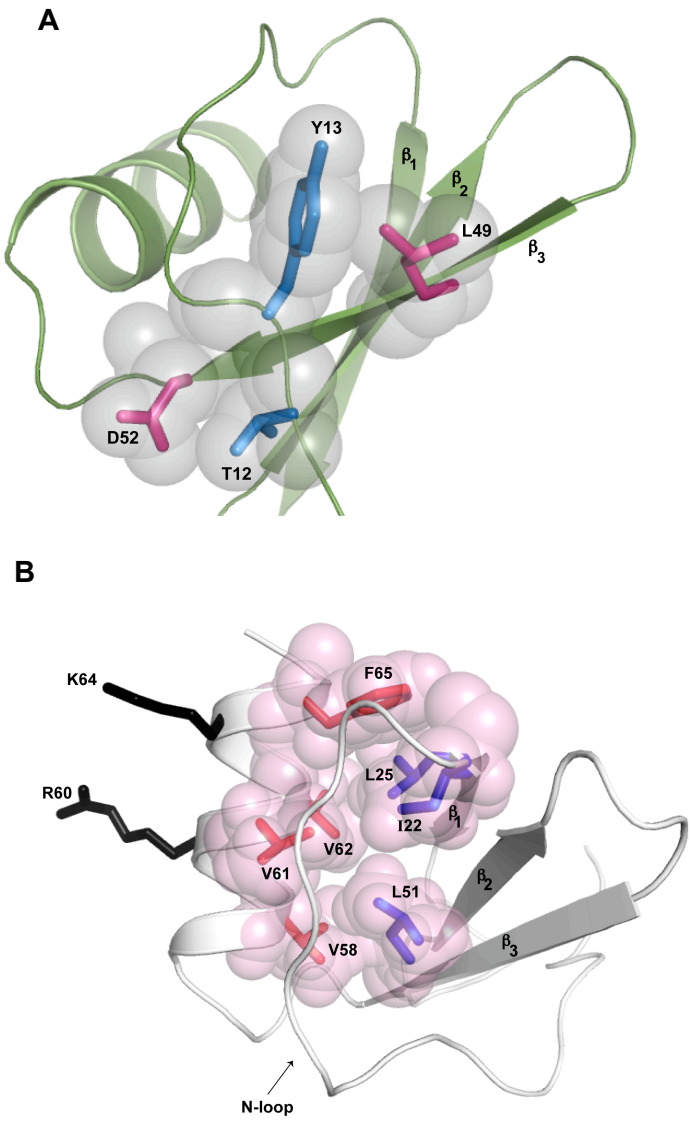

FIGURE 2.4 Binding-induced indirect coupled interactions in third *β*-strand residues (panel A). A molecular plot of the IL-8 monomer showing packing interactions between the N-loop residues Thr12 and Tyr13 (blue) and the third *β*-strand residues Asp52 and Leu49 (pink). Spheres are shown to highlight the side chain packing. One of the methyl groups of Leu49 is packed against the aromatic ring of Tyr13, and the side chain carboxylate of Asp52 is in contact with the hydroxyl side chain of Thr12. Coupled interactions in the C-terminal helix **(panel B)**. A molecular plot of the IL-8 monomer showing the packing interactions between the C-terminal helical residues, Val58, Val61, Val62, and Phe65 (red), and the *β*-strand residues, Ile22, Leu25, and Leu51 (blue). Spheres are shown to highlight the side chain packing. Solvent-exposed residues Arg60 and Lys64 are shown in black. The plots were rendered using PyMOL (96).

Binding of the IL-8 WT and Trapped R26C Dimer

WT IL-8 dissociates at micromolar concentrations (K_d ~10 μM) and therefore is predominantly dimeric at the NMR concentrations used in this study. Most interestingly, we observed a set of new peaks emerging during the latter titration points (>1:1 molar ratio), whose chemical shifts correspond to those of the monomer-bound N-domain complex **(Figure 2.5)**. These observations indicate receptor N-domain binding induces dissociation of the dimer–receptor complex to the monomer–receptor complex. Previous titration studies did not report similar binding-induced dissociation (51, 93) and can be mainly attributed to the fact that in their studies the final molar ratio was ~1:1, whereas we carried out titration up to >10-fold excess of the receptor N-domain.

In order to better understand the structural basis of dimer binding and binding-induced dissociation of the dimer-bound complex, we also carried out NMR studies of the disulfide-trapped R26C IL-8 dimer. The trapped R26C dimer has been shown to behave like the WT dimer but does not dissociate (41). We observe that the extent of overall chemical shift perturbation in the trapped dimer is substantially lower compared to the monomer. In addition to perturbation of the N-loop, third β-strand, and the C-terminal helical residues, perturbation of the second β-strand residues is also observed **(Figure 2.6)**. Two previous NMR titration studies of WT IL-8 binding to the CXCR1 N-domain showed a similar chemical shift perturbation profile, including perturbation of the 40s residues (51, 93). On the basis of monomer NMR data (vide supra), only N-loop residues are involved in direct binding, and any chemical shift perturbation for other regions, such as the 40s residues, should be due to indirect coupling interactions. Therefore, 40s residues in the dimer cannot be involved in direct binding, suggesting mechanism(s) other than binding should be contributing to the chemical shift change.

We observe binding-induced NMR line broadening in the trapped dimer to be distinctly different from the monomer. In the case of the monomer, significant line broadening was observed only for those residues that are involved in binding either by direct or by coupled interactions and could be described as due to exchange between free

and receptor-bound form. On initial binding, these peaks in the monomer become weak and disappear and then reappear, becoming stronger at later titration points as the population of the bound form dominates; these residues also show the largest binding-induced chemical shift perturbations **(Figure 2.1)**. However, in the case of trapped dimer, resonances of almost all residues become weak or completely disappear at later points **(Figures 2.6, panel B)**. Most importantly, we observe no correlation between the extent of peak intensity change and chemical shift perturbation, indicating that the line broadening in the dimer is caused by mechanisms other than exchange between the free and bound forms. For instance, in the trapped dimer, Arg47 shows a small binding-induced chemical shift change, but its line broadening is similar to Ser44 that shows the largest chemical shift change **(Figures 2.6 and 2.7)**. However, in the monomer, Arg47 shows minimal chemical shift change and minimal line broadening, and Ser44 shows significant chemical shift change and significant line broadening **(Figures 2.1 and 2.7)**.

In order to better understand the dynamic characteristics of the trapped dimer, we also carried out ^{15}N–T_2 relaxation measurements of the free and receptor-bound form. We could characterize the relaxation properties of all of the residues of the trapped dimer except for the overlapped resonances **(Figure 2.8)**. In stark contrast, we could measure relaxation values of only ~25% of the residues in the bound form due to significant line broadening. Peaks corresponding to the dimer interface β_1 as well as the β_2 and β_3 residues broaden out, and only peaks corresponding to the N-terminal, C-terminal helix, and loop residues are observed **(Figure 2.8)**. Indeed, previous relaxation measurements of the free WT dimer show residues of the β-strand, including those at the dimer interface, exhibit chemical exchange line broadening (108). Consistent with our observations from the trapped dimer, the authors conclude that these residues undergo concerted rather than independent motions due to extensive H-bonding and packing interactions.

Global line broadening is evidence of increased dynamics in the bound form, providing a snapshot of events that precede dissociation of the bound complex. We

propose that binding induced conformational changes disrupt dimer–interface interactions resulting in the dissociation of the complex, and that the receptor-bound dimer is thermodynamically unfavored and the receptor-bound monomer is the favored state.

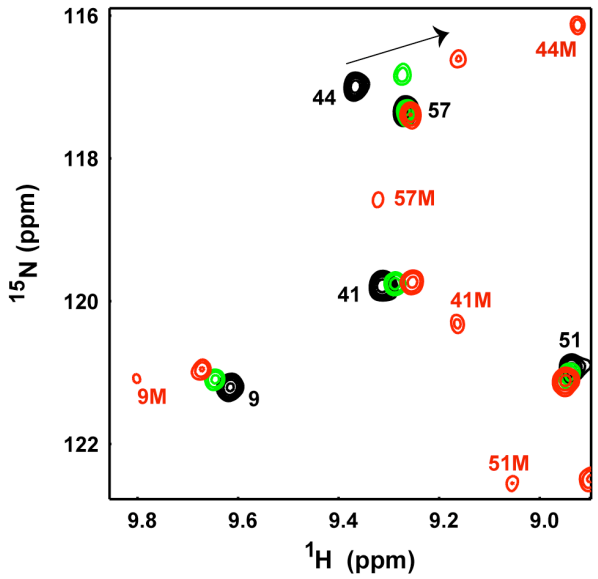

FIGURE 2.5 Binding-induced dissociation of the WT IL-8 dimer. A section of the ^{15}N–^{1}H HSQC spectra showing binding-induced chemical shift changes in the WT dimer and the appearance of bound monomer (labeled as M in red). The peaks are color coded for peptide:protein molar ratios of 0 (black), 2.7 (green), and 11.2 (red).

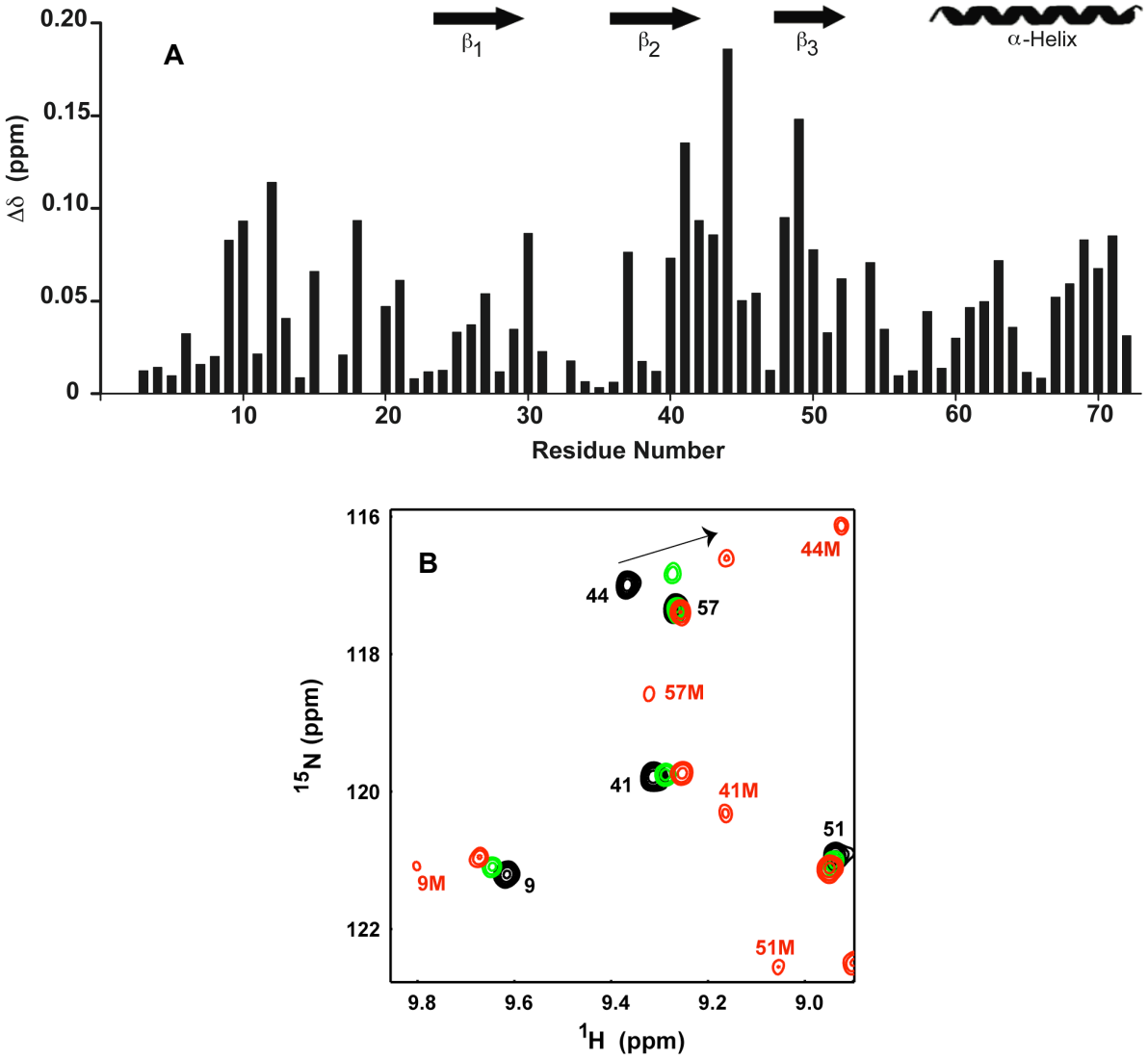

FIGURE 2.6 Binding-induced chemical shift changes in the trapped IL-8 dimer (panel A). The regions showing significant perturbations are the N-loop, second β-strand, third β-strand, and the C-terminal helix. For residues that completely broaden out in the bound form (Gln8, Thr12, Lys15, Lys20, Leu25, Arg26, Glu48, and Asp52), shift changes are calculated from the last observable titration point, and data do not exist for four prolines (residues 16, 19, 32, and 53). A section of the ^{15}N–^{1}H HSQC titration spectra showing binding-induced chemical shift changes in the IL-8 trapped dimer **(panel B)**. The peaks are color coded for peptide:protein molar ratios of 0 (black), 1.4 (green), and 2.6 (red). Data for higher molar ratios are not shown as peaks either disappear or are significantly weak.

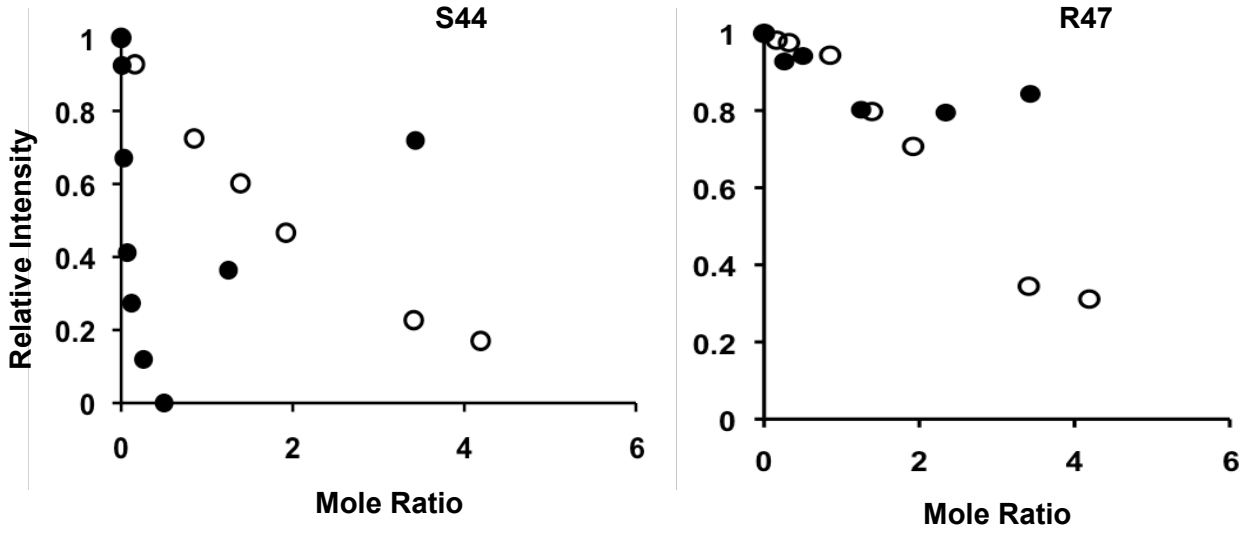

FIGURE 2.7 Binding-induced line broadening in dimer vs. monomer. Binding-induced intensity changes for the trapped dimer (○) and the monomer (●) are shown for residues Ser44 and Arg47. Line broadening and chemical shift changes are correlated for the monomer but not for the trapped dimer.

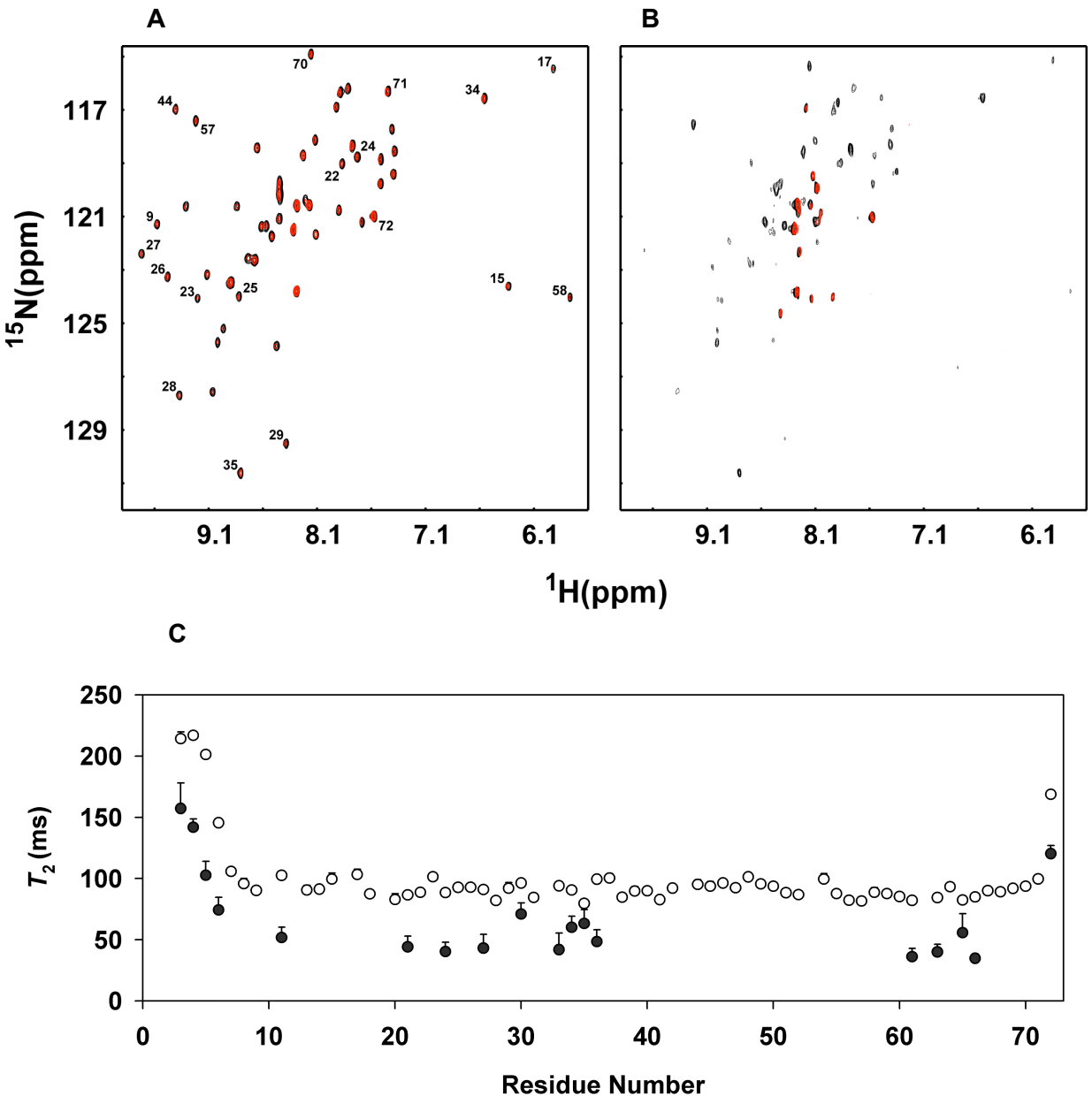

FIGURE 2.8 Relaxation properties of free and bound trapped IL-8 dimer. Overlay of a section of the ^{15}N-T_2 relaxation data when there is no relaxation delay (τ=0; black) and at T_2 delay of τ=70 ms (red) of the free **(panel A)** and the receptor peptide-bound **(panel B)** trapped dimer. The bound spectrum is shown at a level where most of the broadened peaks are visible and is not to scale with respect to the unbound spectrum. In contrast to the free monomer where most peaks are still visible at a T_2 delay of τ=70 ms, additional peaks have disappeared in the bound form. The dimer interface residues and the characteristic upfield shifted peaks are labeled. **(Panel C)** Plot of T_2 values for the free and bound trapped dimer. Due to poor s/n ratio in the bound form, T_2 values could be fitted only for 18 residues.

Binding Affinities of the Monomer and Dimer

The apparent binding constants for the IL-8(1–66) monomer and the trapped R26C dimer were obtained by fitting binding induced chemical shift changes from the titration experiments. We observe that the monomer binds the CXCR1 N-domain with an affinity of ~10 μM, and the trapped R26C dimer binds with an affinity of ~340 μM. Our measured binding constant for the IL- 8(1–66) monomer is similar to the previously measured value of ~8 μM using ITC (109). Previous studies have shown that the trapped dimer binds the intact CXCR1 receptor with ~70 fold lower affinity than the trapped monomer (41). Our observation that the trapped dimer binds the isolated CXCR1 N-domain with ~35 fold lower affinity indicates that most of the reduced binding is due to reduced affinity to the receptor N-domain site. All of these observations together emphasize that the dimer is the low-affinity ligand and the monomer is the high-affinity ligand for the CXCR1 receptor.

Linkage Scheme

Results from our titration studies allow us to discuss the linkage scheme of the binding of the monomer and dimer to the N-domain **(Figure 2.9)**. The individual steps involve binding of the monomer to the receptor N-domain (ΔG_1), binding of the dimer to the receptor N-domain (ΔG_2), dissociation of the dimer to monomer (ΔG_3), and dissociation of the N-domain-bound dimer to the N-domain-bound monomer (ΔG_4). On the basis of calculated binding constants (K_d) from our NMR titration studies, free energies of monomer and dimer binding to the CXCR1 N-domain are $\Delta G_1 = -13.9$ kcal mol^{-1} K^{-1} and ΔG_2 is -5.0 kcal mol^{-1} K^{-1}. The free energy of dimer dissociation has been measured from both ITC and ultracentrifugation methods, $\Delta G_3 = 7.4$ kcal mol^{-1} K^{-1} (97). Therefore, free energy for dissociation of the receptor-bound dimer (ΔG_4) is calculated to be -1.5 kcal mol^{-1} K^{-1}. Our observation that binding-induced dissociation of the dimer–

receptor N-domain complex is thermodynamically favorable suggests that such dissociation also occurs on dimer binding to the intact CXCR1 receptor.

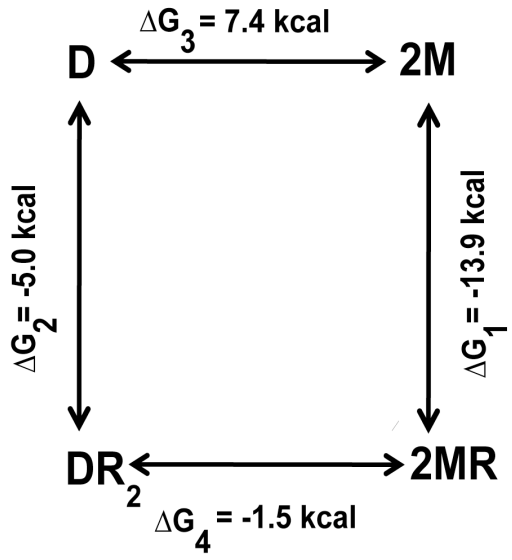

FIGURE 2.9 A thermodynamic linkage scheme representing the binding of the monomer and trapped dimer to the CXCR1 N-domain.

DISCUSSION

IL-8 belongs to the subclass of CXC chemokines that have the characteristic N-terminal "ELR" motif. All ELR chemokines recruit and activate neutrophils by binding two receptors, CXCR1 and CXCR2. Only IL-8 is a high-affinity ligand for CXCR1, whereas all neutrophil-activating chemokines including IL-8 are high-affinity ligands for CXCR2. We have shown previously that our trapped IL-8 dimer binds CXCR1 compared to CXCR2 with much lower affinity and that dissociation of the WT dimer is essential for binding CXCR1 with high affinity (41, 110). Structure–function studies have shown that

mutating IL-8 N-loop residues results in greater loss for CXCR1 binding, indicating that properties of N-loop residues are more stringent for CXCR1 binding (64, 76, 80).

On the basis of our current data, we propose that the protein core of IL-8 functions as a structural scaffold that is not rigid, but dynamic and that a network of direct and indirect backbone–backbone, backbone–side chain, and side chain–side chain interactions are involved in the binding of IL-8 to the CXCR1 N-domain. Residues that span the entire N-loop participate in binding to the N-domain, and a combination of polar, electrostatic, and hydrophobic/packing interactions mediate this event. Sequence analysis reveals that the receptor N-domain is highly negatively charged and shows characteristics of an unstructured or minimally structured domain, and so it can be envisioned that the receptor N-domain binds IL-8 by the fly-casting mechanism (111). The structure of the complex also reveals aromatic/hydrophobic/packing interactions between IL-8 aromatic and receptor Pro/aromatic residues and electrostatic interactions between IL-8 Lys and receptor N-domain Asp/Glu residues. Our NMR data show that the receptor N-domain engages the entire N-loop for the binding, which contrasts previous models, where a subset of highly clustered hydrophobic N-loop residues was defined as the binding site (49, 64).

We propose that binding engagement by multiple N-loop residues triggers propagated conformational changes throughout the protein and that these changes play a critical role in mediating binding affinity and function. Considering that binding-induced structural and dynamic changes are extensive, we propose that this binding event as active and not passive. It is possible that site-I binding results in conformational changes in the receptor triggering downstream interactions and/or triggers changes that are essential for site-II binding of IL-8 N-terminal ELR residues to the receptor extracellular domain which triggers downstream signaling events for function.

Binding of several CXC (SDF-1α and IP-10) and CC (RANTES, eotaxin, eotaxin-2) chemokines and CX_3C chemokine fractalkine to their receptor N-domains has been studied using NMR spectroscopy (14, 23, 24, 48, 94, 112). These studies show not

only that binding predominantly perturbs chemokine N-loop residues but also chemokine-dependent perturbation of other regions of the protein. For instance, fractalkine binding to the CX_3CR1 N-domain results in significant perturbation of N-terminal and 30s loop residues, whereas these residues showed negligible chemical shift changes in IL-8 (24). These observations together suggest that indirect coupling interactions play a critical role for binding of most chemokines and that these interactions play a variety of functional roles from contributing to binding affinity, receptor selectivity, and/or receptor activation.

IL-8 function involves binding to receptors on neutrophils and to glycosaminoglycans (GAG) on the endothelial cell surface. Under transient conditions of injury or infection, IL-8 levels are upregulated and are translocated from the injury site to the bloodstream, and so its concentration will vary continuously as a function of space and time. Indeed, using a trapped monomer, trapped dimer, and the WT, we observe that the WT exists as both monomers and dimers *in vivo* and that the IL-8 dimer is extremely potent in its ability to recruit neutrophils in a mouse model (113). Whereas mice express only the CXCR2 receptor on neutrophils, humans express both CXCR1 and CXCR2 receptors, suggesting that the two receptors play distinctly different roles in humans. IL-8 plays the dual role of recruiting neutrophils to the site of infection and eliciting cytotoxic activities at the site of infection. These events have to be coordinated as the initial receptor engagement should lead to recruitment and chemotaxis, and receptor activation leading to cytotoxic event should not be triggered until late at the site of infection. It is believed in humans that CXCR2 plays a more active role for trafficking neutrophils into the tissue and CXCR1 is more active for eliciting cytotoxic events (82). Consistent with our observations, the IL-8 dimer is less active for CXCR1-related functions (45), suggesting *in vivo* IL-8 dimerization negatively regulates CXCR1 function.

Interestingly, the role of dimerization seems to vary from chemokine to chemokine. CXC chemokine SDF-1α dimerizes like IL-8, but receptor-binding properties of the SDF-1α dimer are distinctly different from the IL-8 dimer (40, 112). Whereas the

structure of the IL-8 dimer–receptor complex reveals binding interactions to only one subunit, the structure of the trapped SDF-1α–receptor complex reveals that the binding involves residues from both subunits of the dimer (42, 51). Whereas binding of the IL-8 dimer to the CXCR1 N-domain results in the dissociation of the complex, binding of the SDF-1α monomer to the CXCR4 N-domain actually results in ligand dimerization (40). Though CXC and CC monomer structures are similar, they dimerize using different regions of the protein. CXC chemokine dimerization involves the third β-strand and α-helical residues, and CC chemokine dimerization involves the N-loop residues. The disulfide-linked CC dimer MIP-1β was shown to be incapable of binding its receptor, and under conditions where both monomer and dimer exist, only the RANTES monomer was shown to bind the CCR5 N-domain (94, 114). Nevertheless, CC chemokine monomer mutants are inactive *in vivo*, indicating that their dimerization is essential for functions other than for binding their GPCR receptors (115).

In summary, our results together indicate that the two fundamental properties shared by chemokines, the ability to exist as monomers and dimers and the interaction of ligand N-loop residues with receptor N-domain residues for binding and function, are not independent but coupled. We propose that such coupling interactions play a critical role in regulating *in vivo* function.

CHAPTER III

THE STRUCTURAL BASIS OF CXCR2 RECEPTOR INTERACTION: INSIGHTS INTO BINDING AFFINITY AND SELECTIVITY OF IL-8 AND MGSA

INTRODUCTION

Chemokine receptors belong to the superfamily of 7-TM GPCRs, and are activated by chemokines that are secreted by the immune cells in response to infection or injury. Chemokine-receptor interactions show a broad range in selectivity, with a single ligand binding just one or multiple receptors, and a single receptor binding multiple ligands. Of particular importance, CXCR1 and CXCR2 receptors bind the subclass of ELRCXC chemokines including IL-8 and MGSA. CXCR1 is specific and binds IL-8 alone with high nM affinity, whereas CXCR2 is promiscuous and binds all ELRCXC chemokines including IL-8 and MGSA with high nM affinity (76, 117).

At physiological conditions, IL-8 and MGSA can exist as monomers and dimers, and therefore CXCR2 function can be mediated by both monomeric and dimeric ligands. Structures of WT IL-8 and MGSA show that they are dimeric, and so it was initially thought that the dimer is the functionally relevant form (15, 18). Subsequently, using trapped IL-8 and MGSA monomers, it was shown the monomer is sufficient for receptor activation (42, 43). Receptor binding studies using trapped IL-8 monomers and dimers have shown that the IL-8 dimer binds CXCR2 with lower affinity but is as active as the monomer in a wide variety of functions (45). At this time, the functional characteristics of monomeric and dimeric MGSA, and the structural basis of how IL-8 and MGSA bind and activate CXCR2 are not known.

Mutagenesis and domain swapping studies of CXCR2 and of its ligands have consistently shown that site-I interaction plays a key role in ligand binding affinity and receptor selectivity (49, 53, 58, 59, 66, 76, 80, 86, 88, 118). However, the molecular basis of how site-I interactions mediate ligand binding affinity and receptor

selectivity is not known. Towards this, I have studied the binding of the IL-8 and MGSA monomers and dimers to the isolated CXCR2 N-domain using NMR spectroscopy. For this purpose, I used designed monomers, IL-8 (1-66) and MGSA (1-67) deletion variants, and the trapped IL-8 R26C and trapped MGSA N27C dimers.

NMR chemical shift perturbation data showed that all the variants bound the CXCR2 N-domain in a similar fashion involving essentially the same set of N-loop residues. However, the measured binding affinities showed that the MGSA monomer compared to the IL-8 monomer binds CXCR2 N-domain with ~6 fold higher affinity, IL-8 monomer and dimer show similar affinities, and the MGSA monomer binds with ~5 fold higher affinity than the MGSA dimer. These observations provide crucial evidence that site-I binding interactions are important, and the measured binding affinities also indicate that binding to site-I is intimately coupled to site-II, and that differential coupling interactions determine overall binding affinities for IL-8 and MGSA monomers and dimers.

EXPERIMENTAL PROCEDURES

Recombinant IL-8 (1-66) monomer, trapped IL-8 R26C dimer and the WT IL-8 dimer are the same as that used for our NMR studies described in Chapter 2. Protein expression and purification of ^{15}N-labeled IL-8 and MGSA variants were performed as described in Chapter 2.

Design of CXCR2 N-domain constructs

Titration studies with the human CXCR2 N-domain involved using two constructs namely, CXCR2 N-domain 43-mer and 25-mer. The sequences of these peptides, and of the full length CXCR2 N-domain are as follows:

CXCR2 N-domain sequences

Full Length MEDFNMESDSFEDFWKGEDLSNYSYSSTLPPFLLDAAPCEPESLEINK

43-mer MESDSFEDFWKGEDLSNYSYSSTLPPFLLDAAPSEPESLEINK

25-mer FWKGEDLSNYSYSSTLPPFLLDAAP

The native CXCR2 N-domain sequence has a cysteine, which was mutated to a serine in the 43-mer to minimize complications due to disulfide bond formation. The peptides were synthesized by solid phase peptide synthesis and their molecular weights were confirmed using MALDI MS.

NMR spectroscopy

For titration experiments involving IL-8 monomers and dimers, ^{15}N-labeled IL-8 (1-66) and trapped R26C IL-8 dimer were prepared in 50 mM sodium acetate buffer, pH 6.0 containing 1mM DSS, 1 mM sodium azide, and 10% $^{2}H_2O$ (v/v). A stock solution of CXCR2 N-domain was prepared in the same buffer, and was titrated to final molar ratios of 4.9, 11.4 and 10.6 for the IL-8 monomer, WT IL-8, and the IL-8 dimer, respectively.

For titration experiments involving ^{15}N-labeled MGSA samples, (1-67) monomer, WT MGSA, and N27C trapped dimer, were prepared in 50 mM potassium phosphate buffer containing 1mM DSS, 1 mM sodium azide, and 10% $^{2}H_2O$ (v/v) at either pH 5.0 or 6.0. A stock solution of CXCR2 N-domain was prepared in the same buffer, and was titrated to final mole ratios of 4.9, 7.1 and 5.2 for the MGSA monomer, WT MGSA, and MGSA dimer, respectively. All titration experiments were carried out at 30˚C. Two-dimensional ^{1}H-^{15}N HSQC spectra were acquired after each titration of the CXCR2 N-domain, with 2048 complex points in the direct ^{1}H dimension and 128 complex points in the indirect ^{15}N dimension.

Effect of pH and temperature on the conformational heterogeneity of MGSA monomer

The effect of pH and temperature on the conformational heterogeneity of the MGSA monomer were studied by acquiring ^{1}H-^{15}N HSQC spectra at pH 4.5, 5.5 and 6.5 at 30˚C, and at 20, 30, and 40˚C at pH 4.5, respectively.

Chemical shift assignments of MGSA monomer

Sequential assignments were performed by acquiring three-dimensional ^{15}N-edited NOESY-HSQC and ^{15}N-edited TOCSY-HSQC spectra with mixing times (τ_m) of 150 ms and 100 ms, respectively at 40°C and pH 4.5 (119). Chemical shifts in all spectra were referenced to DSS (98). All spectra were acquired using either Varian Unity Plus 600 or INOVA 800-MHz spectrometers equipped with field gradient accessories, processed using NMRPipe (99), and analyzed using NMRView (100).

RESULTS AND DISCUSSION

Choice of CXCR2 N-domain

NMR binding studies to the IL-8 monomer were carried out using two CXCR2 N-domain constructs, 25-mer and 43-mer. Initially, the binding of the 25-mer to the IL-8 monomer was studied. Previous binding studies using CXCR1 N-domain peptides of different lengths showed that a 24-mer is sufficient for receptor binding affinity (Chapter 2). Therefore, a 25-mer CXCR2 N-domain peptide (R2-25mer) was designed on the basis sequence alignment with the CXCR1 N-domain 24mer (R1-24mer).

Titration of the R2-25mer induced selective perturbations ($\Delta\delta$ >0.06 ppm) of the N-loop and third β-strand residues **(Figure 3.1, panels A and B)**. The calculated binding constants indicate that the R2-25mer, compared to the R1-24mer, binds the IL-8 monomer with ~70 fold lower affinity (K_d ~720 μM for R2-25mer vs. ~10 μM for R1-24mer). The measured low binding affinity suggested that the R2-25mer could be missing some critical binding residues, and therefore a longer 43-mer peptide (R2-43mer) was designed.

R2-43mer induced larger chemical shift perturbations ($\Delta\delta$ >0.1 ppm) for the N-loop, third β-strand, and C-terminal helical residues **(Figure 3.1, panels C and D)**. A comparison of the binding-induced chemical shift changes for the two peptides indicate essentially the same set of residues are involved in binding, though extent of perturbation was lower for the R2-25mer **(Figure 3.1, panel E)**. Calculation of the

binding affinities indicate that the R2-43mer compared to the R2-25mer binds IL-8 monomer with ~6 fold higher affinity (K_d ~130 μM for the R2-43mer vs. K_d ~720 μM for the R2-25mer) (**Figure 3.1, panel F)**. From a thermodynamic perspective, the observation that the binding of the same residues results in different affinities suggests that the differences are due to entropic and not necessarily enthalpic factors. It is likely that the higher affinity of the R2-43mer is due to lower loss of binding-induced conformational entropy. ITC measurements for the binding of IL-8 monomer to R2-43mer showed that it is enthalpically favored and entropically neutral (ΔH -5.5 kcal mol^{-1}; TΔS, 0.2 kcal mol^{-1}). ITC experiments for the binding of the R2-25mer could not be performed because of its weak binding affinity. The solubility of R2-25 mer was > 1000 μM and that of the R2-43 mer was ~700 μM. Though the R2-25mer had better solubility than the R2-43mer, the R2-43mer was used for the titration experiments because of its higher binding affinity to the monomer.

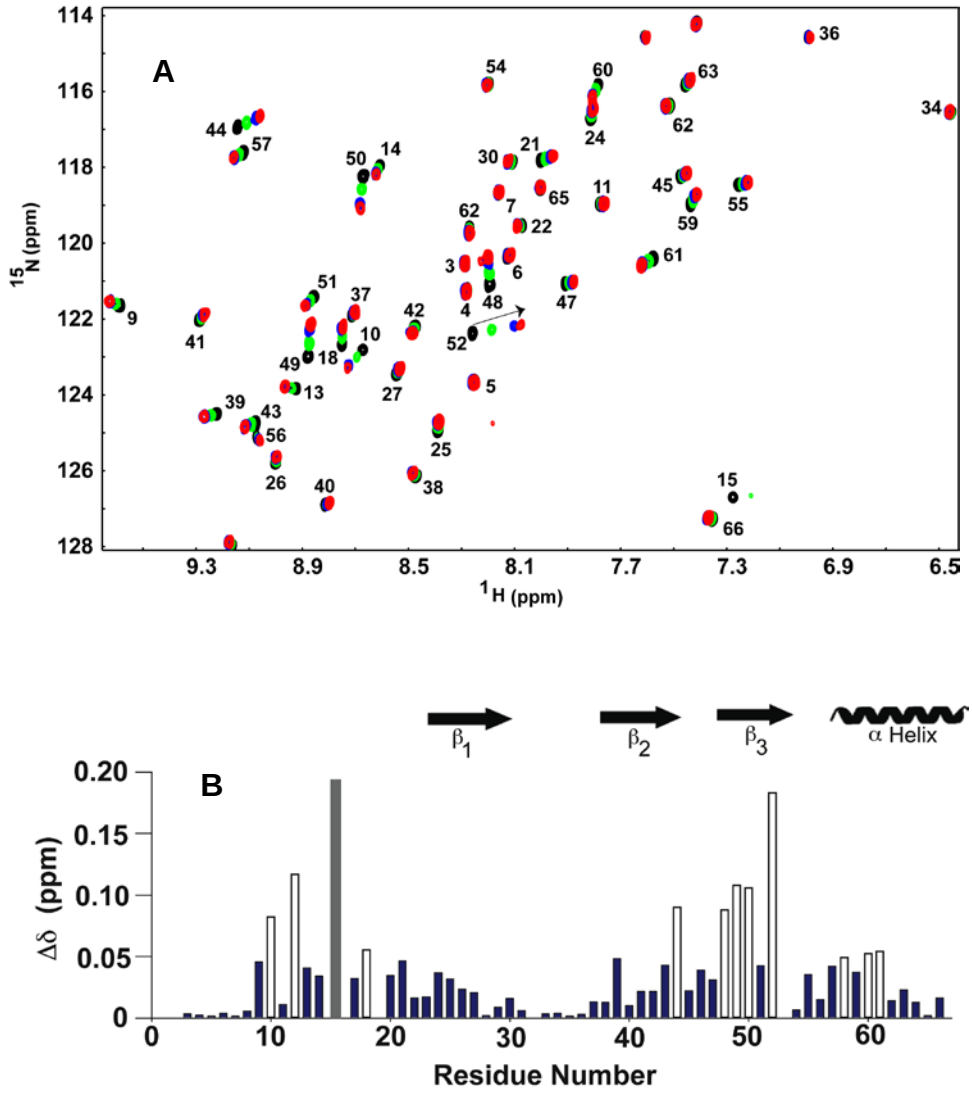
A
B
C
^{15}N (ppm)
^{1}H (ppm)
Δδ (ppm)
Residue Number
β1
β2
β3
α Helix

D

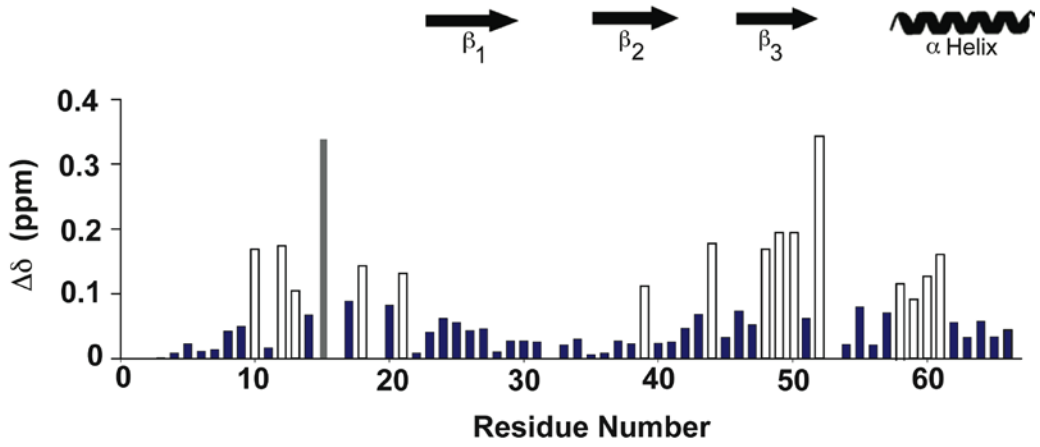
β1
β2
β3
α Helix
0.4
0.3
0.2
0.1
0
Δδ (ppm)
0
10
20
30
40
50
60
Residue Number

E

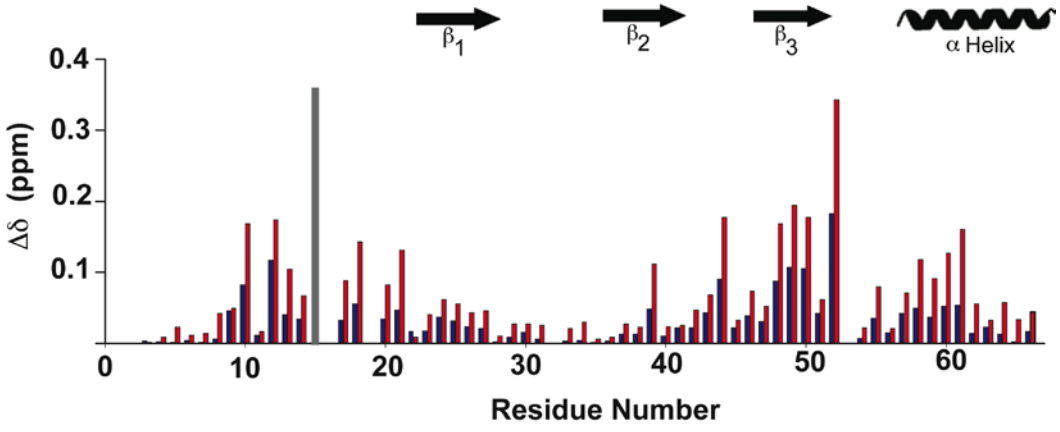
β1
β2
β3
α Helix
0.4
0.3
0.2
0.1
0
Δδ (ppm)
0
10
20
30
40
50
60
Residue Number

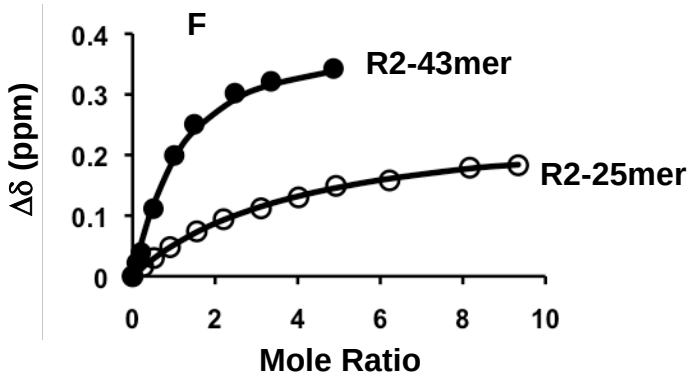

Figure 3.1 Binding of the IL-8 monomer to CXCR2 N-domain.
Panels A and C. Sections of ^{1}H-^{15}N HSQC spectra showing the chemical shift changes on binding to R2-25-mer and R2-43-mer. Peaks are color coded for peptide:protein mole ratios of 0 (black), 1.6 (green), 6.2 (blue) and 9.3 (red) for the binding of the R2-25mer and that of 0 (black), 0.2 (green), 1.0 (blue) and 4.9 (red) for the binding of the R2-43mer. Histogram plots showing the total chemical shift changes in the IL-8 monomer on binding to R2-25mer and R2-43mer are shown in **panels B and D** respectively, and the plot comparing the perturbations on binding to both peptides is shown in **panel E**. Residues showing relatively higher perturbations represented by open white bars. Lys15 disappears during titration, and is represented by a grey bar, which is shown at the same height as the maximum shift change observed for Asp52 to indicate that its perturbation should be similar to or higher than that of Asp52. Residues 16, 19, 32 and 53 are prolines. **Panel F** shows the fitted chemical shift data for the binding of both peptides.

Characterization of CXCR2 N-domain-IL-8 monomer interactions

During the titration, line broadening of a number of peaks was observed, but there was no direct correlation between chemical shift perturbation and line broadening. For instance, Leu49 shows significant binding-induced chemical shift change but its line broadening profile is similar to Gly31, which shows minimal binding-induced chemical shift change **(Figure 3.2)**. Therefore, line broadening cannot be due to the exchange between the free and bound forms, and so the discussion of the binding is confined to the chemical shift perturbation data.

Role of the N-loop residues: Large perturbations were observed for the N-loop residues Ile10, Thr12, Tyr13, His18 and Phe21, and to a lesser extent for residues

Ser14, Phe17 and Lys20, **(Figure 3.3, panel B)**. ASA calculations indicate that Ile10, Ser14, Lys15, and Lys20 are solvent exposed (ASA ~0.8) and so must be involved in direct contact interactions with the receptor residues. On the other hand, residues Thr12, Tyr13, His18, and Phe21 are partially buried (ASA ~0.3-0.6) **(Figure 3.3)**. As the N-loop is conformationally flexible, these residues can either contact the receptor directly or can influence the binding of Ile10, Ser14, Lys15, and Lys20 through propagated conformational changes as a result of indirect coupled interactions. These data together show that the CXCR2 N-domain engages the entire N-loop through direct and indirect packing and electrostatic interactions.

An interesting observation was made for Lys15, that it disappears completely during titration due to line broadening **(Figure 3.1)**. The peak was not observed even at the highest receptor concentration, and this observation was made even with the R2-25mer which binds with much lower affinity **(Figure A1)**. Sequence analysis of the receptor N-domains show the presence of multiple Asp/Glu residues. Therefore, line broadening of Lys15 suggests that it is conformationally dynamic in the bound form and that it could be interacting with different negatively charged Asp/Glu residues in the receptor N-domain.

Role of the third β-strand residues: The third β-strand residues that are significantly perturbed are Glu48, Leu49, Cys50, and Asp52. Among these residues, Glu48 is the only solvent exposed residue, whereas the remaining residues are buried and are involved in favorable packing interactions with the N-loop residues. Interestingly, Asp52 shows the largest perturbation among all residues though it is largely buried (ASA ~0.2). The structure shows that Leu49, Leu51 and Asp52 interact with the N-loop residues Thr12 and Tyr13 through packing interactions, and so binding induced structural changes must be responsible for the observed changes (26) **(Figure 3.4, panel A)**.

Chemical shift perturbation data show that Cys50 compared to Cys9 is perturbed to a large extent **(Figure 3.1, panel D)**. The structure of the monomer shows that the Cys9-Cys50 disulfide bridge tethers the conformationally flexible N-loop to the third β-strand (26); therefore, structural perturbations of the N-loop

residues can be indirectly transmitted to the third β-strand via coupling interactions through the Cys9-Cys50 disulfide bridge.

Role of the C-terminal helix: Significant perturbations are observed for Val58, Gln59, Arg60, and Val61 in the C-terminal helix. Among these residues, Arg60 is the only residue that is solvent exposed, Gln59 is partially buried, and Val58 and Val61 are buried and involved in packing interactions with the β-strand residues **(Figure 3.4, panel B)**. We also observe that buried residues Trp57, Val62, Phe65 and Leu66 are minimally perturbed **(Figure 3.1, panel D)**, and so the perturbations of Val58, Gln59, Arg60 and Val61 cannot be due to direct, but due to indirect coupled interactions as a result of propagated conformational changes.

Other regions: Regions that show minimal perturbations are the N-terminus, first and second β-strand, 30s and 40s loops and the 50s turn residues **(Figure 3.1, panel D)**. Ile39 (second β-strand) and Ser44 (40s loop) are the only residues that show significant chemical shift perturbations **(Figure 3.1, panel D)**. Ile39 is packed against Val58 in the C-terminal helix, and Leu51 in the third β-strand (**Figure 3.4**). Asp52, which is adjacent to Leu51 is packed against the N-loop residue, Thr12, and so Ile39 is perturbed due to structural changes propagated from the third β-strand. The structure of the IL-8 monomer shows backbone-backbone H-bonding interaction between Ser44 and Phe21 in the N-loop **(Figure 3.4, panel C)**. Therefore, Phe21 could be involved in propagating binding-induced conformational changes to Ser44.

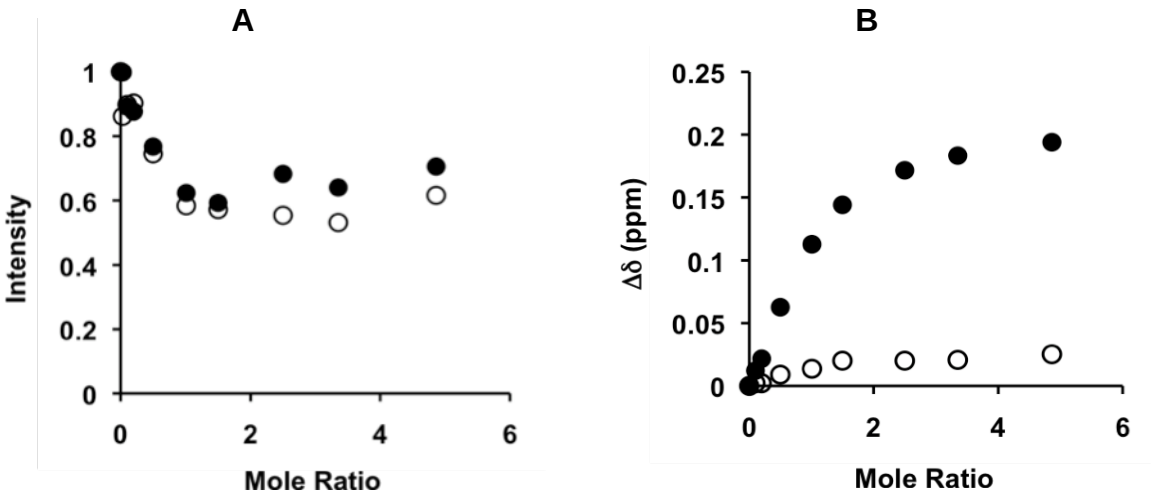

Figure 3.2 Line broadening analysis in the IL-8 monomer on binding to CXCR2 N-domain (43-mer). (A) intensity and **(B)** chemical shift (Δδ) changes as a function of mole ratio are shown for residues Leu 49 (•) and for Gly 31 (○).

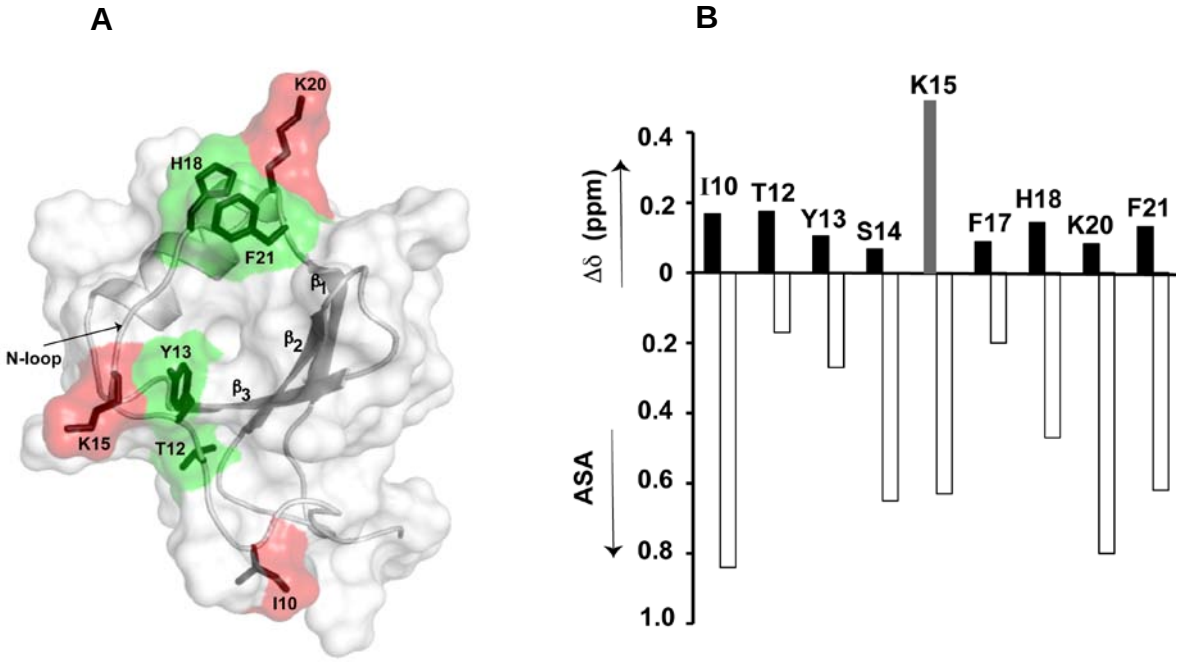

Figure 3.3 Role of the N-loop residues.
A molecular plot of the IL-8 monomer showing the N-loop residues involved in CXCR2 N-domain binding **(panel A)**. The solvent exposed residues, Ile10, Lys15 and Lys20 are highlighted in red, and partially buried residues, Thr12, Try13, His18, and Phe21 are highlighted in green. A plot of the chemical shift change (top y-axis) and the side chain ASA (bottom y-axis) of the IL-8 monomer N-loop residues show that they are not necessarily correlated **(panel B)**. Lys15 disappears due to line broadening and is represented by a grey bar. The ASA of the IL-8 monomer (PDBid 1IKM) was calculated using the program VADAR (116).

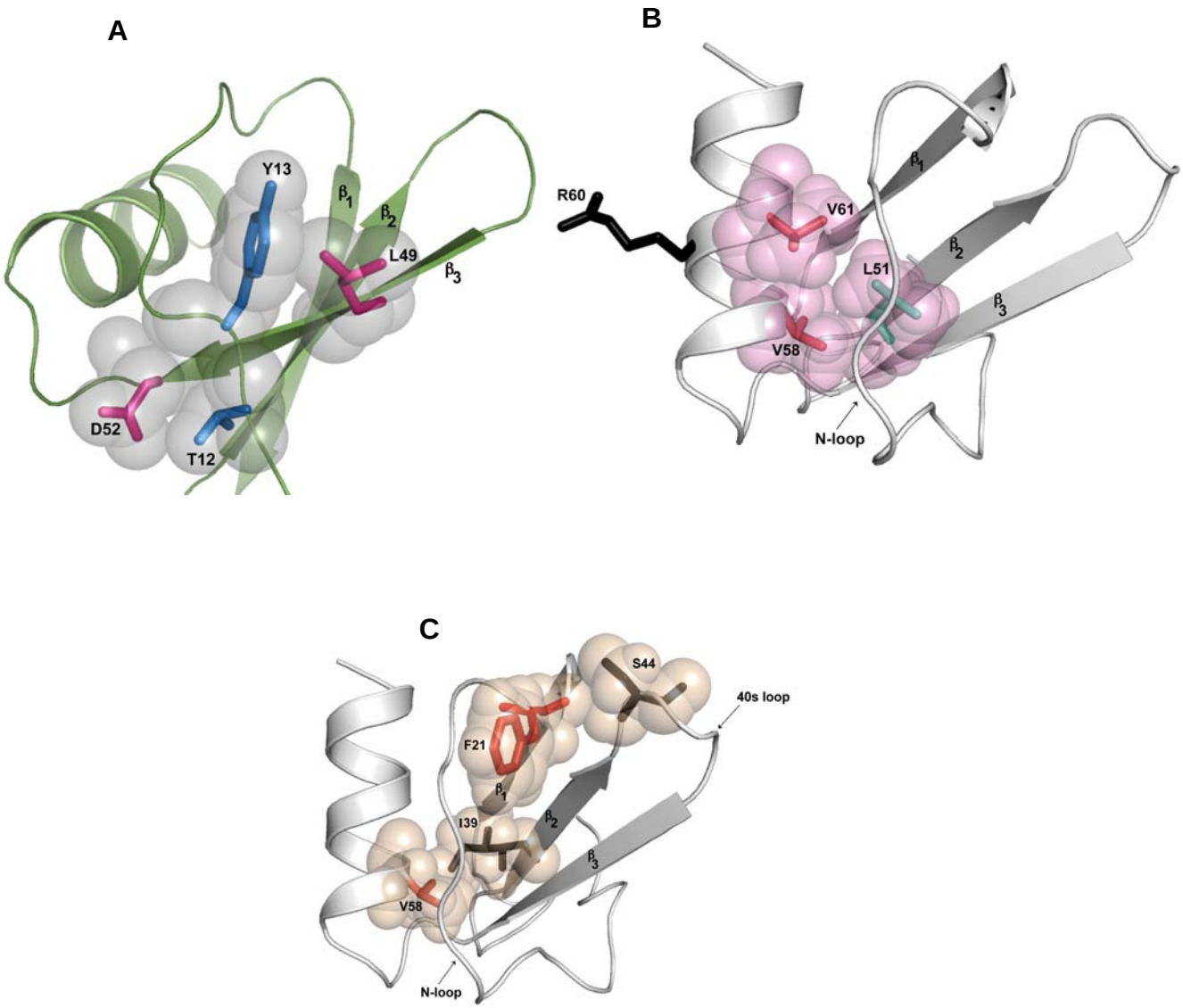

Figure 3.4 CXCR2 N-domain binding induced indirect coupled interactions in the IL-8 monomer. Panel A shows packing interactions between N-loop residues Thr12 and Tyr13 (blue) and the third β-strand residues Asp52 and Leu49 (pink)**. Panel B** shows packing interactions between the C-terminal helix residues Val58 and Val61 (red), and the β-strand residue, Leu51 (cyan). **Panel C** shows packing interactions between the second β-strand residue Ile39 (black) and the C-terminal helix residue Val58 (red), and backbone-backbone interactions between Ser 44 in the 40s loop (black) and the N-loop residue, Phe21 (red).

Design of an obligate MGSA monomer and the trapped MGSA N27C dimer

Previously, it was shown that the designed IL-8(1-66) deletion mutation is an obligate monomer at mM concentrations used in NMR studies (38). This mutant was designed by deleting the last six C-terminal helix residues that were observed to be part of the dimer interface in the structure. The MGSA monomer was designed by deleting the last six C-terminal helix residues as the structure showed that these residues are most likely involved in dimerization. Indeed, analytical ultracentrifugation studies showed that the MGSA (1-67) deletion mutant is a monomer at concentrations used for NMR studies (data not shown).

The trapped MGSA N27C dimer was designed in a similar manner as that of the trapped IL-8 R26C dimer by substituting a disulfide across the dimer interface at the site of 2 fold symmetry (described in chapter 2). This mutation does not perturb the dimer interface, as the chemical shifts of most resonances in the ^{1}H-^{15}N HSQC spectra of the trapped MGSA N27C dimer were similar to that of the WT MGSA dimer (18) **(Figure 3.5)**.

Characterization of CXCR2 N-domain-MGSA interactions

Conformational heterogeneity of MGSA as a function of pH. NMR titration experiments with the IL-8 monomer were carried out at pH 6.0, and so titration experiments with the MGSA monomer were initially carried out at pH 6.0. Two different chemical shifts for several residues were observed in the ^{1}H-^{15}N HSQC spectrum at pH 6.0 indicating the presence of two conformers. However, at pH 5.0 and 4.5, fewer peaks were observed with majority of the resonances at pH 4.5 corresponding to a single major conformer **(Figures 3.6 and 3.7,** also see **Figure A2)**. Analytical ultracentrifugation studies show that the MGSA deletion mutant is a monomer at all pH values indicating that the pH-induced conformational heterogeneity is not due to dimerization. The effect of temperature at pH 4.5 shows that higher temperatures (40 vs. 20°C) minimize the heterogeneity **(Figure 3.8)**.

The phenomenon of conformational heterogeneity as a function of pH was also observed for the WT MGSA dimer. However, the pH had an opposite effect as decreasing the pH increased the relative population of the minor conformer. However, increasing the temperature decreases the heterogeneity **(Figure A3)**. Previous NMR studies did not report any heterogeneity, and the reason for the differences between our MGSA and those published in literature is not clear (18, 20). Molecular weight determination by mass spectrometry and DNA sequence analysis did not detect any problems, and our preparations show the same high level of receptor activity as published in literature. It is possible that the differences could be a reflection of how the proteins are purified. Several groups have made similar observations with other chemokines, where differences in dimerization affinities and mode of dimerization have been reported for the same chemokine (21, 39, 120, 121).

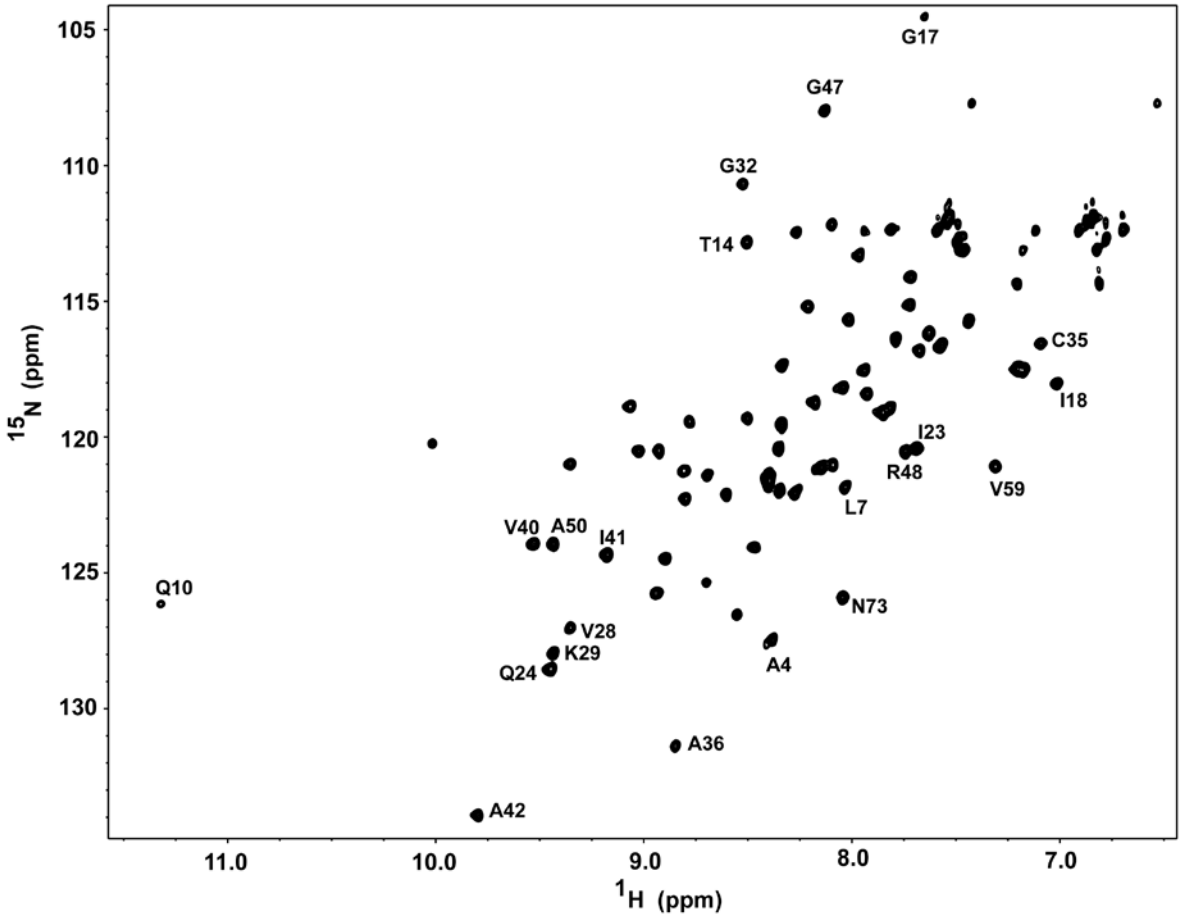

Figure 3.5 ^{1}H-^{15}N HSQC 800 MHz NMR spectrum of the trapped N27C MGSA dimer at pH 6 and 30°C. Residues that could be unambiguously assigned are labeled.

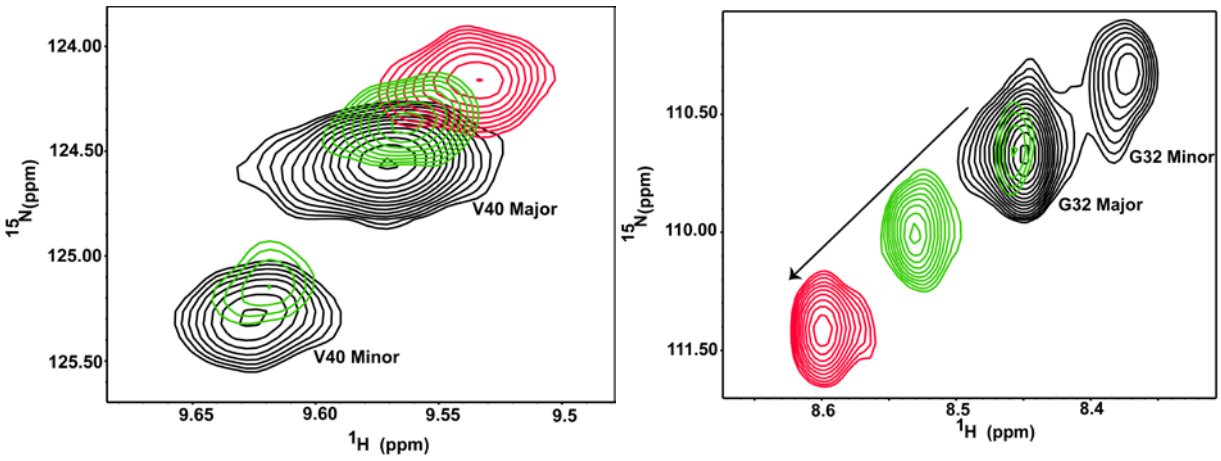

Figure 3.6 pH induced conformational heterogeneity of MGSA monomer. Sections of ^{1}H-^{15}N HSQC spectra at 30°C showing the major and minor conformers of Val40 and Gly32 at pH 6.0 (black), 5.5 (green), and 4.5 (red). The arrow indicates the direction of movement of the major conformer of Gly32.

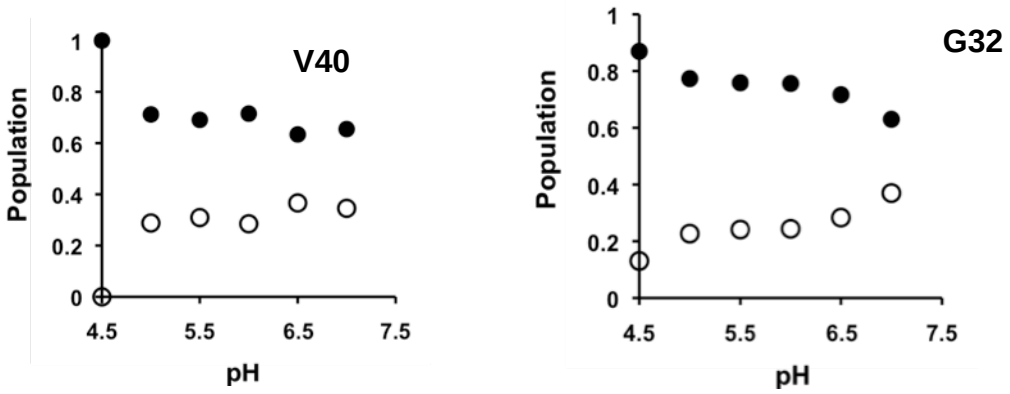

Figure 3.7 Effect of pH on conformational heterogeneity of MGSA monomer. Population of the major (•) and the minor conformers (○) are shown for residues Val40 and Gly32 as function of pH at 30°C.

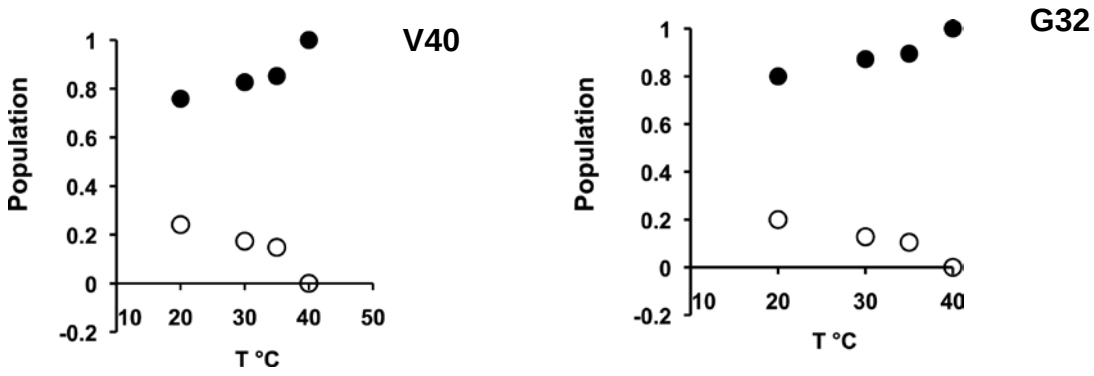

Figure 3.8 Effect of temperature on the conformational heterogeneity of MGSA monomer. Populations of the major (•) and the minor conformers (○) of residues Val40 and Gly32 as a function of temperature, and at pH 4.5 are shown.

Binding of the MGSA monomer to CXCR2 N-domain

Binding studies with the MGSA monomer were carried out at pH 5.0 and not at pH 4.5 due to the insolubility of the R2-43mer at pH 4.5. Chemical shift assignments were carried out at pH 4.5 and the assignments were transferred to the ^{1}H-^{15}N HSQC titration spectra at pH 5.0 **(Figure 3.9) (Table A1)**.

Titration of the R2-43mer into ^{15}N labeled MGSA monomer results in significant chemical shift changes ($\Delta\delta > 0.1$ ppm) for the N-loop, second β-strand, 40s turn, and third β-strand, and the C-terminal helical residues **(Figure 3.10)**. Line broadening analysis did not provide any useful information as even peaks that show minimal chemical shift changes broaden out during titration. Therefore, only chemical shift perturbation was used for analysis.

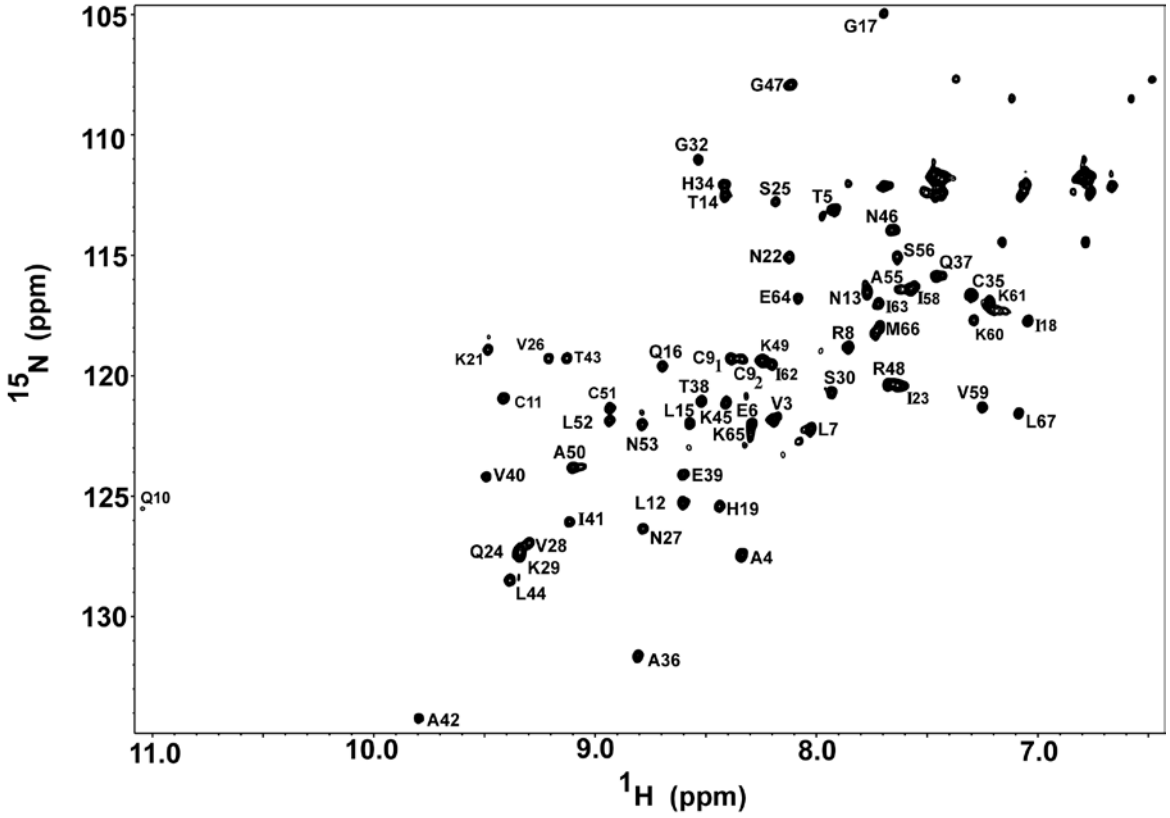

Figure 3.9 ^{1}H-^{15}N HSQC 600 MHz NMR spectrum of the MGSA monomer at pH 4.5 and 30°C.

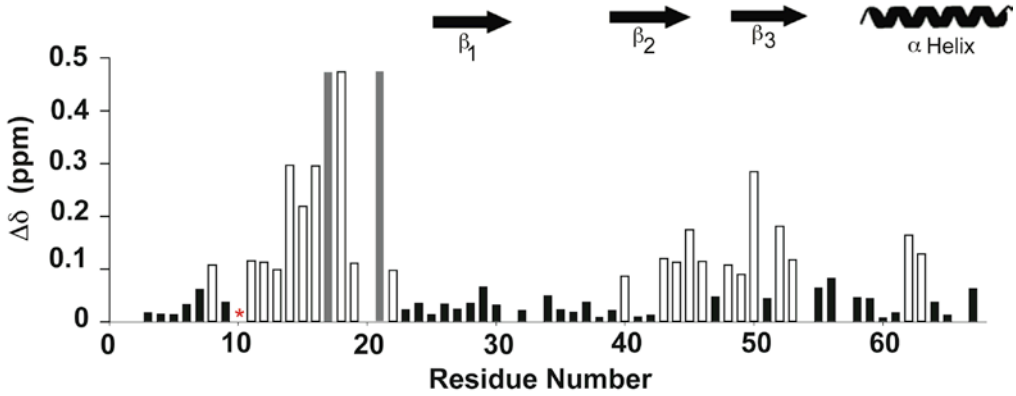

Figure 3.10 CXCR2 N-domain binding induced chemical shift changes in the MGSA monomer. A histogram showing the binding-induced chemical changes (Δδ, ppm) of the major conformer residues. Residues showing significant perturbations are represented as open white bars. Chemical shift change for Gly17 and Lys21 are represented as grey bars, as the peaks corresponding to these residues disappear during titration due to line broadening. The grey bars are shown at the same height as that of Ile18, which shows the maximal chemical shift change. Chemical shift change for Gln10 is not available as its peak is line broadened in the free form and is represented by a red asterisk, and residues 20, 31, 33, 54 and 57 are prolines.

Role of the N-loop residues: Large chemical shift perturbations were observed for N-loop residues, Thr14, Leu15, Gln16, Gly17, Ile18, and Lys21, and to a lesser extent for residues Leu12, Gln13, His19, Lys21 and Asn22. Furthermore, peaks corresponding to Gly17 and Lys21 completely disappear in the bound form suggesting that these are conformationally dynamic in the bound form. The structure of MGSA shows that these residues span the entire length of the N-loop **(Figure 3.11)**. Among these residues, Leu12, Gln13, Gln16, His19, and Lys21 are solvent exposed (ASA ~0.6-0.8), Leu15, Ile18 and Asn22 are partially buried (ASA ~0.4-0.5), and Gly17 is completely buried **(Figure 3.11)**. Unlike IL-8, the available mutagenesis data on MGSA is not as extensive. In fact, the only mutagenesis data available are for residues Leu12, His19, and Lys21. Ala mutants of these residues bind with ~10-fold reduced affinity to CXCR2 (74, 79). However, loss of CXCR2 receptor activities for Leu12 and His19 Ala mutants are much higher indicating that binding affinities are not correlated with their activities. Even though His19 is perturbed to a lesser extent compared to the other N-loop residues, clearly it plays an important role in CXCR2 binding and function.

Large chemical shift perturbation of residues Thr14, Leu15, Gln16, Gly17, Ile18, and Lys21 indicate that these residues are important for CXCR2 N-domain binding. The structure shows that Leu15 and Gly17 are packed against the protein core, and the side chains of Ile18 and Asn22 are partially buried and are in close proximity to each other **(Figure 3.11)**. As the N-loop is conformationally dynamic, it is possible that the side chains of Leu15, Gly17 and Ile18 become exposed and engage in binding or these residues can indirectly influence the binding of the solvent exposed residues. A more conclusive picture on the role of these residues on CXCR2 binding can be obtained by studying the effect of mutating these N-loop residues on receptor binding affinity and function.

Role of the second β-strand residues: The second β-strand residues that are significantly perturbed are Val40, Thr43, and Leu44 **(Figure 3.10)**. These residues are completely buried and are involved in packing interactions, and so cannot be involved in direct binding. Packing interactions are also observed between Val40 and Leu52 in the third β-strand, and Leu52 is packed against Leu15 in the N-loop. Also, Leu44 is

packed against Asn22 in the N-loop **(Figure 3.12)**. Therefore, perturbation of the second β-strand residues are due to binding induced structural changes propagated through packing interactions.

Role of the 40s turn residues: The 40s turn residues that show significant perturbations are Lys45 and Asn46 **(Figure 3.10)**. These residues are partially buried in the structure (ASA ~0.5). The side chain of Lys45 interacts with the backbone of Lys21, and Asn46 is adjacent to Lys45. Therefore, these residues are perturbed as a result of indirect coupled interactions propagated from Lys21 **(Figure 3.12)**.

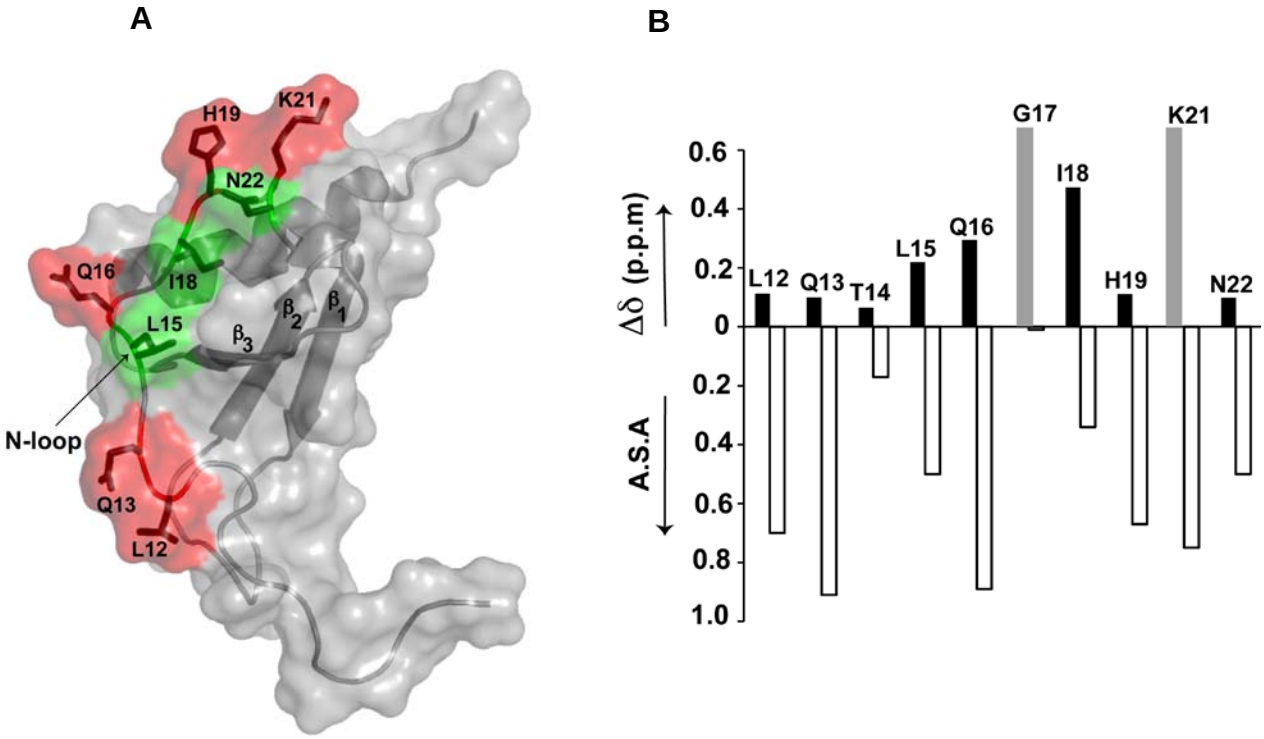

Figure 3.11 Role of the N-loop residues in the MGSA monomer. A molecular plot of a single subunit of MGSA (PDB ID: 1MGS (18)) showing the N-loop residues involved in CXCR2 N-domain binding **(panel A)**. Solvent exposed residues Leu12, Gln13, Gln16, His19 and Lys21 are highlighted in red, and partially buried residues Leu15, Ile18 and Asn22 are highlighted in green. A plot comparing the chemical shift change (top y-axis) and the side chain ASA (bottom y-axis) show that they are not necessarily correlated **(panel B)**. Chemical shift changes of Gly17 and Lys21 are not available due to line broadening and are represented by a grey bar. The grey bar is shown at the same height as that of Ile18, which shows the maximum chemical shift change.

Role of the Third β-strand residues: The third β-strand residues that show significant perturbations are Arg48, Lys49, Ala50, Leu52, and Asn53, whereas Cys51 shows minimal perturbation **(Figure 3.10)**. Among these residues, only Arg48, and Lys49 are solvent exposed (ASA ~0.7), while the others are largely buried and involved in packing interactions against the N-loop residues. For instance, Ala50 is packed against Leu15, Leu52 is packed against Ile18, and Asn53 is packed against Thr14, and so binding induced structural changes from the N-loop can be propagated to these residues (**Figure 3.11**).

Previous studies have shown that mutating Lys49 to Ala results in reduced receptor binding and function, whereas mutating Arg48 to Ala results in minimal loss of receptor binding and function (79). Since the CXCR2 N-domain has several Asp/Glu residues, it was concluded that Lys49 might be part of the CXCR2 binding site (7). In the case of Arg48, perturbation could be due to indirect interactions and/or that it plays only a minor role in direct receptor binding.

Role of the C-terminal helix residues: We observe significant perturbations for only two C-terminal helical residues, Ile62 and Ile63 **(Figure 3.10)**. Ile62 is packed against Gly17, and Ile63 is packed against Val40, and so the perturbations of these residues must be due to indirect coupled interactions **(Figure 3.12)**.

Role of the N-terminal residues: Binding induced perturbations are evident in the N-terminal residues, Glu6, Leu7, and Arg8 **(Figure 3.10)**. These residues are involved in site-II binding. The observation that site-I binding of MGSA results in perturbations in the N-terminus suggests that binding induced indirect coupled interactions are propagated to site-II. These structural changes could orient the 'ELR' residues for optimal interaction at site-II mediating coupling between the two sites.

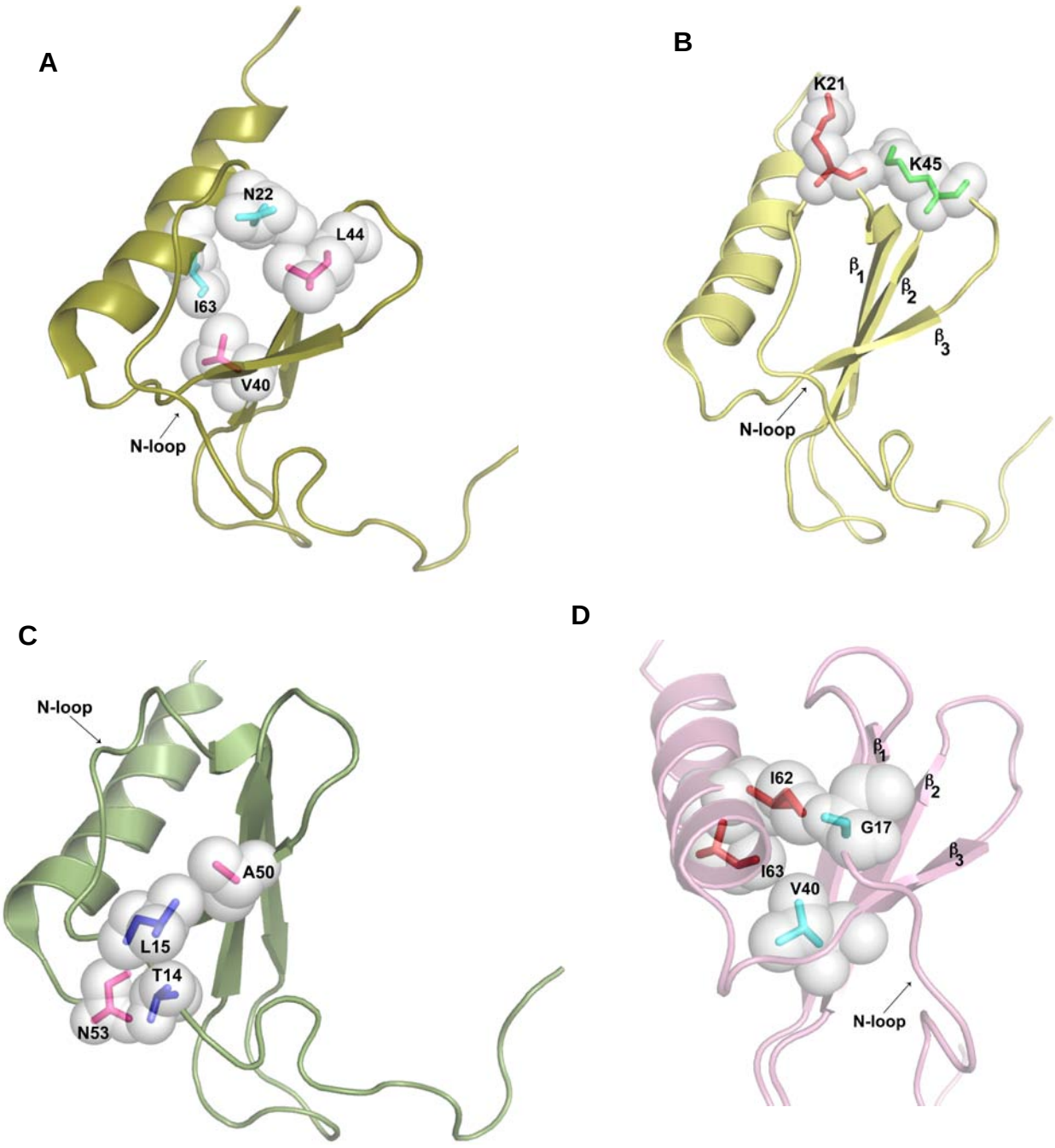

Figure 3.12 CXCR2 N-domain binding induced indirect coupled interactions in the MGSA monomer. Molecular plots of a single subunit of MGSA showing packing interactions in the second β-strand, 40s turn, third β-strand and the C-terminal helix **(Panels A-D)**. The spheres are shown to highlight the packing interactions.

CXCR2 site-I binding affinities of IL-8 and MGSA

On the basis of structure-function data of IL-8 and MGSA, the current proposed model for the two-site interaction for a ligand-receptor pair takes into account that binding interactions are not simply additive, but coupled (13, 91). According to this model, the binding affinity is described by the following equation:

$$\Delta G_{binding} = \Delta G_{site\text{-}I} + \Delta G_{site\text{-}II} + \Delta G_{coupling} \qquad (3.1)$$

where, $\Delta G_{binding}$ is the free energy associated with the overall receptor interaction, $\Delta G_{site\text{-}I}$ and $\Delta G_{site\text{-}II}$ are the free energy changes required for site-I and site-II interactions, and $\Delta G_{coupling}$ is the coupling free energy change between the two sites. $\Delta G_{coupling}$ could be positive or negative; in the former situation, the binding at site-I increases the free energy required for binding at site-II, and in the latter case, the binding at site-I decreases the free energy required for binding at site-II. To calculate $\Delta G_{coupling}$, it is essential to measure the free energy changes of the individual interactions in the context of the intact receptor. Elimination of site-I for measuring $\Delta G_{site\text{-}II}$ is not possible because site-I interaction involves multiple N-loop residues. Deleting the 'ELR' residues does not result in a binding affinity that is measurable, and N-terminal 'ELR' mutants bind with low affinity (18, 56, 68, 79). In principle, site-II interaction should be measured using a peptide containing the 'ELR' residues, but such studies could not detect any binding suggesting that the interaction is weak and should be ~100 μM or lower (65). Therefore measuring either $\Delta G_{site\text{-}I}$ or $\Delta G_{site\text{-}II}$ is not straightforward. At this time, it is not known whether there are any differences in the site-II binding affinities of the IL-8 and MGSA 'ELR' residues. However, since these residues are conserved, it can be assumed that $\Delta G_{site\text{-}II}$ is similar. I have now measured $\Delta G_{site\text{-}I}$ by studying the interaction of IL-8 and MGSA monomers and dimers to the isolated CXCR2 N-domain. $\Delta G_{binding}$ is known from previous studies, and assuming that $\Delta G_{site\text{-}II}$ is similar for the binding of both ligands, we have calculated $\Delta G_{coupling}$ using eq 3.1.

CXCR2 N-domain binding affinities of the IL-8 monomer and dimer

CXCR2 N-domain binding affinities of the IL-8 monomer and dimer are similar, and so $\Delta G_{site\text{-}I}$ is similar **(Table 3.1) (Figure 3.13, panel A)**. However, intact receptor binding affinities are lower for the IL-8 dimer compared to the monomer (41, 45). Therefore, similar $\Delta G_{site\text{-}I}$values do not explain why the IL-8 monomer binds with higher affinity. The calculated $\Delta G_{coupling}$ for different site-II binding affinities show that the coupling is positive if site-II binding affinity ($K_{d\ site\text{-}II}$) is 100 μM or lower. Negative coupling can occur if $K_{d\ site\text{-}II}$ is between 0.1 to 1 μM. Since $K_{d,\ site\text{-}II}$ should be 100 μM or lower, the coupling is most likely positive for the binding of the IL-8 monomer and the dimer, and the $\Delta G_{coupling}$ is always higher for the monomer compared to the dimer.

CXCR2 N-domain binding affinities of the IL-8 monomer and MGSA monomer

IL-8 and MGSA monomers bind with similar nM affinities to the intact CXCR2 receptor (41, 76). However, the MGSA monomer binds the CXCR2 N-domain with ~6 fold higher affinity than the IL-8 monomer **(Figure 3.13, panel B)**. For similar $\Delta G_{site\text{-}II}$ values, $\Delta G_{coupling}$ is higher for the IL-8 monomer compared to the MGSA monomer **(Table 3.2)**. Though the CXCR2 binding affinities of IL-8 and MGSA monomers are similar, differences in the coupling free energies are observed. Similar to what is observed for the IL-8 monomer, the calculated $\Delta G_{coupling}$ values for MGSA monomer also indicate that negative coupling can occur if $K_{d\ site\text{-}II}$ is 1 μM or higher, whereas positive coupling occurs if $K_{d\ site\text{-}II}$ is 100 μM or lower. At this time, it is not clear how the differences in coupling free energies are related to the receptor activity of the IL-8 and MGSA monomer.

CXCR2 N-domain binding affinities of the MGSA dimer and MGSA monomer

CXCR2 N-domain binding studies with the MGSA dimer showed that the trapped MGSA dimer binds with ~5 fold lower affinity than the MGSA monomer **(Figure 3.13)**. MGSA dimer is observed to bind the intact CXCR2 receptor with ~5 fold lower affinity compared to the MGSA monomer and WT indicating that the differences in the binding affinity is essenitally due to the differences in site-I binding

affinity. Therefore, the coupling is essentially the same for both the MGSA monomer and dimer for CXCR2 binding interactions.

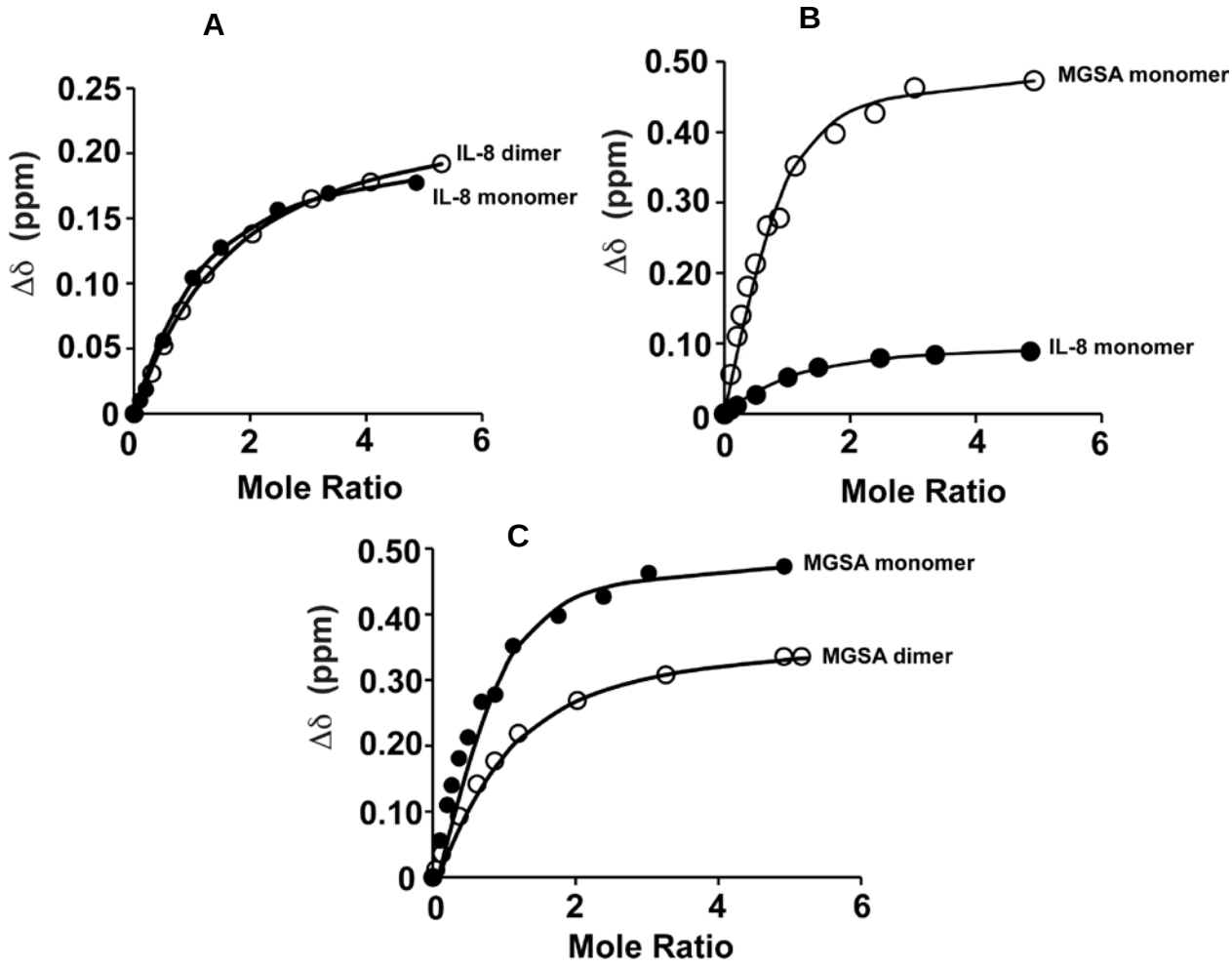

Figure 3.13 CXCR2 N-domain binding affinities of IL-8 and MGSA. Comparison of the CXCR2 N-domain binding profiles of IL-8 monomer and dimer **(panel A)** and the IL-8 monomer and MGSA monomer **(panel B)**, and the MGSA monomer and MGSA dimer **(panel C)** are shown. The binding profiles represent residues, Ser44 **(panel A)**, Phe17 for the IL-8 monomer, and Ile18 for the MGSA monomer and dimer **(panels B and C)**. The binding affinities of the IL-8 monomer, the IL-8 dimer, MGSA monomer and MGSA dimer obtained from fitting the chemical shift changes are 133 ± 14 μM, 187 ± 50 μM, 21± 3 μM and 86 ± 18 μM respectively.

Table 3.1 Calculation of $\Delta G_{coupling}$ for CXCR2 binding of IL-8 monomer and dimer.

Variant	$K_{d\ site-I}$ (μM)	ΔG_{site-I} (kcal mol^{-1})	$K_{d\ site-II}$ (μM)	$\Delta G_{site-II}$ (kcal mol^{-1})	$K_{d\ binding}$ (nM)	$\Delta G_{binding}$ (kcal mol^{-1})	$\Delta G_{coupling}$ (kcal mol^{-1})
IL-8 $_{Monomer}$	133	-5.4	0.1	-9.7	0.5	-12.9	2.2
	133	-5.4	1	-8.3	0.5	-12.9	0.8
	133	-5.4	10	-6.9	0.5	-12.9	-0.6
	133	-5.4	100	-5.5	0.5	-12.9	-2.0
	133	-5.4	1000	-4.2	0.5	-12.9	-3.3
IL-8 $_{Dimer}$	187	-5.2	0.1	-9.7	9	-11.2	3.7
	187	-5.2	1	-8.3	9	-11.2	2.3
	187	-5.2	10	-6.9	9	-11.2	0.9
	187	-5.2	100	-5.5	9	-11.2	-0.5
	187	-5.2	1000	-4.2	9	-11.2	-1.8

Table 3.2 Calculation of $\Delta G_{coupling}$ for CXCR2 binding of IL-8 monomer and MGSA monomer.

Variant	$K_{d\ site-I}$ (μM)	ΔG_{site-I} (kcal mol^{-1})	$K_{d\ site-II}$ (μM)	ΔG_{site-I} (kcal mol^{-1})	$K_{d\ binding}$ (nM)	$\Delta G_{binding}$ (kcal mol^{-1})	$\Delta G_{coupling}$ (kcal mol^{-1})
IL-8 $_{Monomer}$	133	-5.4	0.1	-9.7	0.5	-12.9	2.2
	133	-5.4	1	-8.3	0.5	-12.9	0.8
	133	-5.4	10	-6.9	0.5	-12.9	-0.6
	133	-5.4	100	-5.5	0.5	-12.9	-2.0
	133	-5.4	1000	-4.2	0.5	-12.9	-3.3
MGSA $_{Monomer}$	21	-6.5	0.1	-9.7	0.5	-12.9	3.3
	21	-6.5	1	-8.3	0.5	-12.9	1.9
	21	-6.5	10	-6.9	0.5	-12.9	0.5
	21	-6.5	100	-5.5	0.5	-12.9	-0.9
	21	-6.5	1000	-4.2	0.5	-12.9	-2.2

Table 3.3 Calculation of $\Delta G_{coupling}$ for CXCR2 binding of MGSA monomer and MGSA dimer.

Variant	$K_{d\ site\text{-}I}$ (μM)	$\Delta G_{site\text{-}I}$ (kcal mol^{-1})	$K_{d\ site\text{-}II}$ (μM)	$\Delta G_{site\text{-}II}$ (kcal mol^{-1})	$K_{d\ binding}$ (nM)	$\Delta G_{binding}$ (kcal mol^{-1})	$\Delta G_{coupling}$ (kcal mol^{-1})
MGSA $_{Monomer}$	21	-6.5	0.1	-9.7	0.5	-12.9	3.3
	21	-6.5	1	-8.3	0.5	-12.9	1.9
	21	-6.5	10	-6.9	0.5	-12.9	0.5
	21	-6.5	100	-5.5	0.5	-12.9	-0.9
	21	-6.5	1000	-4.2	0.5	-12.9	-2.2
MGSA $_{dimer}$	100	-5.5	0.1	-9.7	2.4	-11.9	3.3
	100	-5.5	1	-8.3	2.4	-11.9	1.9
	100	-5.5	10	-6.9	2.4	-11.9	0.5
	100	-5.5	100	-5.5	2.4	-11.9	-0.9
	100	-5.5	1000	-4.2	2.4	-11.9	-2.2

CONCLUSIONS

Ligand binding affinity is the first step for the regulation of receptor function, but affinity is also closely linked to selectivity. It is now well established that the two-site interaction of chemokines is important for modulating binding affinity and selectivity of chemokine receptors. However, it does not provide a comprehensive description of how ligand binding at site-I modulates overall receptor binding affinity. To our knowledge, this is the first study using the isolated CXCR2 N-domain for gaining insights into how site-I binding influences overall CXCR2 affinity. The differences in the CXCR2 N-domain affinities of the designed IL-8 and MGSA monomers and trapped IL-8 and MGSA dimers indicate that site-I interaction plays differential roles. I propose that site-I interaction plays an important role in imparting binding affinity, however the differential coupling between site-I and site-II determines overall CXCR2 binding affinity. Future structural studies of IL-8 and MGSA complexed with the CXCR2 N-domain should provide further insights into how the individual receptor N-domain residues mediate ligand binding affinity and selectivity.

CHAPTER IV

NOVEL COUPLED INTERACTIONS MEDIATE IL-8-RECEPTOR BINDING: A CRITICAL ROLE FOR A SOLVENT EXPOSED HYDROPHOBE

INTRODUCTION

Interleukin-8 (IL-8), one of the best-studied members of the chemokine subfamily, exerts its function by binding and activating receptors that belong to the G-protein coupled receptor (GPCR) class. Sequence and structure analysis reveal that the N-loop contains a highly conserved solvent exposed hydrophobe, which is unusual as large non-polar residues are usually buried and involved in packing interactions. Furthermore, this residue is adjacent to the CXC/CC motif and the cysteines in this motif form disulfide bridges that tether the N-loop and the N-terminus regions involved in receptor binding to the protein core. This residue corresponds to Ile10 in IL-8, and most likely plays a key role in receptor binding and function by interacting directly with the receptor N-domain (site-I).

Mutagenesis studies have shown that compared to WT[1] IL-8, I10A mutant binds with ~30 fold lower affinity to neutrophil receptors, and is ~20 fold less active in elastase and calcium release assays (66, 49). These data indicate that binding affinity and functional activity which could be separable functions, are nevertheless correlated and that Ile10 is important for high affinity agonist binding and function (87). Consistent with previous receptor binding studies, we also observed that I10A*[1] binds the intact CXCR1 receptor with ~24 fold reduced affinity compared to WT*[1]. So in this study, Ile10 was conservatively mutated to Ala, and the effect of the mutation on receptor binding of IL-8 at site-I was studied.

[1]WT denotes IL-8 (1-72); WT* and I10A* denote 1-66 versions of the protein. The (1-66) deletion IL-8 mutant binds and has the same activity as the WT IL-8.

Interestingly, I10A* mutant binds the CXCR1 receptor N-domain essentially with the same affinity as WT*, and NMR data show that Ala10 is conformationally flexible in the free form and becomes more structured in the bound form. These are quite unexpected results as one would have expected the reduced binding of I10A to the intact receptor is due to reduced binding to the receptor N-domain. These results indicate a novel paradigm by which a solvent exposed hydrophobe plays a key role not as much as participating in direct binding interactions, but indirectly by influencing binding at a remote site via coupling interactions for optimal binding affinity and function.

EXPERIMENTAL PROCEDURES

Cloning, expression and purification of ^{15}N-labeled IL-8(1-66) I10A mutant

The I10A mutant was generated by mutating Ile10 to Ala on the WT* plasmid that was cloned in the pet32Xa vector at the LIC site. PCR amplification was carried out using the upstream primer and the downstream primers as follows respectively.

5'-GAACTTAGATGTCAGTGCGCAAAGACATACTCCAAACCTTTC-3'

5'-GAAAGGTTTGGAGTATGTCTTTGCGCACTGACATCTAAGTTC-3'

Mutagenesis was performed using QuickChange Site-Directed Mutagenesis kit (Stratagene Inc., La Jolla, CA, USA). Protein expression and purification of recombinant ^{15}N-labeled I10A was carried out as described for WT* in chapter 2. Purity and molecular weight of I10A* was confirmed using analytical HPLC and MALDI MS. The CXCR1 N-domain (24-mer) was synthesized using solid phase peptide synthesis and is the same as that used for the titration experiments described in Chapter 2.

NMR spectroscopy

Titration of unlabeled CXCR1 N-domain 24-mer into ^{15}N-labeled I10A* was carried out similar to that of WT* as described in Chapter 2. The titration was carried

out until essentially no further changes in chemical shifts were observed. The final peptide to protein mole ratio for the I10A mutant was 4.2. Two-dimensional ^{1}H-^{15}N HSQC spectra were acquired with 2048 complex points for direct ^{1}H and 128 complex points for indirect ^{15}N dimension. All spectra were recorded using Varian INOVA 800-MHz spectrometers equipped with field gradient accessories. The spectra were processed using NMRPipe (99) and analyzed using NMRView (100). Binding constants (K_d) were calculated as described in Chapter 2.

NMR line shape analysis

To determine the kinetics of binding of I10A* and the WT* to CXCR1 N-domain, line shapes of the backbone amide resonances that were well resolved in the ^{1}H-^{15}N HSQC titration spectra were analyzed. Residues that showed significant chemical shift differences between the free and the bound forms were selected and the line widths (LW) were calculated from Lorentzian line shape fitting of the cross peaks in the ^{1}H acquisition dimension of the ^{1}H-^{15}N HSQC titration spectra. The line shape fitting was performed using an in house fitting program, giving the apparent transverse relaxation rates, R_{2app}, which is related to the LW in *Hz* by the equation,

$$LW = \frac{R_{2app}}{\prod} \tag{4.1}$$

The two-state exchange process can be described by the McConnell equations, giving R_{ex} (105, 122). Therefore, R_{2app} for a two state chemical exchange process occurring in the moderately fast time scales is described by the following equation,

$$R_{2app} = p_f \times R_{2f} + p_b \times R_{2b} + R_{ex} \tag{4.2}$$

where, R_{ex} is given by the following equation,

$$R_{ex} = \frac{4 \times \prod^2 \times {p_f}^2 \times p_b \times \Delta\omega^2}{k_{off}} \tag{4.3}$$

where, p_f and p_b are the populations of the free and the bound forms, respectively. Since the binding constant is known, p_f and p_b are determined from the concentrations of the bound protein for each titration point. R_{2f} and R_{2b} are the relaxation rates in the

free and the bound forms in s^{-1}, Δw is the chemical shift difference between the free and bound forms in *Hz*, and k_{off} is the off constant in s^{-1}. k_{off} was determined from eq. 4.2 by nonlinear least square fitting of the R_{2app} values with the fitted parameters being, k_{off}, R_{2f} and R_{2b}.

Surface Plasmon Resonance studies

Binding studies of WT* and I10A* were carried out at the Center for Biomolecular Interaction Analysis core facility at University of Utah. A CXCR1 N-domain (25-mer) peptide with a free cysteine at the C-terminus was first synthesized using solid phase peptide synthesis. The 25-mer was coupled at a density of 2000 RU to a CM5 Biacore sensor chip using standard sulfo-maleimidobenzoyl-N-hydroxysulfosuccinimide ester (sulfo-MBS) thiol coupling. The proteins were dissolved at 1mg/ml concentration in phosphate buffer saline (PBS) pH 8, and binding studies were carried out at starting protein concentrations of 8 and 11 μM, respectively in a two-fold dilution series at 25°C. The response (RU) was measured as a function of time (s) at 9 concentrations, and the experiments were performed in triplicates. The data were fitted to a 1:1 interaction model to determine the binding constant (K_d), off rate constant (k_{off}) and on rate constant (k_{on}).

Isothermal Calorimetry studies

ITC experiments were performed using a Microcal VP-ITC system at 25°C as described previously (123). The proteins and the CXCR1 N-domain 24-mer peptide were extensively dialyzed against 50 mM HEPES, 50 mM NaCl, pH 8, centrifuged, filtered and degassed. Protein concentrations were measured using amino acid analysis and ranged from 0.1 to 0.85 mM for WT*, and 0.006 to 0.07 mM for the CXCR1 N-domain 24-mer. Protein and peptide concentrations for the binding I10A* were 0.13 and 0.006 mM respectively. The 1.42 ml sample cell and the syringe were first washed with soap solution, rinsed with water and then with the dialysis buffer. The CXCR1 N-domain 24-mer and the ligand were loaded into the sample cell and the syringe, respectively. For WT*, a total of 35 injections were performed with the first five injections being 3 μl each and the remaining 25 injections being 9 μl each with 6 min equilibration time between injections. For I10A*, a total of 32 injections

were performed with the first three injections being 1 μl and the remaining 29 injections being 6 μl each with 6 min equilibration time between injections. The data were fitted to a single-site model using nonlinear least square fitting in Microcal Origin for ITC version 5.0 by varying the stoichiometry (n), association constant (K_a), and the binding enthalpy (ΔH).

RESULTS AND DISCUSSION

Studies described in Chapter 2 showed that the binding of WT* to CXCR1 N-domain induces significant chemical shift perturbation and line broadening of N-loop residues, Ile10, Lys15 and Lys20. These residues are solvent exposed, non-sequential and span the entire N-loop, and therefore proposed to play a critical role in the initial docking of the ligand to the N-domain **(Figure 4.1)**. In this study, the role of the steric bulk of Ile10 was studied by mutating it to Ala.

Effect of the Ile10 to Ala mutation on the secondary and tertiary structure

Differences in backbone chemical shift amide protons can serve as sensitive probes to monitor structural and dynamic changes in proteins (124-127). Amide proton shift differences between WT* and I10A* were similar except for residues at and around the site of substitution **(Figure 4.2)**. The largest amide protein shift difference of ~0.2 ppm is observed for Ala10. If the random coil shift differences between Ile and Ala are taken into consideration, then the difference for the Ile to Ala decreases from 0.2 ppm to 0.05 ppm. This difference is small and can be directly attributed to the substitution. These results are also consistent with the results from previous NMR studies of the I10A mutant designed on the WT IL-8 template, which showed that the Ile→Ala substitution does not perturb the overall tertiary structure (128).

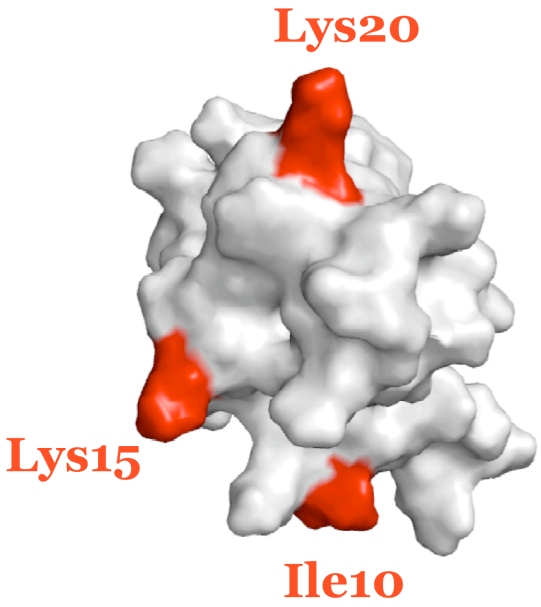

Figure 4.1 Ile10 is the only solvent exposed hydrophobe in the N-loop. A molecular plot of IL-8 highlighting the solvent exposed N-loop residues, Ile10, Lys15 and Lys20 (shown in red). The plot was rendered using the program PyMOL (96).

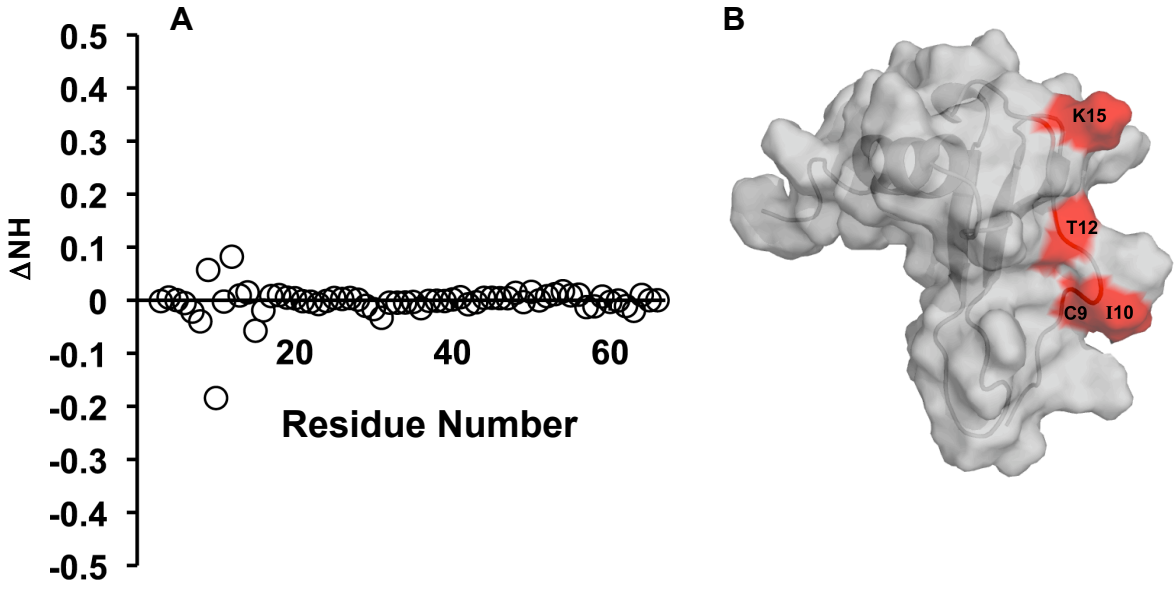

Figure 4.2. Mutation of Ile10 to Ala does not perturb the structure. **Panel A.** A plot showing the differences in backbone amide shifts (○) between WT* and I10A*. **Panel B.** A molecular plot of the IL-8 monomer highlighting residues showing the largest backbone amide shift differences, Δδ >0.05 ppm (shown in red).

*Binding induced total chemical shift changes of I10A**

CXCR1 N-domain binding to the WT* and I10A* induces very large chemical shift changes **(Figures 4.3 and 4.4)**. Magnitude of the changes were similar between WT* and I10A* except for Ile10, which showed higher chemical shift perturbation in WT* compared to I10A* **(Figure 4.4)**. These data together indicate that both I10A* and WT* bind in a similar fashion, and involve the same set of residues for CXCR1 N-domain binding.

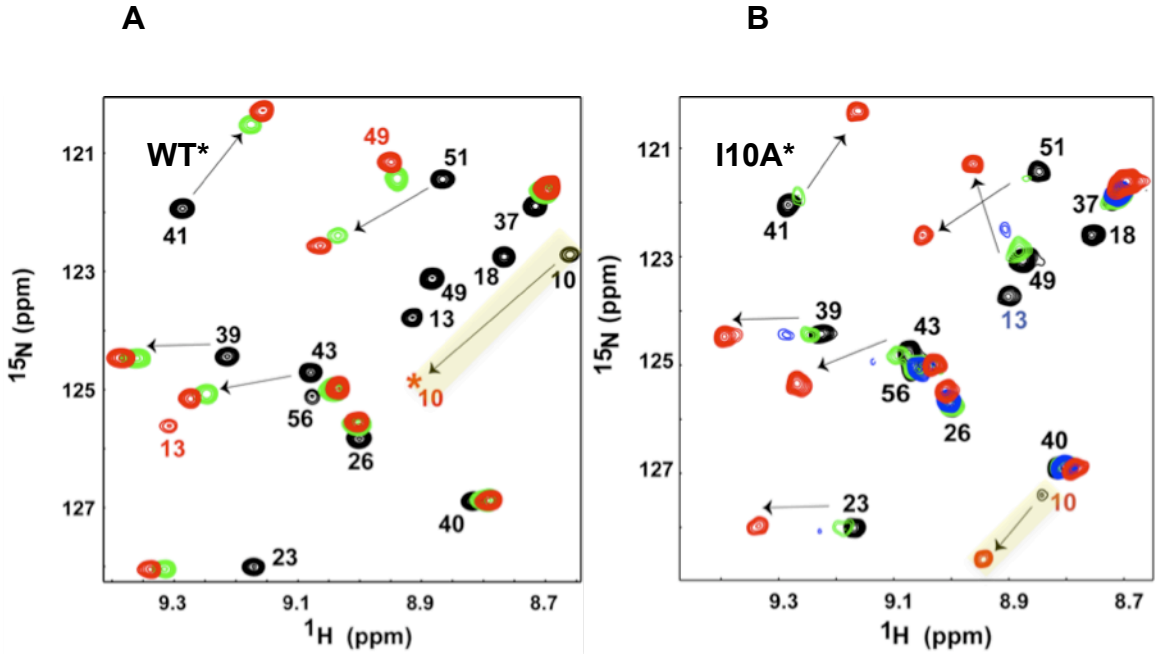

Figure 4.3 CXCR1 N-domain binding induced chemical shift changes in WT* and I10A*. Sections of ^{1}H-^{15}N HSQC titration spectra showing the chemical shift perturbations in WT* **(panel A)** and I10A* **(panel B)**. Arrows indicate the direction of peak movement and for residues, Ile10, Tyr13 and Leu49 showing large chemical shift changes in the WT*, the final bound peaks are labeled in red. Chemical shift changes of Ile10/Ala10 are highlighted in yellow. Peak position for Ile10 in the bound form of WT* is not detected at the contour level shown and therefore is denoted by a red asterisk. Tyr13 in I10A* is labeled in blue due to peak disappearance during titration. Peaks are color coded for peptide:protein mole ratios of 0 (black), 1.2 (green) and 3.4 (red) in the WT* spectra and 0 (black), 0.1 (green), 0.3 (blue) and 4.2 (red) in the I10A* spectra, respectively.

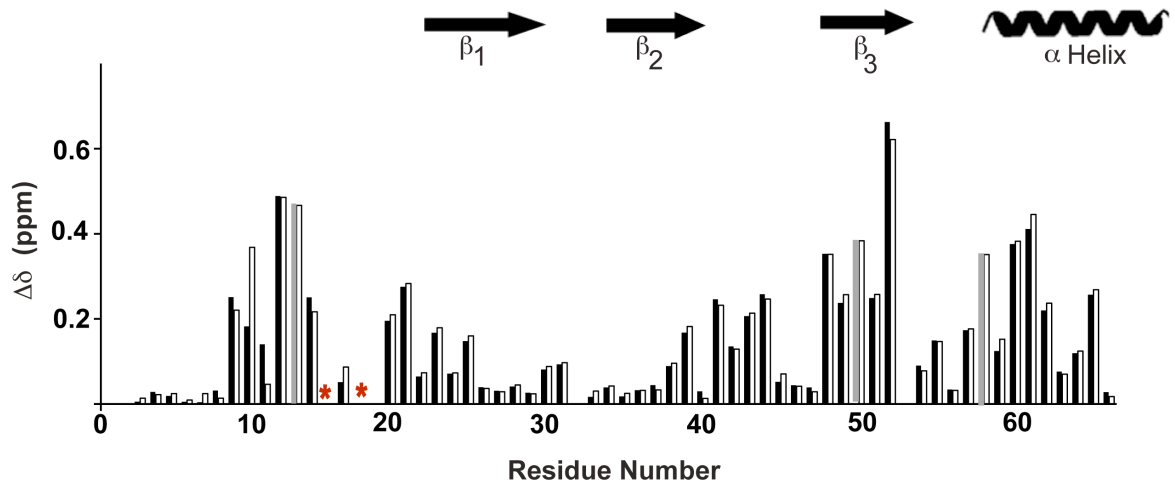

Figure 4.4 CXCR1 N-domain binding induced chemical shift changes between I10A* and WT*. A histogram showing the total chemical shift changes as a function of residue number for I10A* (black bars) and WT* (open white bars). Lys15 and His18 disappears completely during titration in both WT* and I10A* and are denoted by red asterisks. Perturbations for Tyr13, Cys50 and Val58 could not be detected in I10A* due to line broadening during titration, and so are represented by grey bars which are shown at the same height as the perturbation observed for the corresponding residues in WT*.

Binding affinity of I10A to CXCR1 N-domain*

Calculation of binding constants from binding-induced chemical shift changes indicate that I10A binds the CXCR1 N-domain with ~2 fold higher affinity compared to WT* **(Figure 4.5)**. However, NMR cannot reliably calculate K_ds in this range, and so any perceived differences have to be interpreted with caution. ITC experiments showed that I10A* binds with slightly higher affinity (< 2 fold) **(Figure 4.7, Table 4.2),** and SPR studies show I10A* binds with slightly lower affinity (< 2 fold) than the WT* **(Figure 4.6, Table 4.1)**.

A summary of the binding constants from different experimental techniques shows differences in the absolute values of the binding constants **(Table 4.3)**. Based on these observations, considering the intrinsic differences among different

techniques, we conservatively conclude that I10A* binds essentially with the same affinity as WT*. Therefore, the 20-40 fold difference in its binding affinity to the intact receptor cannot be explained on the basis of the differences in binding to the N-domain alone. These results are quite remarkable as one would have expected mutating an N-loop residue would result in reduced binding affinity to site-I. For both proteins, binding affinities for site-II should be the same, and so the differences in the binding affinities to the intact receptor implies that the binding of Ile10 is positively coupled to site-II for receptor binding and function.

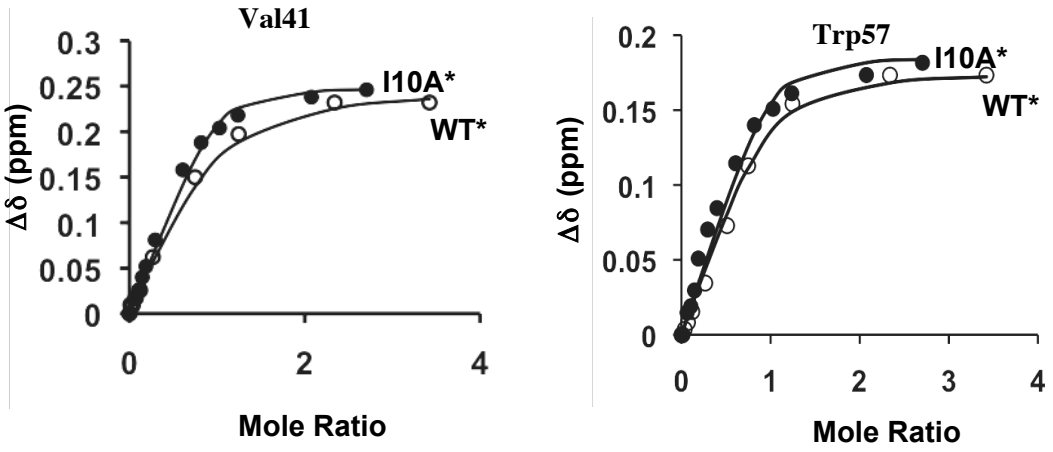

Figure 4.5. Binding affinities of WT* and I10A* to CXCR1 N-domain determined by NMR. Binding induced chemical shift changes (Δδ, ppm) as a function of mole ratio are shown for Val41 and Trp57 in WT* (○) and I10A* (●).

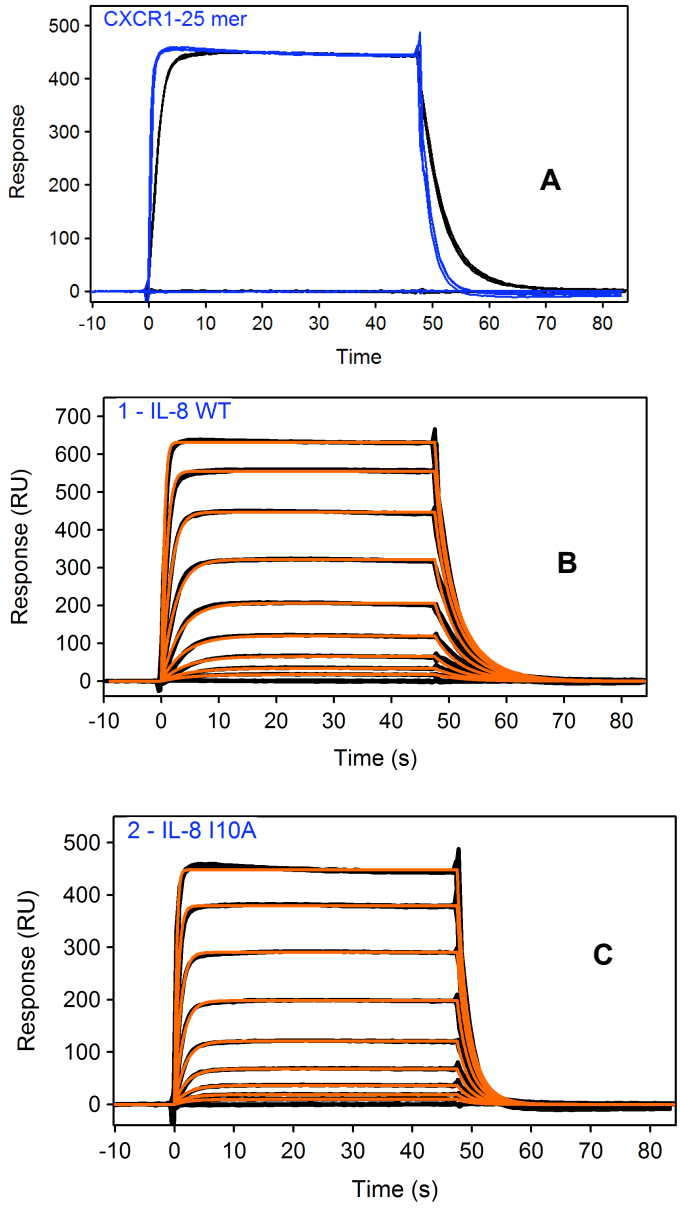

Figure 4.6 Determination of CXCR1 N-domain binding affinities of WT* and I10A* by SPR. Panel A shows the response data (RU) at a single concentration as a function of time for the binding of WT* (black line) and I10A* (blue line). **Panels B and C** show the response data at 9 different concentrations as a function of time (s) for WT* and I10A* respectively. The data collected in triplicates highly overlap indicating the reproducibility of the experiments.

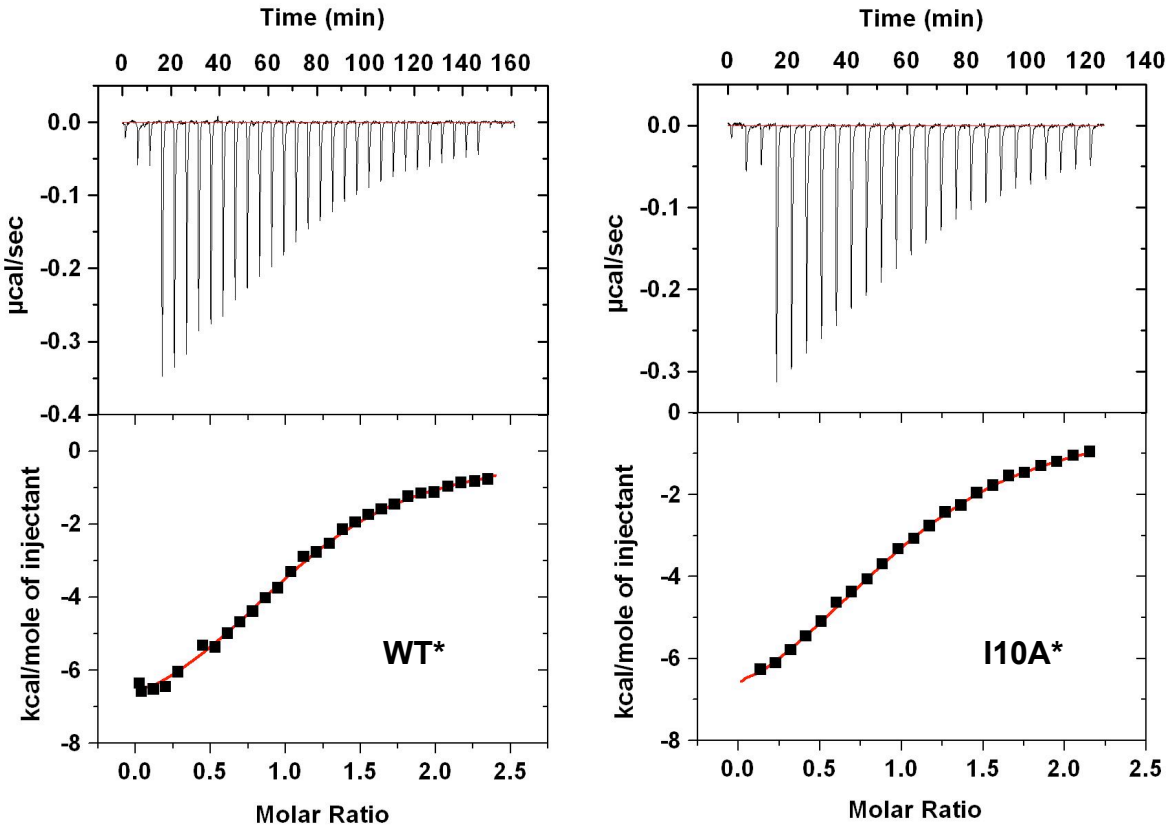

Figure 4.7 ITC binding studies of WT* and I10A* to CXCR1 N-domain. Representative ITC profiles for the binding of WT* and I10A* at 25°C are shown. The upper panels represent the ITC thermograms, and the lower panels represent the fitted binding isotherms.

Table 4.1 SPR binding results for CXCR1 N-domain binding of WT* and I10A*.

IL-8 variant	$k_{on} \times 10^5$ ($mol^{-1}s^{-1}$)	k_{off} (s^{-1})	K_d (μM)
WT*	3.7 ± 0.1	0.5 ± 0.1	1.4 ± 0.1
I10A*	3.3 ± 0.1	0.8 ± 0.1	2.4 ± 0.1

Table 4.2 ITC results for CXCR1 N-domain binding of WT* and I10A*.

IL-8 variant	n	K_d (μM)	ΔG (kcal mol^{-1})	ΔH (kcal mol^{-1})	TΔS (kcal mol^{-1})
WT*	1.2	3.5 ± 0.2	-7.4 ± 0.1	-10.3 ± 0.1	-2.9 ± 0.1
	1.1	4.6 ± 0.2	-7.2 ± 0.1	-8.3 ± 0.1	-1.1 ± 0.1
	1.1	1.5 ± 0.2	-7.9 ± 0.1	-8.1 ± 0.3	-0.2± 0.1
	1.0	1.9± 0.2	-7.8 ± 0.1	-9.4 ± 0.5	-1.6 ± 0.1
I10A*	1.0	2.4 ± 0.2	-7.7± 0.1	-8.9 ± 0.4	-1.2 ± 0.1
	1.0	2.1 ± 0.1	-7.7± 0.1	-8.8 ± 0.4	-1.0 ± 0.1

Table 4.3 Summary of the binding affinities of I10A* and WT* to CXCR1 N-domain.

IL-8 variant	Binding constants, K_d (μM)		
	NMR	SPR	ITC
WT*	9.5 ± 2	1.4 ± 0.1	2.8 ± 1.4
I10A*	3.1 ± 1	2.4 ± 0.1	2.3 ± 0.5

*Binding-induced line broadening in I10A**

The exchange regimes for the binding of WT* and I10A* to CXCR1 N-domain is moderately fast on NMR times scales **(Figure 4.3)**. Studies described in Chapter 2 showed that binding induced line broadening changes can serve as probes to monitor structural/dynamic changes. Therefore, the line broadening changes in the WT* and I10A* were compared by monitoring relative intensity changes of the peaks as a function of mole ratio as defined by the following equation:

$$\text{Relative Intensity} = \text{Intensity}_{\text{bound}}/\text{Intensity}_{\text{unbound}} \qquad (4.4)$$

Steeper line broadening profiles were observed for some residues in I10A* compared to WT* suggesting that the off rate constant (k_{off}) for the binding is lower for I10A* **(Figure 4.8)**. In particular, the largest relative intensity change was observed for Ala10 compared to other residues such Lys20 and Leu51 in the mutant suggesting that Ala10 becomes more structured in the mutant compared to WT*. Future experiments on the dynamics in the free and the bound form should provide a more conclusive picture on the binding induced dynamic changes in WT* and I10A*.

*Kinetic basis of interaction of WT*and I10A* with CXCR1 N-domain*

Dissociation constants (K_d) provide information on the relative affinities of CXCR1 N-domain interaction of WT* and I10A*, whereas kinetic constants (k_{on} and k_{off}) provide information on the association and dissociation kinetics. The dissociation constant is defined as by the following equation:

$$K_d = k_{off}/ k_{on} \qquad (4.5)$$

For most ligand-receptor interactions, k_{on} is diffusion limited, and is ~10^6-10^8 $M^{-1}s^{-1}$ (129). NMR is very powerful for obtaining both microscopic K_d and k_{off} values for the binding of the individual residues. The microscopic k_{off} values can be obtained from NMR line shape analysis when the exchange regimes are moderately fast on NMR time scales (103). From eq 4.2, it is evident that exchange line broadening due to chemical shift differences between the free and the bound form, $\Delta\omega$ and also k_{off} can affect the transverse relaxation rate, R_{2app}.

For ligand binding in the moderately fast time scale, increased line broadening is due to increase in R_{2app} values. At the same p_b values, the extent of line broadening was higher in I10A* implying k_{off} must be lower for I10A* compared to the WT*. The k_{off} values obtained from the line shape analysis of the individual residues in WT* is ~1000 to 2000 s^{-1} **(Figure 4.9).** Therefore, for the binding of WT*, the calculated k_{on} is 10^8 $M^{-1}s^{-1}$ as the K_d and k_{off} are 10 μM and 1000 s^{-1}. As shown from our NMR studies, I10A* binds with K_d ~3 μM, then the calculated k_{off} is ~300 s^{-1} if k_{on} is unaltered (~10^8 $M^{-1}s^{-1}$). For a k_{off} of ~300 s^{-1}, binding induced line broadening should be higher than what is observed (**Figure 4.10**). k_{off} values determined from line width measurements at each titration point for three residues indicate that they are similar for I10A* and WT* within experimental error (k_{off} ~1000 s^{-1}) suggesting that the differences in the binding affinities between WT* and I10A* is most likely due to differences in k_{on} (**Figures 4.9 and 4.10**). Due to poor s/n ratio, k_{off} values for most residues in I10A* could not be determined in a reliable manner. On the other hand, we cannot rule out the possibility that the K_d of WT* is not 3 fold, but 2 fold lower than I10A*, and that both k_{on} and k_{off} are essentially the same between the two variants. If different, it is difficult to quantitate it due to the small differences in the binding between the two variants.

A comparison of the absolute k_{off} values obtained from NMR studies and SPR studies shows that the dissociation rates from NMR studies are ~1000-2000 fold faster than that obtained from SPR studies (**Table 4.1 and Figure 4.9**). SPR studies showed that the I10A* mutant dissociates from the complex 2 fold faster than the WT* (**Table 4.1**). Also the SPR studies were performed with the CXCR1 N-domain peptide immobilized on a chip, and this could impose a constraint on the flexibility of the N-domain peptide, which could reflect on the k_{off} values, whereas NMR studies are performed in solution. Moreover, the buffer conditions used for SPR studies were different from those used for NMR studies, which could show differences in the k_{off}.

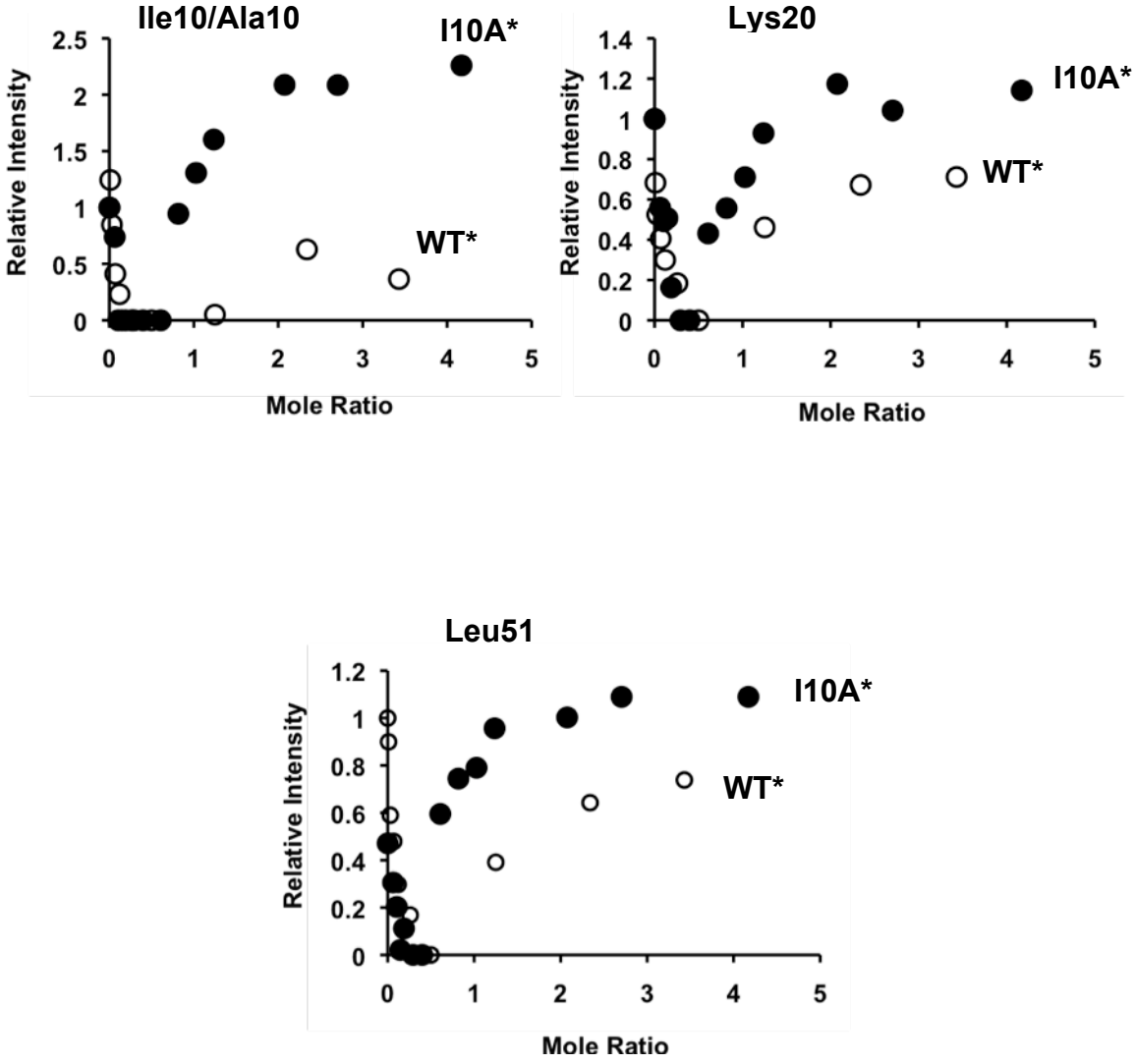

Figure 4.8 CXCR1 N-domain binding induced line broadening analysis in WT* and I10A*. Relative intensity changes as function of peptide to protein mole ratio are shown for residues Ile10/Ala10, Lys20 and Leu51 in the WT* (○) and I10A* (●).

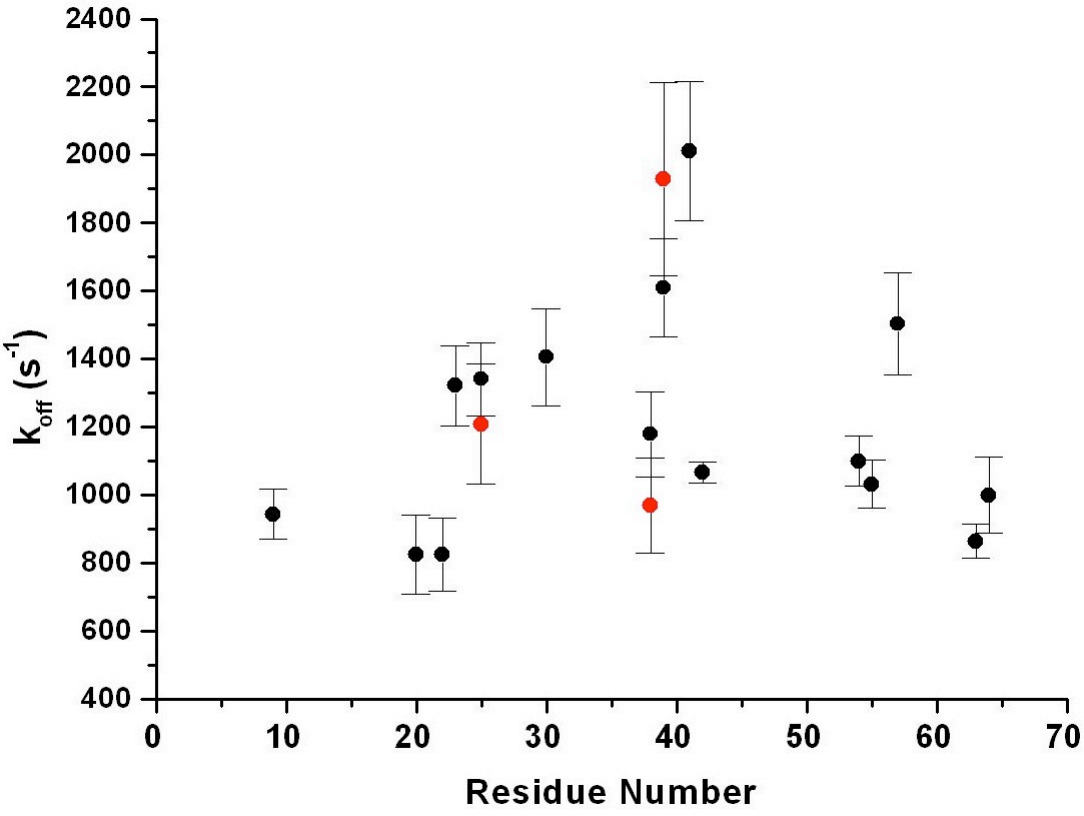

Figure 4.9 Kinetic off-rate constants determined from NMR line shape analysis of the residues in WT* on binding to CXCR1 N-domain. A plot showing the k_{off} values of the residues in WT* (•) and I10A* (•).

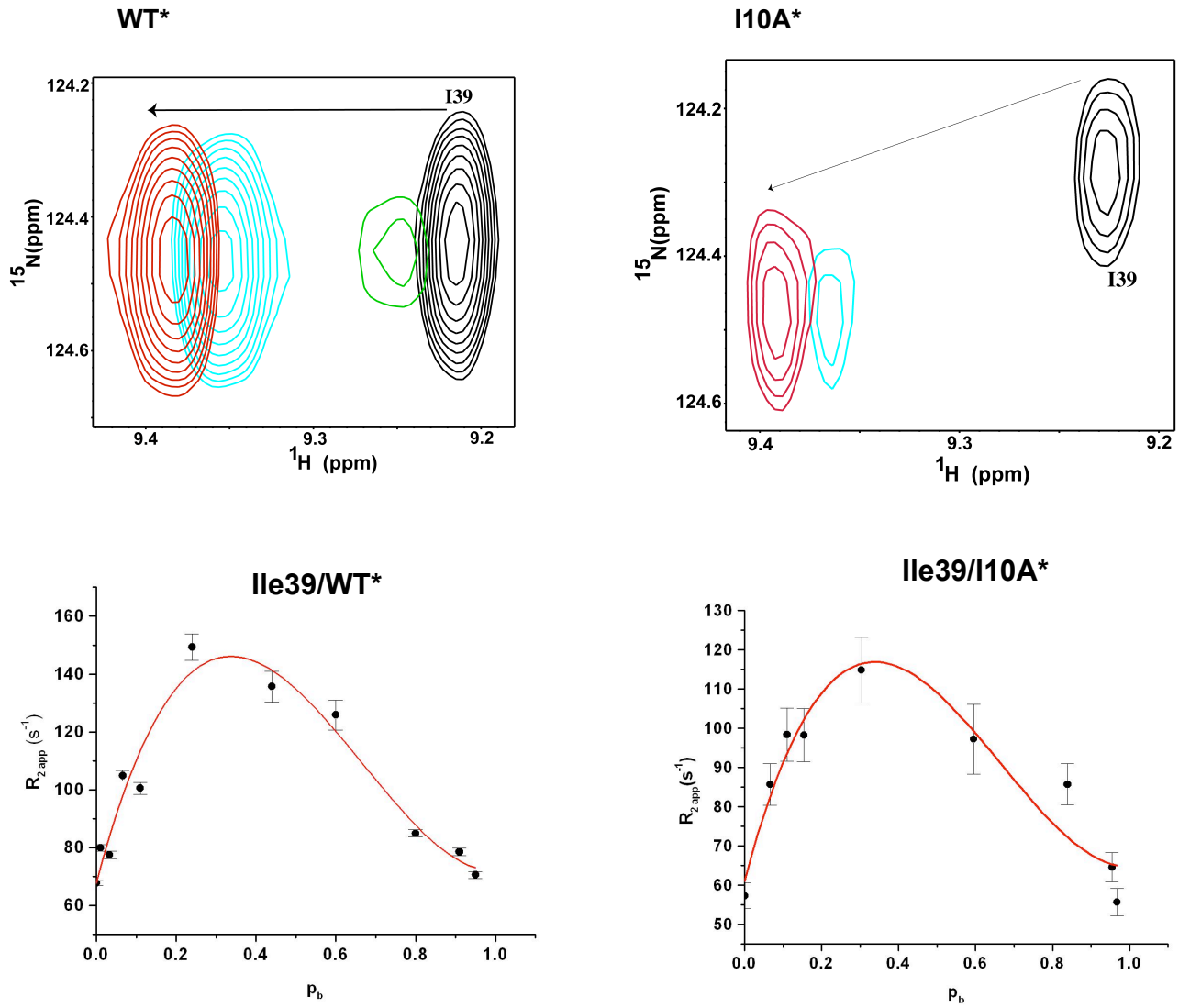

Figure 4.10 Kinetic analysis of the binding of WT* and I10A* to CXCR1 N-domain. ^{1}H-^{15}N HSQC titration spectra of Ile39 showing the intensity changes in WT* and I10A* **(upper panels)**. Peaks are color coded according for p_b values of 0 (black), 0.24 (green), 0.60 (blue), 0.8 (cyan) and 0.97 (red). $R_{2\ app}$ fits as a function of p_b for Leu25 in the WT* and I10A*, respectively **(lower panels)**. k_{off} values obtained from both the fits are 1609 ± 143 s^{-1} for WT* and 1928 ± 284 s^{-1} for I10A*.

Most chemokines have a large hydrophobe (Ile/Leu/Val/Phe/Tyr) at the position corresponding to Ile10 in the IL-8 N-loop **(Figure 4.11),** indicating a evolutionarily conserved function for this residue and that it plays a key role in modulating receptor binding and function. Indeed, it has been shown for many protein families that evolutionarily conserved residues usually belong to a network of amino acids that mediate propagation of signals from one site to another through energy transduction mechanisms and/or through correlated motions (130, 131). Our data indicate that the steric bulk of Ile10 seems to play only a marginal role in direct site-I binding interactions, and therefore Ile10 must play an indirect role via coupling interactions between site-I and site-II.

Structural basis of Ile10-mediated coupled interactions

Binding studies indicate that the I10A* binds with similar affinity to site-I as the WT*, but the resulting structural/dynamic changes do not allow optimal presentation of the N-terminal ELR residues, and so results in reduced intact receptor binding affinity and activity **(Figure 4.12)**. In thermodynamic terms, the total free energy of receptor binding, ΔG_{total} is represented by the following equation:

$$\Delta G_{total} = \Delta G_{site\text{-}I} + \Delta G_{site\text{-}II} + \Delta G_{coupling} \qquad (4.6)$$

where, $\Delta G_{site\text{-}I}$ and $\Delta G_{site\text{-}II}$ are the free energy changes required for site-I and site-II interactions, and $\Delta G_{coupling}$ is the coupling free energy change between the two sites (13).

Positive coupling implies site-I interaction decreases the free energy of binding required for site-II interaction, whereas negative coupling implies site-I interaction increases the free energy of binding for site-II interaction. $\Delta G_{site\text{-}II}$ should be similar for WT* and I10A* since the ELR residues are conserved. We observe from our ITC studies that $\Delta G_{site\text{-}I}$ for I10A* range from -7.6 to -7.8 kcal mol^{-1} and that of WT* range from -7.1 to -8 kcal mol^{-1} and therefore, $\Delta\Delta G_{site\text{-}I}$ varies from ~ 0.2-0.7 kcal mol^{-1}. Therefore, a 2 fold difference in the binding affinity translates to a very small difference in $\Delta G_{site\text{-}I}$ between the two variants. Binding studies to the intact CXCR1 receptor show that binding affinity of WT* and I10A* to CXCR1 is 2 nM

(ΔG_{total}= -11.8 kcal mol^{-1}) and 48 nM (ΔG_{total}= -9.9 kcal mol^{-1}), respectively. Therefore, this 24 fold reduction in the intact receptor binding affinity of I10A* must be due to differences in the coupling free energies ($\Delta\Delta G_{coupling}$) between the two sites. From eq 4.6, $\Delta\Delta G_{coupling}$ is calculated to be ~-2.0 kcal mol^{-1}.

ITC data also showed that the ΔH and $T\Delta S$ values for the binding of WT* and I10A* seems to be similar within experimental error, and that the binding is enthalpically favored and entropically disfavored **(Table 4.2)**. Factors that contribute towards favorable enthalpy typically include van der Waals, hydrogen-bonding and electrostatic interactions, and those that contribute towards favorable entropy are increased dynamics, and release of water on binding. Considering small differences and also that the structures of the receptor-bound complexes are not available, discussing the enthalpic and entropic contributions in terms of structural basis and molecular mechanisms should be done with caution. Future high-resolution structure determination of the complex should identify intermolecular contacts between the ligand and the receptor N-domain residues, and therefore should allow more meaningful discussion on the different pairwise interactions that contribute to favorable enthalpy. Further, factors that contribute to favorable entropy is less well understood. Discussion of entropic factors is not straightforward without knowledge on the conformational flexibility and dynamic motions before and after ligand binding. Future experiments on the NMR relaxation studies of WT* and I10A* in the free and in the bound form should provide a more conclusive picture on how the binding induced changes in the dynamics of WT* and I10A* correlate with the enthalpic and entropic changes observed from the ITC experiments.

In summary, we conclude that the side chain steric bulk of Ile10 in IL-8 plays a key role in mediating coupling interactions to site-II. This is the only study to our knowledge, which shows that mutating a functionally important solvent exposed hydrophobe in a chemokine has only marginal effect for site-I binding, but most remarkably plays an important role in communication to site-II resulting in overall optimal receptor binding affinity and function.

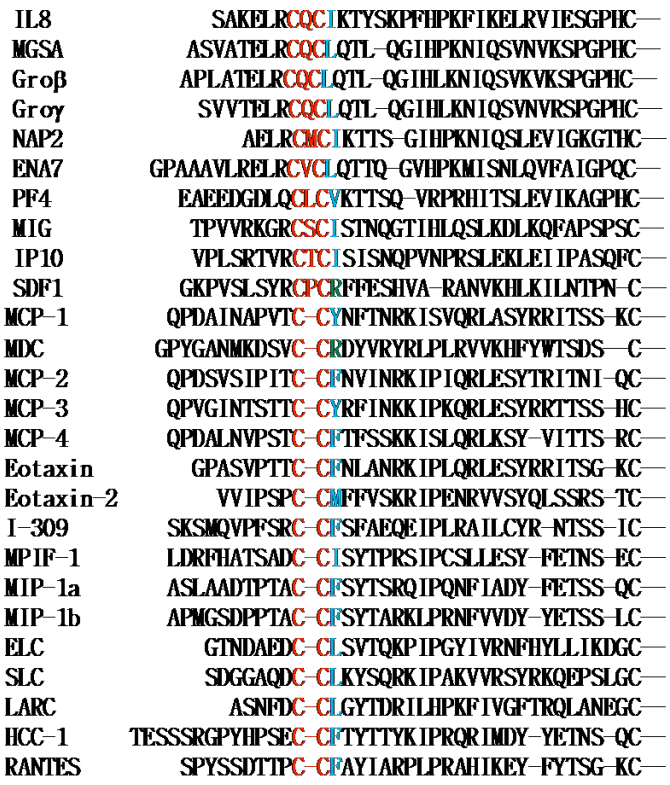

Figure 4.11 Residues corresponding to Ile10 in IL-8 are highly conserved. Sequences of CXC and CC chemokines are shown to indicate that the solvent exposed hydrophobe in the N-loop (shown in blue) is conserved. CXC and CC motifs are shown in red.

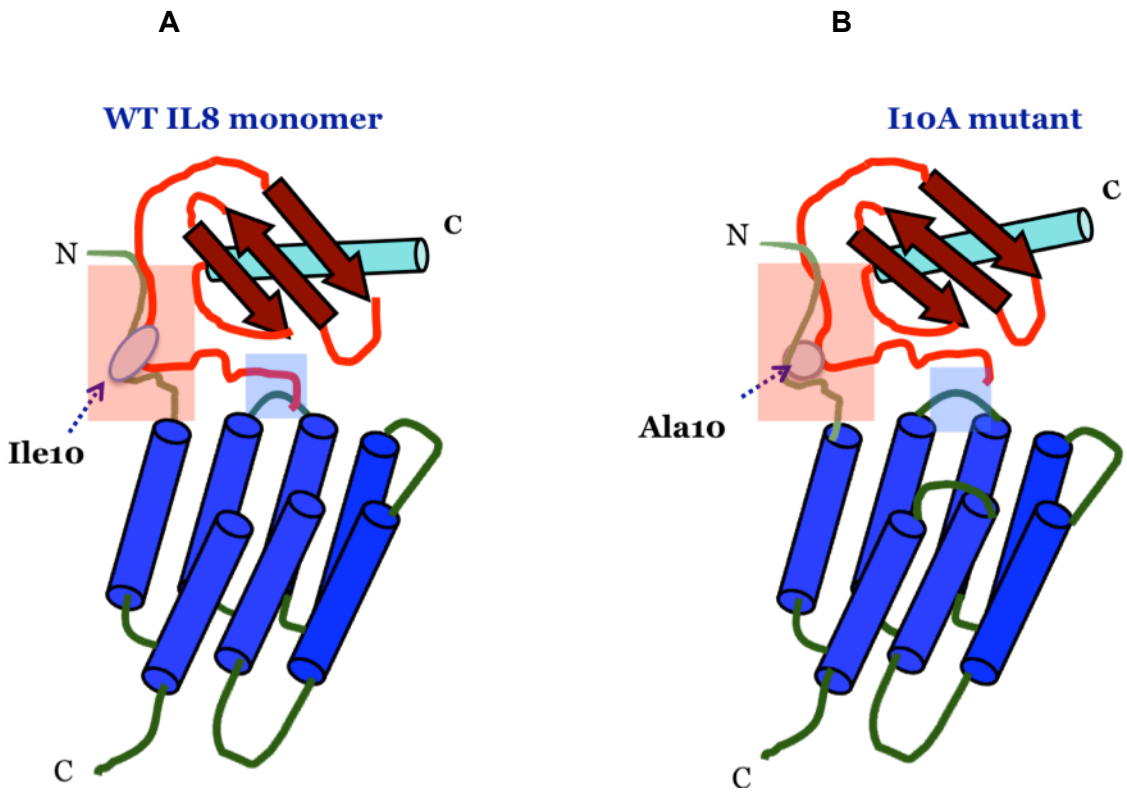

Figure 4.12 A schematic model that describes the role of the steric bulk of Ile10 in CXCR1 interaction. Site-I interaction of residue 10 (highlighted in pink) in WT* **(panel A)** and I10A* **(panel B)** are similar, but differences are observed at site-II (highlighted in blue) indicating that the steric bulk of Ile10 plays a role in coupling between site-I and site-II.

CHAPTER V

DESIGNING INHIBITORS THAT TARGET IL-8-RECEPTOR INTERACTION

INTRODUCTION

IL-8, one of the earliest chemokines discovered, plays a key role in neutrophil recruitment during host defense against infection and injury. A growing body of evidence suggests that it is intimately involved in the onset and progression of numerous inflammatory and autoimmune diseases, and so is an extremely attractive drug target (7, 132-135). Receptor binding of IL-8 is one of the key steps that trigger neutrophil activation and recruitment during host defense leading to further downstream signaling events. Therefore, IL-8-receptor interaction can be exploited as a drug target for developing potential therapeutics against inflammatory diseases. This requires knowledge of the ligand and receptor structures, as well as insights into the structural basis of receptor binding and function. Ligand structures are known, whereas structures of the receptor and of the ligand-receptor complex are not known.

Structure-function data indicate that IL-8 binds its receptors CXCR1 and CXCR2 with high nM affinity (41). This involves interactions between the ligand N-loop and the receptor N-domain (site-I), and the IL-8 N-terminus and the receptor exoloops/transmembrane residues (site-II) (13, 49, 51, 58, 64, 76, 80, 88, 89, 93). Sequence analysis of both ligands and receptors and also of chemokine structures show the largest difference for site-I residues. For instance, CXCR1 and CXCR2 share 77% sequence identity, whereas the N-domain shows less than 50% identity. Structure-function studies have also shown that site-I interactions play a major role in determining both specificity and affinity (13, 58, 86, 88, 91, 92).

High throughput screening (HTS) of small molecule libraries is the conventional approach used in drug discovery. Most pharmas, and in recent times, universities use this approach because it is relatively straightforward and the methodologies are well established. Furthermore, designing a HTS assay for

screening of small molecules does not require *a priori* knowledge of the ligand or receptor structures. More than 50% of the drugs discovered via HTS target GPCRs, and so considerable effort has been expended for discovering inhibitors for chemokine receptors (136). Indeed, HTS methods employed by pharmaceutical companies have resulted in the identification of a number of hits that target the chemokine receptor, and some of these molecules are in the early phase clinical trials. Nevertheless, the disadvantage of the HTS approach is the lack of knowledge of the molecular basis of how and where the hits bind the target.

An alternate strategy is the rational drug design approach, which makes use of the knowledge of the structures of the ligands, receptors, and ligand-receptor complexes. In this strategy, small molecules identified via HTS approaches are further optimized for higher affinity and potency, or peptidomimetics are designed that mimic the ligand/receptor binding sites. This approach is less popular for reasons that it is time consuming, requires significant initial investment, and moreover, the structures of the target are always not available. However, this approach could be quite powerful for designing second-generation molecules from those hits initially identified via HTS screening approaches.

In this study, we ask whether targeting the ligand instead of the receptor could result in potential small molecule inhibitors. Targeting the ligand allows neutralizing chemokine function at the site of insult. It is now well established that IL-8 binds its receptors at site-I with μM affinity (91, 109). Therefore, design of a small molecule inhibitor should bind IL-8 N-loop with similar or ideally higher affinity and specificity, and thus prevent site-I interaction. Towards accomplishing this goal, two approaches were used.

The first approach involved development of a fluorescence-based HTS assay for screening small molecule inhibitors that will bind IL-8 and thus prevent its interaction with the receptor N-domain. For this purpose, the N-terminus of the CXCR1 N-domain was fluorescently labeled, and changes in the fluorescence polarization (FP) and total fluorescence (TF) were monitored on binding to IL-8. Assay development involved optimizing the incubation time and temperature for

binding, testing for assay reproducibility and reliability, and testing the effect of DMSO on the binding.

The second approach was to use the knowledge gained from the structure-function studies on IL-8. The structure of IL-8 monomer shows that the N-loop and the third β-strand residues form a well-defined CXCR1 N-domain binding hydrophobic groove (26) **(Figure 5.1)**; ITC studies described in chapter 4, as well as previous studies showed that the binding of the IL-8 monomer to the CXCR1 N-domain is enthalpically favored and entropically disfavored (109). Therefore, to minimize the loss of binding induced conformational entropy, a cyclic CXCR1 N-domain was designed by linking the C-terminus of the linear peptide to the N-terminus using a disulfide bond. Results from these studies, including progress and hurdles faced are discussed and some potential strategies for inhibiting IL-8-receptor interaction are outlined.

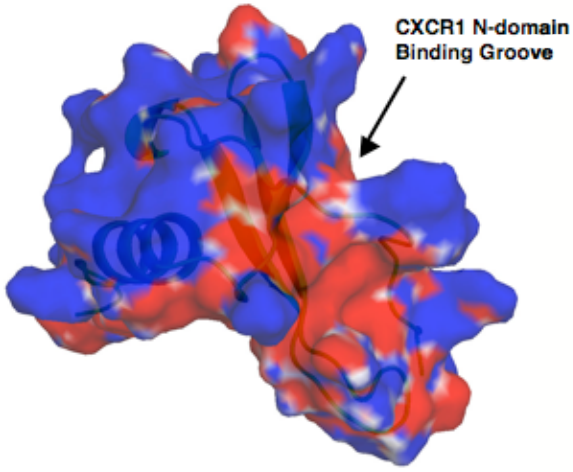

Figure 5.1 Schematic of the IL-8 monomer showing the CXCR1 N-domain binding groove. The hydrophobic binding groove for CXCR1 N-domain is formed by the IL-8 N-loop and the third β-strand residues.

EXPERIMENTAL PROCEDURES

Protein expression and purification for high throughput assay development

Expression and purification of recombinant IL-8 (1-66) monomer was performed in BL21DE3 *E. coli* using previous established procedures (91, 109). The lyophilized protein was dialyzed against the fluorescence assay buffer, 50 mM NaCl, 50 mM HEPES, pH 8.0 and the purity and molecular weight was confirmed using analytical HPLC and MALDI-MS respectively.

Unlabeled CXCR1 N-domain (24-mer) was synthesized using solid phase peptide synthesis and is the same as that used for the NMR binding studies described in chapter 2. The fluorescently labeled CXCR1 N-domain (FITC 24-mer) consists of a fluorescein isothiocyanate (FITC) tag at the amino terminus, and was also synthesized using solid phase peptide synthesis.

General methods

For HTS experiments involving fluorescence assay development and optimization for high throughput screening, fluorescence polarization (FP) and total fluorescence (TF) were measured on the binding of the IL-8 monomer to the FITC 24-mer. All FP and TF measurements were carried out in a 384-well, low-volume, black round-bottom polystyrene NBS microplate (Corning) using a Spectromax M5 plate reader (Molecular Devices, Sunnyvale, CA, USA). Addition of reagents was carried out using Biomek FXp dual arm robot (Beckman Coulter Inc. USA) The polarization values are reported in millipolarization units (mP) and the TF were measured at an excitation wavelength of 485 nm and an emission wavelength of 538 nm. The data were fitted using SigmaPlot 10 to determine the window size (ΔmP), binding constant (K_d) and inhibition constant (K_i).

Optimizing the incubation time for the binding of the IL-8 monomer to FITC 24-mer

The optimal incubation time required for performing the high throughput assay, was determined as follows. To each well, 10 μl of 100 nM FITC 24-mer and 10 μl of increasing concentrations of the IL-8 monomer were added to the assay buffer

(50 mM NaCl, 50 mM HEPES, pH 8). FP and TF measurements were measured at RT and 4°C for incubation times, 0, 0.15, 0.45, 1, 2, 6, 8 hrs. The data were fitted to obtain the binding constant, K_d.

Competitive inhibition experiments with unlabeled 24-mer

The inhibition constant, K_i or IC_{50} for competitive inhibition of the binding of FITC 24-mer using the unlabeled 24-mer was determined as follows. To each well, 10 μl of increasing concentrations of excess unlabeled CXCR1 N-domain 24-mer (0.007 nM-59.3 μM) and 10 μl of IL-8 bound FITC 24-mer (master mix) were added. The final concentrations of the FITC 24-mer and IL-8 monomer in the master mix were 0.1 μM and 2.34 μM, respectively. FP and TF values were read at RT and the data was fitted to estimate ΔmP and IC_{50}, which is the half maximal concentration for the inhibition of the unlabeled peptide.

Calculation of Z' factor

To calculate the Z' factor, the binding assay was carried out in a 384 well plate using a constant amount of IL-8 monomer, 2.3 μM, and FITC 24-mer, 0.1 μM. The experiment was carried out with unlabeled 24-mer concentrations 5 μM, 10 μM and 20 μM.

The 384-well plate was split into three sections, with each section containing 8 columns and 16 rows. To the first section containing 10 μl of buffer in each well, 10 μl of a mixture containing IL-8 monomer and FITC 24-mer at concentrations, 2.3 μM and 0.1 μM, respectively were added. The TF of the binding of the IL-8 monomer to the FITC 24-mer was measured for the positive control. To the second section containing 10 μl of buffer in each well, 10 μl of FITC 24-mer at final concentration of 0.2 μM was added and the TF was measured for the negative control. To section three, 10 μl of a mixture containing IL-8 monomer and FITC 24-mer at concentrations, 2.3 μM and 0.1 μM, respectively were added to 10 μl of unlabeled 24-mer with concentrations of either 5 μM, 10 μM or 20 μM. The TF was measured for the inhibition of unlabeled 24-mer as the positive control.

The Z' factor was calculated for both the binding of the IL-8 monomer to the FITC-24 mer, and for the inhibition of unlabeled 24-mer using the formula,

$$Z'\,factor = 1 - 3 \times \left(\sigma_p - \sigma_n\right) / \left(\mu_p - \mu_n\right) \qquad (5.1)$$

where, σ_p and σ_n are the standard deviations of the positive control and the negative control, and μ_p and μ_n are the means of the positive and the negative controls respectively.

Effect of DMSO on the binding

The objective was to test the effect of DMSO on the binding since the small molecule library to be screened is dissolved in DMSO, The effect of DMSO on the binding of the IL-8 monomer was tested by adding 10 µl of 5% DMSO in the assay buffer containing FITC 24-mer at 0.1 µM, and 10 µl of increasing concentrations of IL-8 monomer. FP and TF values were read and the data was fitted to estimate $K_{d.}$

Nonlinear least square fitting

All FP and TF data were fitted to a single site model using a four-parameter fit with Sigma Plot 10 using the equation,

$$Y = B + \frac{\Delta mP}{\left(1 + 10^{X - \log_{10} K_d}\right)} \qquad (5.2)$$

where, Y is either FP or TF, ΔmP is the window size, B is the average of the FP or TF value corresponding to free IL-8, X are the IL-8 concentrations and K_d is the binding constant.

Design of the cyclic CXCR1 N-domain peptidomimetic

Design of cyclic peptides against IL-8 requires using the principles of peptidomimetic design (137). One of the principles of designing a peptidomimetic is to optimize the ring size to increase the affinity as well as the potency. This strategy has been employed to successfully design cyclic peptides for other protein classes

(138). The cyclic CXCR1 N-domain was designed by linking the C-terminus of the linear CXCR1 N-domain (24-mer) to the N-terminus using a disulfide bond. The peptide was synthesized using solid phase peptide synthesis. The sequence of the cyclic peptide is shown below.

NMR Spectroscopy

For NMR binding studies with the cyclic CXCR1 N-domain, ^{15}N labeled IL-8 (1-66) monomer was expressed and purified as described in chapter 2. Titration of the cyclic CXCR1 N-domain (24-mer) into ^{15}N labeled IL-8 (1-66) monomer was carried out similar to the titration studies involving the linear cyclic CXCR1 N-domain (24-mer) as described in chapter 2. The final peptide:protein molar ratio was 7.5. Two-dimensional ^{1}H-^{15}N HSQC spectra were acquired with 2048 complex points for direct ^{1}H and 128 complex points for indirect ^{15}N dimension. All spectra were recorded using Varian INOVA 800-MHz spectrometers equipped with field gradient accessories. The spectra were processed using NMRPipe (99) and analyzed using NMRView (100).

RESULTS

Design of a fluorescence assay for HTS of small molecules

Developing a robust and sensitive high throughput fluorescence-based assay is fundamental for screening small molecules that will inhibit IL-8-receptor binding at site-I. For this purpose, we used FP and TF. FP exploits the property that the polarization is proportional to the size of the protein complex. TF measures the change in the fluorescence intensity of the protein in its free vs. complexed state. FP has been successfully used to identify small molecule compounds that inhibit a wide variety of protein-protein interactions (139). The approach was to monitor the binding

of the FITC 24-mer to IL-8 using FP and TF. FP and TF measurements provide information on the screening parameters such as binding affinity as measured by the K_d, and window size (ΔmP), which represents the dynamic range of the assay in units of milli polarization and is defined as the difference in polarization between the free and the bound N-domain peptide.

Time course experiments

Initial experiments involved optimizing the incubation time required for the binding of the IL-8 monomer to the FITC 24-mer. It was observed that the binding resulted in a change in both FP and TF. TF resulted in a larger window size compared to FP (ΔmP ~70 units for TF vs. 30 units for FP). Therefore, only TF was used to monitor the binding of the monomer to the FITC 24-mer. It was observed that the IL-8 monomer binds the FITC 24-mer with an affinity of ~0.4 μM. We observed that K_d and ΔmP at RT and at 4°C did not vary as a function of incubation time and temperature **(Figure 5.2 and Table 5.1)**. Therefore, all TF measurements were carried out at RT without any incubation time.

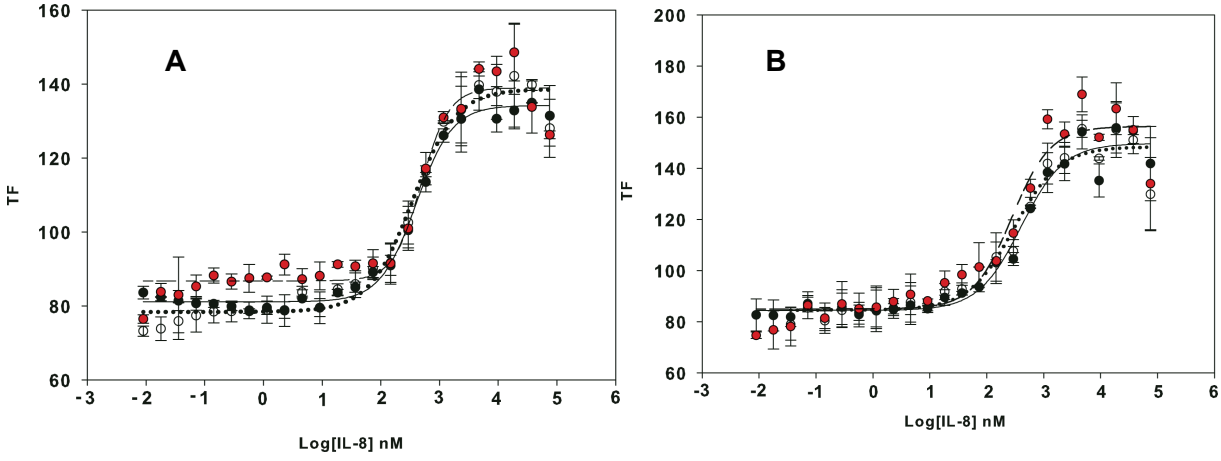

Figure 5.2 Time course experiments on the binding of the IL-8 monomer to FITC 24-mer. FITC 24-mer binding induced change in TF (y-axis) at RT **(panel A)** and at 4°C **(panel B)** are plotted against IL-8 monomer concentration in log units (x-axis) for incubation times 0 (○), 1 (•) and 8 hrs (•), respectively.

Table 5.1 A summary of the time course experiments on the binding of the IL-8 monomer to FITC 24-mer. The binding measurements using TF were carried out at RT and 4 °C and the incubation time, binding constant (K_d) and window size (ΔmP) are reported.

At RT	Time (hrs)	K_d (μM)	ΔmP
	0	0.4 ± 0.04	53 ± 1
	0.15	0.4 ± 0.06	64 ± 1
	0.45	0.4 ± 0.04	60 ± 1
	1	0.4 ± 0.06	60 ± 1
	2	0.4 ± 0.06	60 ± 1
	6	0.4 ± 0.07	60 ± 1
	8	0.5 ± 0.08	52 ± 1
At 4°C	0	0.4 ± 0.07	65 ± 1
	0.15	0.3 ± 0.06	67 ± 1
	0.45	0.2 ± 0.06	75 ± 1
	1	0.3 ± 0.06	69 ± 2
	2	0.3 ± 0.06	64 ± 1
	6	0.3 ± 0.07	71 ± 2
	8	0.3 ± 0.07	71 ± 2

Competitive inhibition experiments

Competitive binding experiments were carried out after determining the final IL-8 concentration at which the binding is 70% complete. This corresponds to an IL-8 concentration of 2.3 μM and ΔmP of 50 units, and was estimated from the binding curve shown in **Figure 5.2, panel A**. Unlabeled peptide was added to the FITC 24-mer bound IL-8 at a concentration that is 100-fold excess over IL-8 concentration. I observed that the unlabeled peptide competed with the labeled peptide with an IC_{50} of 2 ± 1 μM **(Figure 5.3)**.

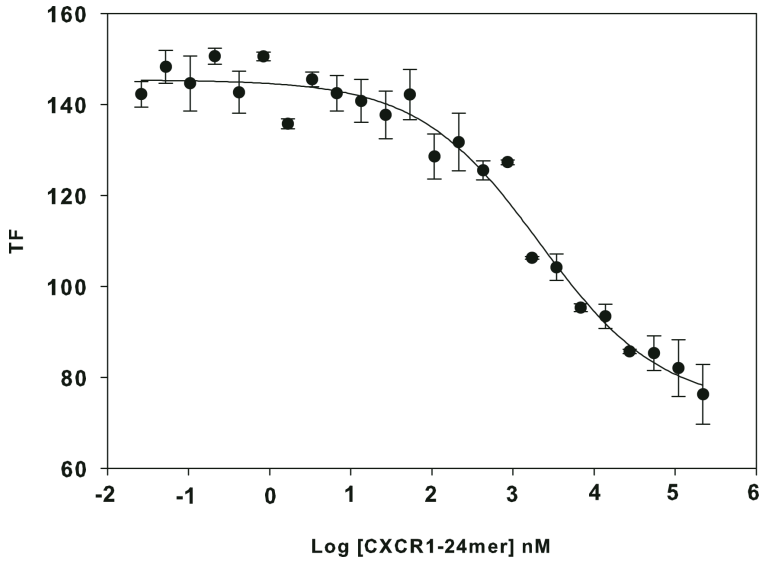

Figure 5.3 Competitive binding of unlabeled CXCR1 N-domain with FITC 24-mer bound to the IL-8 monomer. The displacement of the FITC 24-mer is measured by recording the TF (•) (y-axis) as a function of CXCR1 N-domain (24-mer) concentration in log units (x-axis). The IC_{50} and ΔmP are 2 ± 1 μM and 71 ± 4 μM, respectively.

Calculation of Z' factor

The quality (precision) and reproducibility of the assay was tested by carrying out Z' factor experiments. A Z' factor of >0.5 indicates that the assay is reliable. The closer the Z' factor is to 1, the more reliable is the assay although it is technically impractical to get a Z' factor of 1. The experiments were repeated twice and at different times and days to account for intra-plate, inter-plate and day-to-day variations in the assay results. The Z' factors for unlabeled peptide concentrations at 5, 10 and 20 μM were ~0.8. From the measured TF values, the % inhibition of the unlabeled peptide was calculated. This was done to determine the cut off % inhibition for identifying a positive hit during the screening process. The experiment at 5 μM unlabeled peptide concentrations was repeated at 2 different days **(Figure 5.4)**. Results showed that there are differences in the average TF values for bound FITC 24-mer, the inhibition of the unlabeled peptide and ΔmP values determined at two different days suggesting poor reproducibility of the experiment.

The Z' factor experiments carried out at 10 and 20 μM peptide concentrations yielded similar results **(Figures 5.5 and 5.6)**. I also observed inter-plate variations and that the % inhibition values were quite similar to that obtained at 5 μM peptide concentrations. Ideally, the % inhibition should increase with increasing unlabeled peptide concentrations. From these experiments, it was concluded that the assay is not reproducible due to large standard deviations in the average TF and ΔmP values and also due to intra-plate, inter-plate and day-to-day variations in the assay results. This is most likely due to low signal to noise and could be overcome if ΔmP is increased.

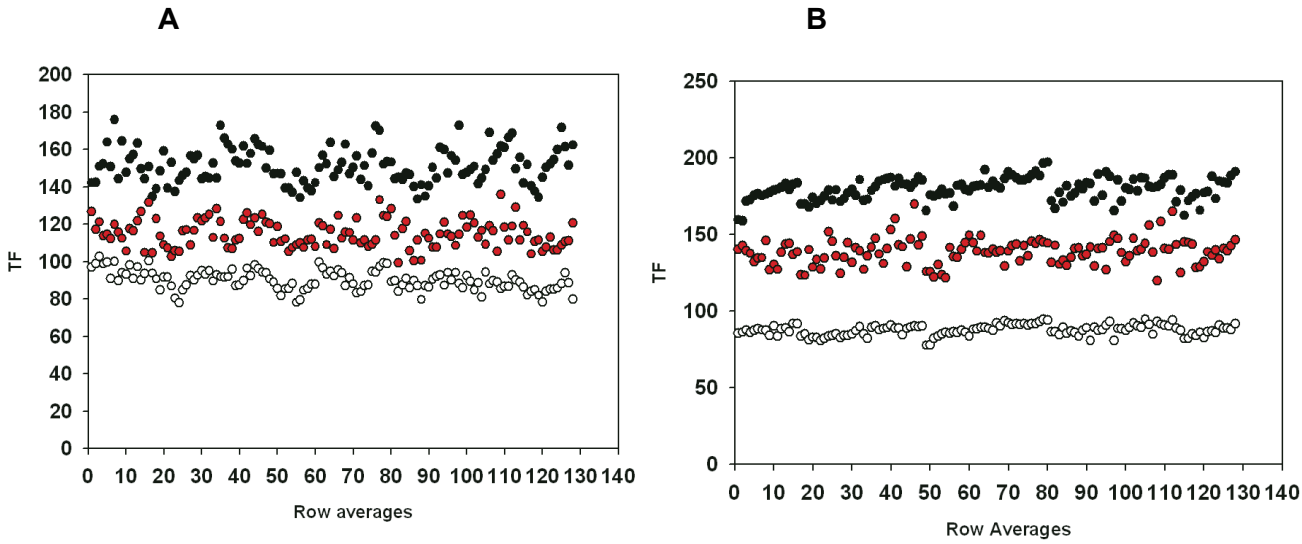

Bound FITC 24-mer = 151 ± 10 µM
Inhibition of unlabeled 24-mer = 115 ± 7 µM
Free FITC 24-mer = 90 ± 5 µM
% inhibition = 60 ± 12
ΔmP= 62 ± 4

Bound FITC 24-mer = 180 ± 7 µM
Inhibition of unlabeled 24-mer=138 ± 9 µM
Free FITC 24-mer = 88 ± 4 µM
% inhibition = 44 ± 9
ΔmP= 92 ± 4

Figure 5.4 Z' factor calculations at 5 µM unlabeled peptide concentration. **Panels A and B** show the row averages for the TF (y-axis) of bound FITC 24-mer (•), free FITC 24-mer (○) and the inhibition of the unlabeled 24-mer peptide at 5 μM concentration (•) on two different days. The average TF, the % inhibition of the unlabeled 24-mer and ΔmP are shown. The Z' factor for the inhibition of the unlabeled peptide is ~0.7.

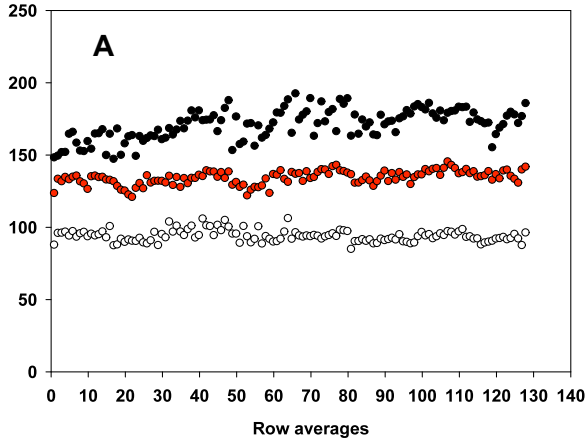

Bound FITC 24-mer = 170 ± 10 µM
Inhibition of unlabeled 24-mer=134 ± 5 µM
Free FITC-24mer = 94 ± 6 µM
% inhibition = 60 ± 9
ΔmP= 77 ± 4

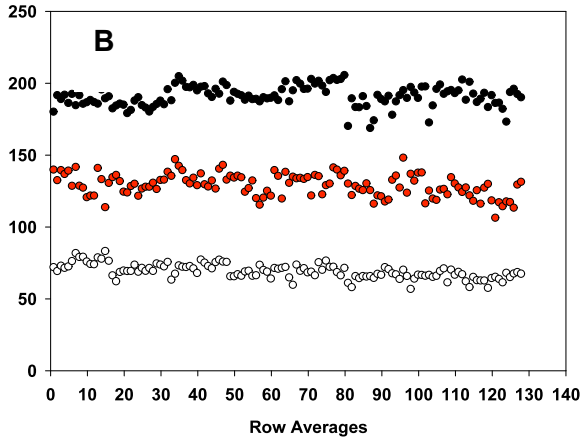

Bound FITC 24-mer = 191 ± 7 µM
Inhibition of unlabeled 24-mer = 127 ± 7.9 µM
Free FITC 24-mer = 69 ± 6 µM
% inhibition = 51 ± 6
ΔmP= 122 ± 2

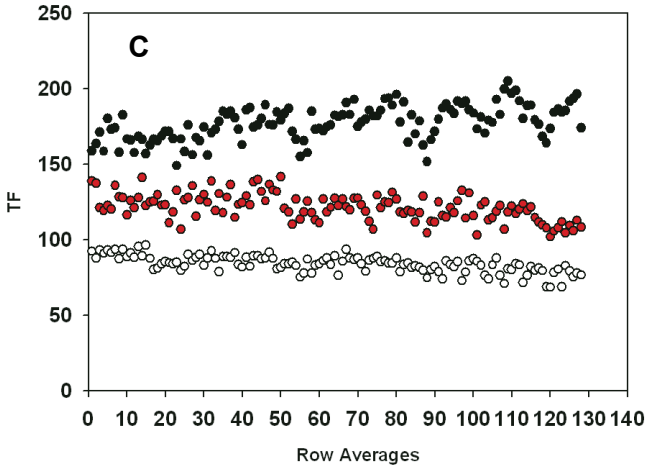

Bound FITC 24-mer = 177 ± 11 µM
Inhibition of unlabeled 24-mer = 121 ± 9 µM
Free FITC 24-mer = 84 ± 6 µM
% inhibition = 60 ± 9
ΔmP = 93 ± 6

Figure 5.5 Z' factor calculations at 10 µM unlabeled peptide concentration. The row averages of the TF (y-axis) of bound FITC 24-mer (•), free FITC 24-mer (○) and the inhibition of the unlabeled 24-mer peptide at 10 μM concentration (•) are shown for day1 **(panel A)** and day 2 **(panels B and C)**. **Panels B and C** represent experiments performed with two different plates. The average TF, the % inhibition of the unlabeled 24-mer and ΔmP are shown. The Z' factor for the inhibition of the unlabeled peptide in all three experiments is ~0.8-0.9.

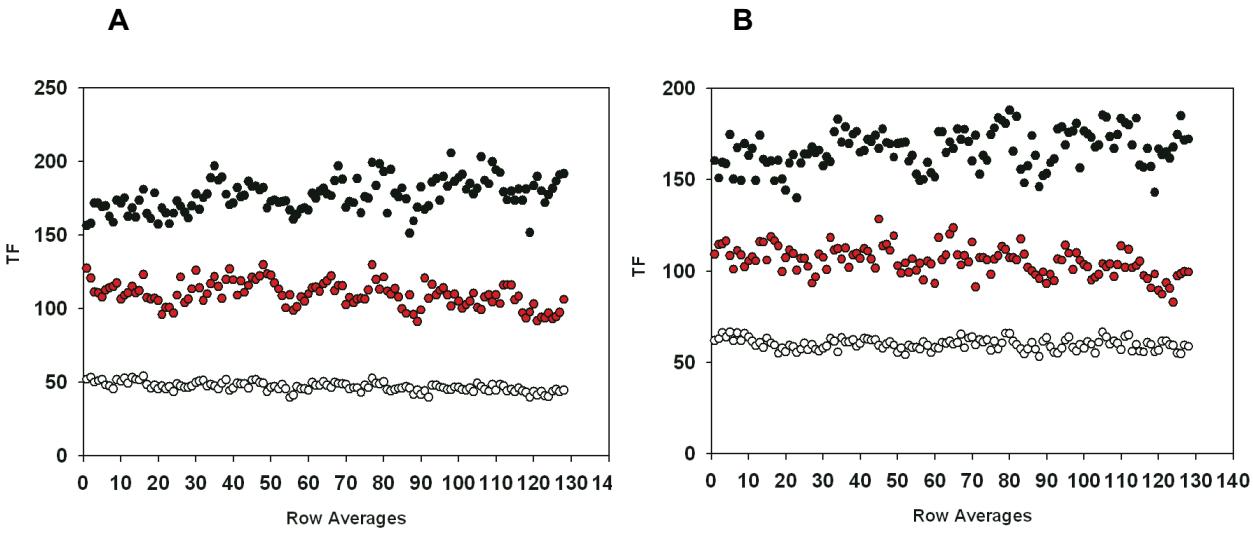

Bound FITC 24-mer = 176 ± 11 µM
Inhibition of unlabeled 24-mer = 109 ± 9 µM
Free FITC 24-mer = 47 ± 3 µM
% inhibition = 51 ± 7
ΔmP = 130 ± 4

Bound FITC 24-mer = 167 ± 10 µM
Inhibition of unlabeled 24-mer = 105 ± 8 µM
Free FITC 24-mer = 60 ± 3 µM
% inhibition = 57 ± 7
ΔmP = 107 ± 7

Figure 5.6 Z' factor calculations at 20 µM unlabeled peptide concentration. The row averages of the TF (y-axis) of bound FITC 24-mer (•), free FITC 24-mer (○) and the inhibition of the unlabeled 24-mer peptide at 20 μM concentration (•) are shown for experiments done with two different plates **(panels A and B)**. The average TF, the % inhibition of the unlabeled 24-mer and ΔmP are shown. The Z' factor for the inhibition of the unlabeled peptide in both experiments is ~ 0.7.

The effect of DMSO

The effect of DMSO was tested from competitive binding experiments of the unlabeled 24-mer in the presence of 5% DMSO. This is the minimal DMSO concentration needed for small molecule screening. The 5% DMSO was incorporated in the assay buffer and the experiment was carried out in the similar way as described for the same assay without DMSO. There was no competition of the unlabeled peptide in 5% DMSO indicating that DMSO interferes in the assay. This experiment was repeated twice to test for reproducibility **(Figure 5.7)**. A control experiment without any DMSO showed that the unlabeled peptide displaced the FITC 24-mer at an IC_{50} of ~0.8 μM.

Alternative solutions

Our studies indicate that using FP is limiting due to the small size difference between the CXCR1 N-domain in its free and the bound form. IL8 is ~7 kDa in size and the CXCR1 N-domain is ~3 kDa. Even when using TF, the signal to noise ratio should be large enough so that the ΔmP is large. Either using a shorter CXCR1 N-domain peptide or increasing the molecular weight of IL-8 could overcome these problems.

Synthesizing a shorter CXCR1 N-domain may not be practical because reducing the size might disrupt some of the key native interactions in the complex. The latter solution is more straightforward as IL-8 can be expressed as a fusion protein. Binding studies with IL-8 fused to a thioredoxin tag was carried out but it was observed that the tag interfered with the binding as the binding affinities measured with and without the tag were not similar. An alternate solution to this is to carry out assay optimization studies with IL-8 fused to a glutathione-S-transferase (GST) tag or other tags.

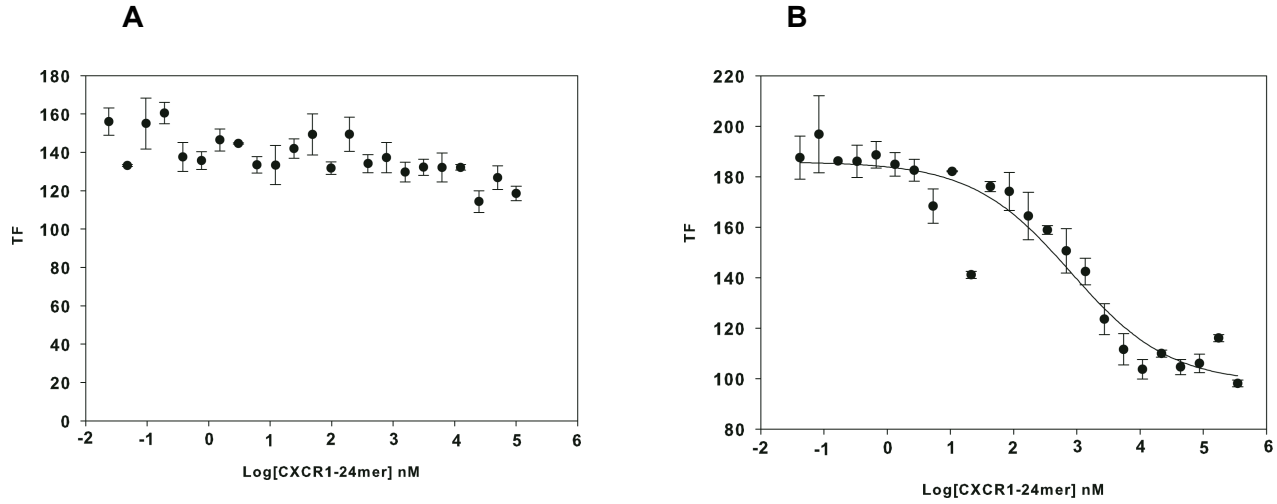

Figure 5.7 Effect of 5% DMSO on the competitive binding of unlabeled 24-mer. Competition of the unlabeled 24-mer with the FITC 24-mer bound to IL-8 monomer in the presence of 5% DMSO **(panel A)** and without DMSO **(panel B)** are shown. The unlabeled peptide displaces the FITC 24-mer bound to the IL-8 monomer at an IC_{50} and ΔmP of 0.9 ± 0.5 μM and 87 ± 4 μM respectively.

Testing for batch to batch variation in the binding assay in the presence of 5% DMSO

The binding assay was carried out with two different batches of IL-8 (1-66) in the presence of 5% DMSO **(Figure 5.8)**. The binding curves did not reach saturation, and so the data could not be fitted to obtain reliable K_d and ΔmP values. This is contrary to what was observed for the binding of IL-8 without DMSO in the buffer, which showed that the binding reached saturation **(Figure 5.2)**. These experiments reiterate that the assays are not reproducible and that there is batch-batch variation in the binding of IL-8.

Summary

Efforts on the optimization of the high throughput fluorescence assays for screening resulted in low signal to noise ratios due to small ΔmP, poor assay reproducibility due to variations in K_d, ΔmP, and batch to batch variations in the assay results.

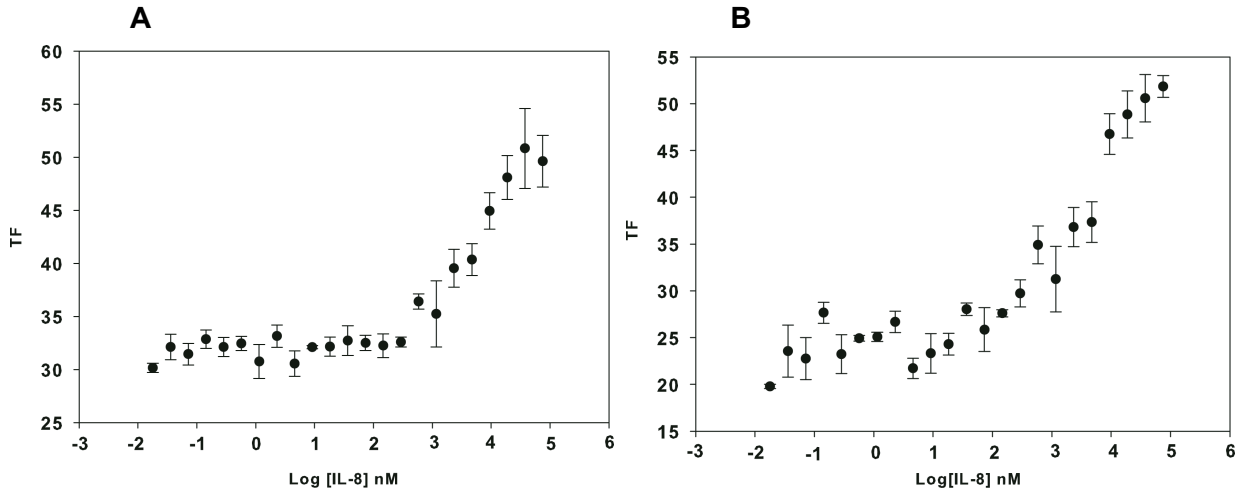

Figure 5.8 Effect of 5% DMSO on the binding of IL-8 monomer. Panels A and B show the binding curves of IL-8 monomer with and without 5% DMSO respectively.

Binding of the IL-8 monomer with cyclic CXCR1 N-domain

ITC studies have shown that the enthalpic and entropic changes on site-I interaction of the IL-8 monomer are ~-8 kcal mol^{-1} and ~-1.2 kcal mol^{-1} (chapter 4), indicating that the binding is enthalpically favored and entropically disfavored. Therefore, to design peptidomimetic that binds with high affinity requires increasing the favorable enthalpic interactions and/or decreasing the unfavorable entropic factors (140, 141). As the structures of the receptors or that of the ligand-receptor complexes are not available, the structural basis of interactions that contribute to enthalpy such as hydrophobic, electrostatic, and H-bonding are not known. Moreover, factors that contribute to favorable entropic changes are more complex and are less well understood. However, it is generally believed that loss of conformational entropy is one of the factors that disfavors binding. Therefore, we hypothesized that designing a cyclic CXCR1 N-domain peptide should minimize the loss of conformational entropy, and result in overall higher binding affinity. Such a strategy has been shown

to result in tighter binding in a number of systems (142, 143). To address this hypothesis, a cyclic CXCR1 N-domain was designed by linking the C-terminus of the linear CXCR1 N-domain 24-mer with the N-terminus using a disulfide bond.

Titration of the cyclic peptide into labeled IL-8 monomer resulted in selective chemical shift perturbations of residues in the N-loop, third β-strand and helix, but the perturbations were significantly lower than what was observed for the linear peptide (Δδ of ~0.05 vs. >0.25 ppm) **(Figure 5.9)**. Binding induced chemical shift perturbations could not be fitted to obtain the binding affinity for the cyclic peptide indicating weak binding (K_d >1mM). Furthermore, ITC studies could not be carried out due to the weak binding affinity, and so the ΔH and ΔS for the interaction of the cyclic peptide are not known. It is most likely that the binding of this cyclic peptide does not allow optimal interactions resulting in loss of favorable enthalpic energy. It is clear that our approach of just using one peptide is limiting, and approaches to increase favorable enthalpic interactions and simultaneously minimize loss of entropy require a more exhaustive study of designing a series of peptides with different linker lengths, and using lactam bridges instead of disulfides.

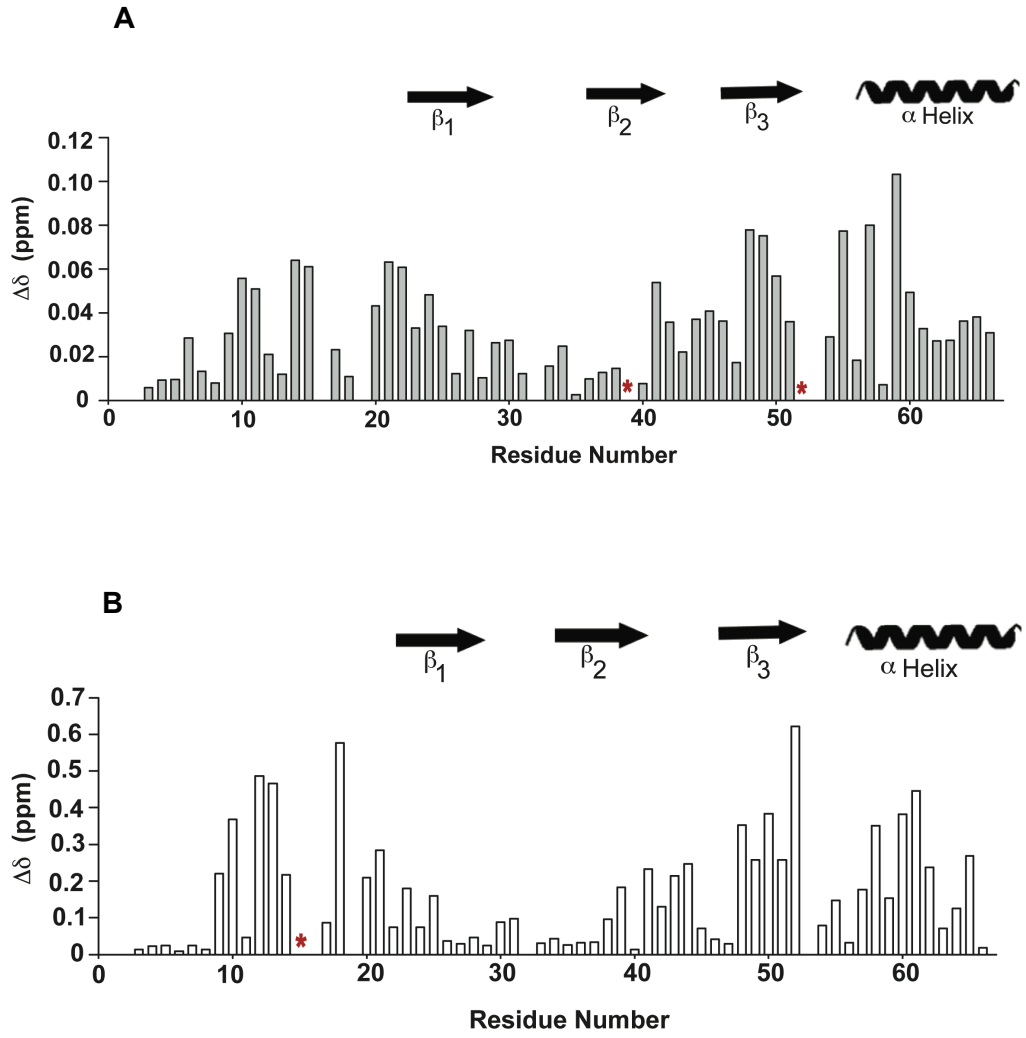

Figure 5.9 Chemical shift perturbations in the IL-8 monomer on binding to cyclic and linear CXCR1 N-domains. Histogram plots showing the total chemical shift perturbations in the IL-8 monomer on binding to cyclic CXCR1 N-domain **(panel A)** and linear CXCR1 N-domain **(panel B)**. The asterisk denotes residues Ile39 and Asp52, which broaden out during titration of the cyclic CXCR1 N-domain and Lys15, which broaden out during titration of the linear CXCR1 N-domain.

DISCUSSION

Chemokines and their receptors play key roles in numerous inflammatory and autoimmune diseases, and so represent a targetable class of molecules for developing anti-inflammatory therapeutics (144). However, this notion often draws skepticism because of the complexity involved in the ligand-receptor interaction. Ligand-receptor interaction involves a single ligand binding multiple receptors, as well as a single receptor binding multiple ligands (13). Also, many ligands are known to dimerize and oligomerize and the receptors are also known to dimerize. So receptor activation can involve binding of monomeric and dimeric ligands, which further contributes towards the complexity.

Despite this skepticism and the question of specificity issues, HTS approaches have successfully identified small molecule inhibitors, and some of them are already in clinical trials (144). The discovery of small molecule drugs against CCR5 for HIV prevention, and against CXCR4 for hematopoietic stem cell mobilization herald the first triumphs for small molecule inhibitors (144). Currently, five inhibitors that target IL-8 receptors are in early phase clinical trials. Four of them target CXCR2 with high specificity, and only one inhibitor called reparixin targets both CXCR1 and CXCR2 (145-150). These inhibitors block receptor activity by binding to site-II, which is highly conserved in sequence among the receptors. Antibodies that target the ligand neutralize the ligand, however the efficacy of the antibodies in clinical trials remains unknown. A CXCR1 N-domain peptidomimetic that was generated by replacing the residues in the center of the peptide that act as a scaffold with a six amino acid hexanoic acid linker showed similar potency in inhibiting IL-8-receptor binding compared to that of the linear CXCR1 N-domain (151).

Our approach is distinctly different in that it targets the ligand, and targets the site-I interaction. Our attempt to develop a HTS assay that target the IL-8 N-loop by competitively inhibiting the binding of the CXCR1 N-domain was not successful. This is because the compatibility of the assay with the target system has to be taken into account during assay development. In this case, the screening window size in the

fluorescence assay was small because of the small change in anisotropy between the N-domain in its free and the bound form. There were additional difficulties such as poor reproducibility and batch-to-batch variations in the assay results. All of these problems highlight the practical limitations of developing assays for HTS approaches.

The second approach of minimizing unfavorable entropic interactions was not successful most likely due to significant loss of favorable enthalpic interactions. However, small molecule cyclic peptidomimetics of polyphemusins, T140 and its analogues that target CXCR4 receptor have been potent in inhibiting HIV infection, cancer metastasis and rheumatoid arthritis (152-154). The peptidomimetics used in these studies are small in size, and are essentially cyclic pentapeptides consisting of key residues that are required for high inhibition potency. In our case, reducing the size of the CXCR1 N-domain becomes an issue as truncation analogs of CXCR1 N-domain exhibits decreased potency in inhibiting IL-8-receptor binding (90).

In summary, on the basis of these studies, and from what is currently known regarding various studies on small molecule drug design for chemokine-receptor interaction, identifying small molecules inhibitors that target the active site of IL-8 is a promising approach towards developing anti-inflammatory therapeutics. Developing a HTS assay is possible if issues such as compatibility of the system and assay reproducibility are accounted for. Successful identification of hits through this process should allow further characterization using structure-based approaches, and can be tested for potency and efficacy *in vivo*. Rational drug design of CXCR1 N-domain peptidomimetics holds promise if the design allows enthalpic and entropic free energy changes to favorably contribute to its interaction. Future studies on the structure determination of the CXCR1 N-domain-IL-8 complex should provide further insights for our HTS and peptidomimetic approaches.

APPENDIX

Table A1 **^{15}N and ^{1}H chemical shifts of MGSA monomer at 40 °C, pH 4.5.**

Residue	^{15}N	HN	H_α		H_β		H_γ			H_δ		H_ε
Val3	121.81	8.19	4.15		2.08		0.92	0.92				
Ala4	127.44	8.33	4.32		1.38							
Thr5	113.11	7.92	4.19		4.28					1.16		
Glu6	122.02	8.30	4.30		2.22	1.97						
Leu7	122.19	8.02	4.27		1.37		1.57			0.86		
Arg8	118.80	7.85	4.74		2.08	1.80	1.57			3.21		
$Cys9_{major}$	119.29	8.38	4.65		3.78	2.72						
$Cys9_{minor}$	119.29	8.34	4.65		3.78	2.72						
Gln10	125.51	11.06	4.29		2.02	1.99						
Cys11	120.93	9.42	4.87		3.17	2.72						
Leu12	125.31	8.60	4.35		1.67	1.67	1.65			0.94		
Gln13	116.54	7.77	4.62		2.34	2.04	2.30	2.30				
Thr14	112.49	8.41	4.59		3.99		1.05					
Leu15	121.97	8.58	4.67		1.64		1.25			0.94	0.68	
Gln16	119.61	8.70	4.46		2.18	2.02	2.46	2.46				
Gly17	104.95	7.67	3.86	3.90								
Ile18	117.70	7.03	4.22		1.69		1.39	1.05	0.72			
His19	125.41	8.43	4.64		3.09	3.09						
Lys21	118.93	9.58	4.25		1.83	1.83	1.35	1.35				
Asn22	115.05	8.13	4.87		3.12	2.75				7.63		
Ile23	120.40	7.63	3.90		1.91		1.63	0.76		0.76		
Gln24	127.21	9.34	4.51		1.86	1.77	2.29	2.29				7.95
Ser25	112.76	8.18	5.38		4.17	3.92						
Val26	119.29	9.21	4.78		1.78		0.76					
Asn27	126.34	8.79	5.69		2.87	2.61						
Val28	126.93	9.29	4.57		2.14		0.82					
Lys29	126.89	9.34	4.71		1.91	1.71						

Residue	^{15}N	HN	H_α		H_β		H_γ		H_δ		H_ε	
Ser30	120.70	7.94	4.76		4.02	4.02						
Gly32	111.02	8.52	4.38	4.03								
His34	112.07	8.39	4.64		3.23	2.94						
Cys35	116.63	7.28	4.68		2.95	2.02						
Ala36	131.64	8.80	4.53		1.45							
Gln37	115.86	7.46	4.77		2.19	1.94	2.34				7.24	6.80
Thr38	121.06	8.52	4.51		3.94		1.16					
Glu39	124.09	8.59	4.88		2.79	1.96	2.34					
Val40	124.17	9.50	4.9		2.23		0.80					
Ile41	126.05	9.12	4.69		1.82		1.49	0.78				
Ala42	134.22	9.80	5.26		1.33							
Thr43	119.27	9.13	4.75		4.19		1.17					
Leu44	128.50	9.39	5.02		2.13	1.75	1.66		0.75			
Lys45	121.14	8.40	3.98		1.77		1.34	1.34				
Asn46	113.95	7.66	4.62		3.26	2.83						
Gly47	107.92	8.13	4.32	3.56								
Arg48	120.35	7.66	4.34		1.88		1.60	1.6	3.57	3.57		
Lys49	119.36	8.24	5.24		1.68		1.53					
Ala50	123.80	9.10	4.66		1.23							
Cys51	121.35	8.93	5.55		3.88	3.13						
Leu52	121.87	8.94	4.93		1.42	1.42	1.60		0.70			
Asn53	122.04	8.78	4.74		2.98	2.79						
Ala55	116.41	7.57	4.34		1.40							
Ser56	115.06	7.65	4.85		4.19	4.19						
Ile58	116.40	7.57	3.88		1.92		1.40	0.88				
Val59	121.31	7.26	3.43		2.34		1.06	0.85				
Lys60	117.68	7.30	3.76		1.91	1.91	1.49					
Lys61	116.94	7.22	4.05		1.92							
Ile62	119.55	8.18	3.54		2.01							
Ile63	117.00	7.71	4.24		1.92							
Glu64	116.78	8.08	3.83		2.13		2.56					
Lys65	122.38	8.30	4.3		2.02	1.98						
Met66	117.96	7.72	4.17		2.08	1.97	2.82	2.44			1.93	
Leu67	121.56	7.08	4.17		1.68		2.09		0.79			

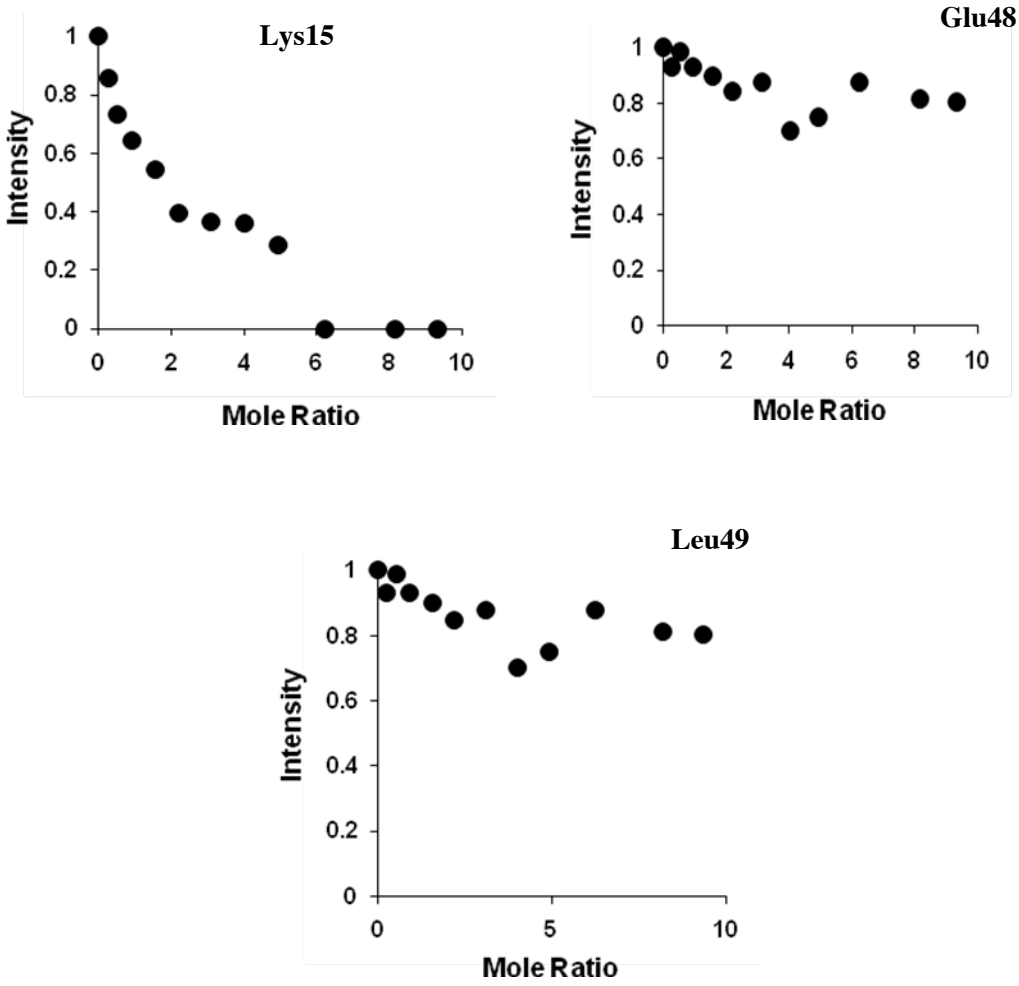

Figure A1. Line broadening in the IL-8 monomer on binding to CXCR2 N-domain R2-25mer. Intensity changes in the IL-8 monomer (y-axis) on binding to R2-25mer as a function of peptide:protein mole ratio (x-axis) are shown for Lys15, Glu48, and Leu49. Glu48 and Leu49 show relatively higher chemical shift perturbations compared to the remaining residues, but do not change in intensity, whereas the peak corresponding to Lys15 disappears during titration.

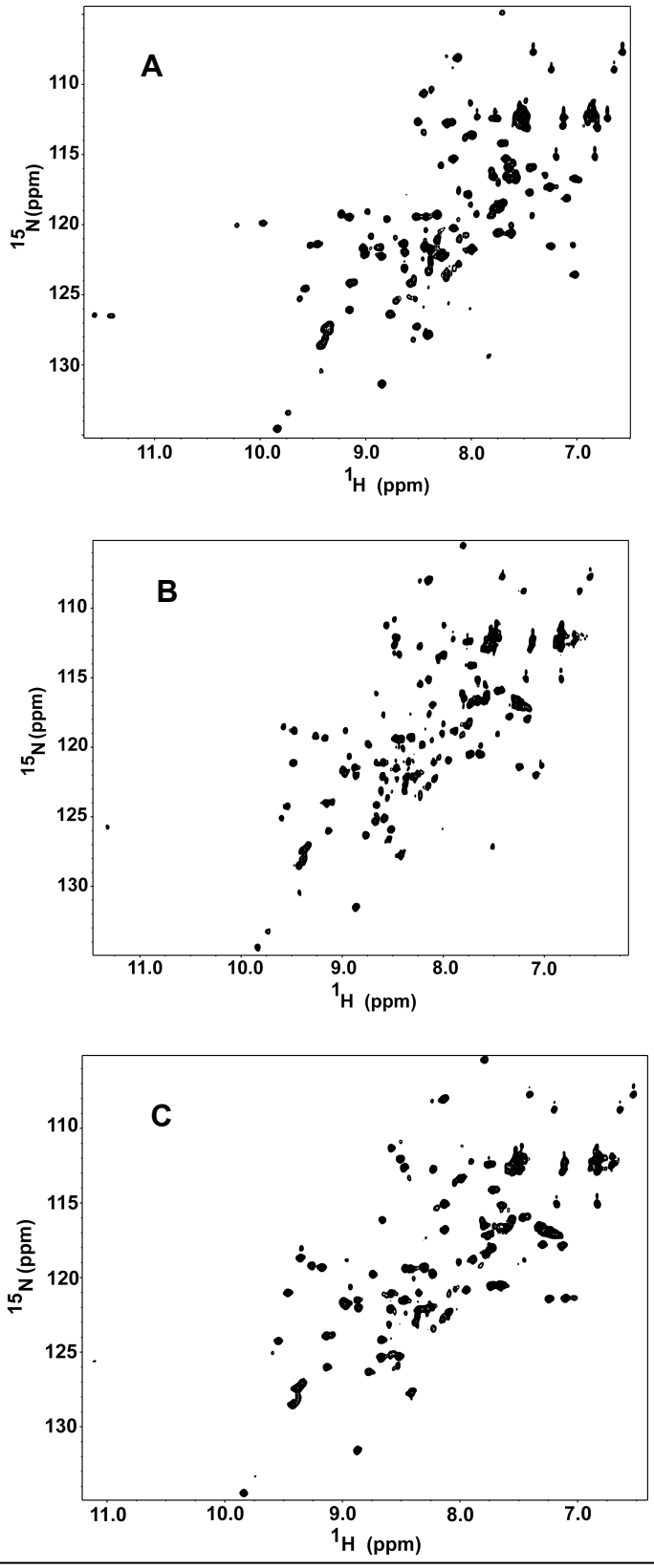

Figure A2. pH induced conformational heterogeneity of MGSA monomer. ^{1}H-^{15}N HSQC spectra of the MGSA monomer at pH 6, 5.5 and 4.5 respectively are shown (**panels A-C**). The data was collected at 30°C using an 800 MHz NMR spectrometer.

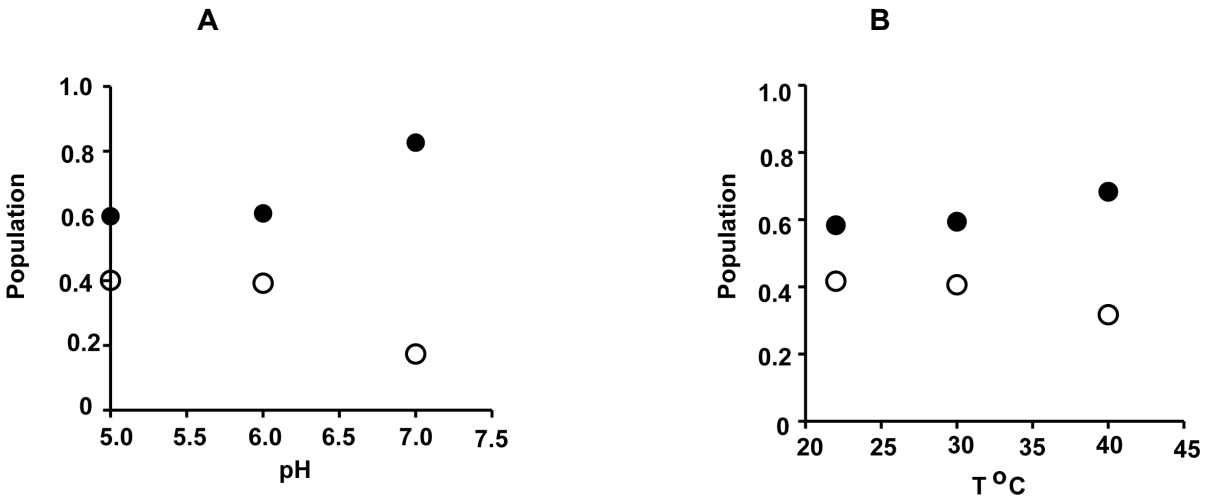

Figure A3. Effect of pH and temperature on the conformational heterogeneity of WT MGSA dimer. Panel A show the populations of the major (●) and the minor conformers (○) for His34 as a function of pH at 30°C. **Panel B** shows the populations of the major (●) and the minor conformers (○) for His34 as a function of temperature, and at constant pH 6.0.

REFERENCES

1. Moser, B., Wolf, M., Walz, A., and Loetscher, P. (2004) Chemokines: multiple levels of leukocyte migration control, *Trends Immunol. 25*, 75-84.

2. Luster, A. D. (2002) The role of chemokines in linking innate and adaptive immunity, *Curr. Opin. Immunol. 14*, 129-135.

3. Lau, E. K., Allen, S., Hsu, A. R., and Handel, T. M. (2004) Chemokine-receptor interactions: GPCRs, glycosaminoglycans and viral chemokine binding proteins, *Adv. Protein Chem. 68*, 351-391.

4. Bonecchi, R., Galliera, E., Borroni, E. M., Corsi, M. M., Locati, M., and Mantovani, A. (2009) Chemokines and chemokine receptors: an overview, *Front. Biosci. 14*, 540-551.

5. Murphy, P. M., Baggiolini, M., Charo, I. F., Hebert, C. A., Horuk, R., Matsushima, K., Miller, L. H., Oppenheim, J. J., and Power, C. A. (2000) International union of pharmacology. XXII. Nomenclature for chemokine receptors, *Pharmacol. Rev. 52*, 145-176.

6. Proudfoot, A. E., Power, C. A., and Schwarz, M. K. Anti-chemokine small molecule drugs: a promising future?, *Expert Opin. Investig. Drugs. 19*, 345-355.

7. Gerard, C., and Rollins, B. J. (2001) Chemokines and disease, *Nat. Immunol. 2*, 108-115.

8. Berger, E. A., Murphy, P. M., and Farber, J. M. (1999) Chemokine receptors as HIV-1 coreceptors: roles in viral entry, tropism, and disease, *Annu. Rev. Immunol. 17*, 657-700.

9. Luster, A. D. (1998) Chemokines--chemotactic cytokines that mediate inflammation, *N. Engl. J. Med. 338*, 436-445.

10. Rajarathnam, K. (2002) Designing decoys for chemokine-chemokine receptor interaction, *Curr. Pharm. Des. 8*, 2159-2169.

11. Rot, A., and von Andrian, U. H. (2004) Chemokines in innate and adaptive host defense: basic chemokinese grammar for immune cells, *Annu. Rev. Immunol. 22*, 891-928.

12. Johnson, Z., Power, C. A., Weiss, C., Rintelen, F., Ji, H., Ruckle, T., Camps, M., Wells, T. N., Schwarz, M. K., Proudfoot, A. E., and Rommel, C. (2004) Chemokine inhibition--why, when, where, which and how?, *Biochem. Soc. Trans. 32*, 366-377.

13. Rajagopalan, L., and Rajarathnam, K. (2006) Structural basis of chemokine receptor function--a model for binding affinity and ligand selectivity, *Biosci. Rep. 26*, 325-339.

14. Booth, V., Keizer, D. W., Kamphuis, M. B., Clark-Lewis, I., and Sykes, B. D. (2002) The CXCR3 binding chemokine IP-10/CXCL10: structure and receptor interactions, *Biochemistry 41*, 10418-10425.

15. Clore, G. M., Appella, E., Yamada, M., Matsushima, K., and Gronenborn, A. M. (1990) Three-dimensional structure of interleukin 8 in solution, *Biochemistry 29*, 1689-1696.

16. Crump, M. P., Gong, J. H., Loetscher, P., Rajarathnam, K., Amara, A., Arenzana-Seisdedos, F., Virelizier, J. L., Baggiolini, M., Sykes, B. D., and Clark-Lewis, I. (1997) Solution structure and basis for functional activity of stromal cell-derived factor-1; dissociation of CXCR4 activation from binding and inhibition of HIV-1, *EMBO J. 16*, 6996-7007.

17. Crump, M. P., Rajarathnam, K., Kim, K. S., Clark-Lewis, I., and Sykes, B. D. (1998) Solution structure of eotaxin, a chemokine that selectively recruits eosinophils in allergic inflammation, *J. Biol. Chem. 273*, 22471-22479.

18. Fairbrother, W. J., Reilly, D., Colby, T. J., Hesselgesser, J., and Horuk, R. (1994) The solution structure of melanoma growth stimulating activity, *J. Mol. Biol. 242*, 252-270.

19. Fernandez, E. J., and Lolis, E. (2002) Structure, function, and inhibition of chemokines, *Annu. Rev. Pharmacol. Toxicol. 42*, 469-499.

20. Kim, K. S., Clark-Lewis, I., and Sykes, B. D. (1994) Solution structure of GRO/melanoma growth stimulatory activity determined by 1H NMR spectroscopy, *J. Biol. Chem. 269*, 32909-32915.

21. Kim, K. S., Rajarathnam, K., Clark-Lewis, I., and Sykes, B. D. (1996) Structural characterization of a monomeric chemokine: monocyte chemoattractant protein-3, *FEBS Lett. 395*, 277-282.

22. Lodi, P. J., Garrett, D. S., Kuszewski, J., Tsang, M. L., Weatherbee, J. A., Leonard, W. J., Gronenborn, A. M., and Clore, G. M. (1994) High-resolution solution structure of the beta chemokine hMIP-1 beta by multidimensional NMR, *Science 263*, 1762-1767.

23. Mayer, K. L., and Stone, M. J. (2000) NMR solution structure and receptor peptide binding of the CC chemokine eotaxin-2, *Biochemistry 39*, 8382-8395.

24. Mizoue, L. S., Bazan, J. F., Johnson, E. C., and Handel, T. M. (1999) Solution structure and dynamics of the CX3C chemokine domain of fractalkine and its interaction with an N-terminal fragment of CX3CR1, *Biochemistry 38*, 1402-1414.

25. Qian, Y. Q., Johanson, K. O., and McDevitt, P. (1999) Nuclear magnetic resonance solution structure of truncated human GRObeta [5-73] and its structural comparison with CXC chemokine family members GROalpha and IL-8, *J. Mol. Biol. 294*, 1065-1072.

26. Rajarathnam, K., Clark-Lewis, I., and Sykes, B. D. (1995) 1H NMR solution structure of an active monomeric interleukin-8, *Biochemistry 34*, 12983-12990.

27. Rajarathnam, K., Li, Y., Rohrer, T., and Gentz, R. (2001) Solution structure and dynamics of myeloid progenitor inhibitory factor-1 (MPIF-1), a novel monomeric CC chemokine, *J. Biol. Chem. 276*, 4909-4916.

28. Skelton, N. J., Aspiras, F., Ogez, J., and Schall, T.J. (1995) Proton NMR Assignments and Solution Conformation of RANTES, a Chemokine of the C-C Type., *Biochemisty 34*, 5329-5342.

29. Tuinstra, R. L., Peterson, F. C., Kutlesa, S., Elgin, E. S., Kron, M. A., and Volkman, B. F. (2008) Interconversion between two unrelated protein folds in the lymphotactin native state, *Proc. Natl. Acad. Sci. U.S.A. 105*, 5057-5062.

30. Warne, T., Serrano-Vega, M. J., Baker, J. G., Moukhametzianov, R., Edwards, P. C., Henderson, R., Leslie, A. G., Tate, C. G., and Schertler, G. F. (2008) Structure of a beta1-adrenergic G-protein-coupled receptor, *Nature 454*, 486-491.

31. Rasmussen, S. G., Choi, H. J., Rosenbaum, D. M., Kobilka, T. S., Thian, F. S., Edwards, P. C., Burghammer, M., Ratnala, V. R., Sanishvili, R., Fischetti, R. F., Schertler, G. F., Weis, W. I., and Kobilka, B. K. (2007) Crystal structure of the human beta2 adrenergic G-protein-coupled receptor, *Nature 450*, 383-387.

32. Park, J. H., Scheerer, P., Hofmann, K. P., Choe, H. W., and Ernst, O. P. (2008) Crystal structure of the ligand-free G-protein-coupled receptor opsin, *Nature 454*, 183-187.

33. Palczewski, K., Kumasaka, T., Hori, T., Behnke, C. A., Motoshima, H., Fox, B. A., Le Trong, I., Teller, D. C., Okada, T., Stenkamp, R. E., Yamamoto, M., and Miyano, M. (2000) Crystal structure of rhodopsin: A G protein-coupled receptor, *Science 289*, 739-745.

34. Cherezov, V., Rosenbaum, D. M., Hanson, M. A., Rasmussen, S. G., Thian, F. S., Kobilka, T. S., Choi, H. J., Kuhn, P., Weis, W. I., Kobilka, B. K., and Stevens, R. C. (2007) High-resolution crystal structure of an engineered human beta2-adrenergic G protein-coupled receptor, *Science 318*, 1258-1265.

35. Rosenbaum, D. M., Rasmussen, S. G., and Kobilka, B. K. (2009) The structure and function of G-protein-coupled receptors, *Nature 459*, 356-363.

36. Czaplewski, L. G., McKeating, J., Craven, C. J., Higgins, L. D., Appay, V., Brown, A., Dudgeon, T., Howard, L. A., Meyers, T., Owen, J., Palan, S. R., Tan, P., Wilson, G., Woods, N. R., Heyworth, C. M., Lord, B. I., Brotherton, D., Christison, R., Craig, S., Cribbes, S., Edwards, R. M., Evans, S. J., Gilbert, R., Morgan, P., Randle, E., Schofield, N., Varley, P. G., Fisher, J., Waltho, J. P., and Hunter, M. G. (1999) Identification of amino acid residues critical for aggregation of human CC chemokines macrophage inflammatory protein (MIP)-1alpha, MIP-1beta, and RANTES. Characterization of active disaggregated chemokine variants, *J. Biol. Chem. 274*, 16077-16084.

37. Lowman, H. B., Fairbrother, W. J., Slagle, P. H., Kabakoff, R., Liu, J., Shire, S., and Hebert, C. A. (1997) Monomeric variants of IL-8: effects of side chain substitutions and solution conditions upon dimer formation, *Protein Sci. 6*, 598-608.

38. Rajarathnam, K., Kay, C. M., Clark-Lewis, I., and Sykes, B. D. (1997) Characterization of quaternary structure of interleukin-8 and functional implications, *Methods Enzymol. 287*, 89-105.

39. Veldkamp, C. T., Peterson, F. C., Pelzek, A. J., and Volkman, B. F. (2005) The monomer-dimer equilibrium of stromal cell-derived factor-1 (CXCL 12) is altered by pH, phosphate, sulfate, and heparin, *Protein Sci. 14*, 1071-1081.

40. Veldkamp, C. T., Seibert, C., Peterson, F. C., De la Cruz, N. B., Haugner, J. C., 3rd, Basnet, H., Sakmar, T. P., and Volkman, B. F. (2008) Structural basis of CXCR4 sulfotyrosine recognition by the chemokine SDF-1/CXCL12, *Sci. Signal. 1*, ra4.

41. Rajarathnam, K., Prado, G. N., Fernando, H., Clark-Lewis, I., and Navarro, J. (2006) Probing receptor binding activity of interleukin-8 dimer using a disulfide trap, *Biochemistry 45*, 7882-7888.

42. Rajarathnam, K., Sykes, B. D., Kay, C. M., Dewald, B., Geiser, T., Baggiolini, M., and Clark-Lewis, I. (1994) Neutrophil activation by monomeric interleukin-8, *Science 264*, 90-92.

43. Rajarathnam, K., Kay, C. M., Dewald, B., Wolf, M., Baggiolini, M., Clark-Lewis, I., and Sykes, B. D. (1997) Neutrophil-activating peptide-2 and melanoma growth-stimulatory activity are functional as monomers for neutrophil activation, *J. Biol. Chem. 272*, 1725-1729.

44. Paavola, C. D., Hemmerich, S., Grunberger, D., Polsky, I., Bloom, A., Freedman, R., Mulkins, M., Bhakta, S., McCarley, D., Wiesent, L., Wong, B., Jarnagin, K., and Handel, T. M. (1998) Monomeric monocyte chemoattractant protein-1 (MCP-1) binds and activates the MCP-1 receptor CCR2B, *J. Biol. Chem. 273*, 33157-33165.

45. Nasser, M. W., Raghuwanshi, S. K., Grant, D. J., Jala, V. R., Rajarathnam, K., and Richardson, R. M. (2009) Differential activation and regulation of CXCR1 and CXCR2 by CXCL8 monomer and dimer, *J. Immunol. 183*, 3425-3432.

46. Laurence, J. S., Blanpain, C., Burgner, J. W., Parmentier, M., and LiWang, P. J. (2000) CC chemokine MIP-1 beta can function as a monomer and depends on Phe13 for receptor binding, *Biochemistry 39*, 3401-3409.

47. Zhou, N., Luo, Z., Luo, J., Liu, D., Hall, J. W., Pomerantz, R. J., and Huang, Z. (2001) Structural and functional characterization of human CXCR4 as a chemokine receptor and HIV-1 co-receptor by mutagenesis and molecular modeling studies, *J. Biol. Chem. 276*, 42826-42833.

48. Ye, J., Kohli, L. L., and Stone, M. J. (2000) Characterization of binding between the chemokine eotaxin and peptides derived from the chemokine receptor CCR3, *J. Biol. Chem. 275*, 27250-27257.

49. Williams, G., Borkakoti, N., Bottomley, G. A., Cowan, I., Fallowfield, A. G., Jones, P. S., Kirtland, S. J., Price, G. J., and Price, L. (1996) Mutagenesis studies of interleukin-8. Identification of a second epitope involved in receptor binding, *J. Biol. Chem. 271*, 9579-9586.

50. Yan, Z., Zhang, J., Holt, J. C., Stewart, G. J., Niewiarowski, S., and Poncz, M. (1994) Structural requirements of platelet chemokines for neutrophil activation, *Blood 84*, 2329-2339.

51. Skelton, N. J., Quan, C., Reilly, D., and Lowman, H. (1999) Structure of a CXC chemokine-receptor fragment in complex with interleukin-8, *Structure 7*, 157-168.

52. Shinkai, A., Komuta-Kunitomo, M., Sato-Nakamura, N., and Anazawa, H. (2002) N-terminal domain of eotaxin-3 is important for activation of CC chemokine receptor 3, *Protein Eng. 15*, 923-929.

53. Schraufstatter, I. U., Ma, M., Oades, Z. G., Barritt, D. S., and Cochrane, C. G. (1995) The role of Tyr13 and Lys15 of interleukin-8 in the high affinity interaction with the interleukin-8 receptor type A, *J. Biol. Chem. 270*, 10428-10431.

54. Pakianathan, D. R., Kuta, E. G., Artis, D. R., Skelton, N. J., and Hebert, C. A. (1997) Distinct but overlapping epitopes for the interaction of a CC-chemokine with CCR1, CCR3 and CCR5, *Biochemistry 36*, 9642-9648.

55. Monteclaro, F. S., and Charo, I. F. (1996) The amino-terminal extracellular domain of the MCP-1 receptor, but not the RANTES/MIP-1alpha receptor, confers chemokine selectivity. Evidence for a two-step mechanism for MCP-1 receptor activation, *J. Biol. Chem. 271*, 19084-19092.

56. Moser, B., Dewald, B., Barella, L., Schumacher, C., Baggiolini, M., and Clark-Lewis, I. (1993) Interleukin-8 antagonists generated by N-terminal modification, *J. Biol. Chem. 268*, 7125-7128.

57. Loetscher, P., Gong, J. H., Dewald, B., Baggiolini, M., and Clark-Lewis, I. (1998) N-terminal peptides of stromal cell-derived factor-1 with CXC chemokine receptor 4 agonist and antagonist activities, *J. Biol. Chem. 273*, 22279-22283.

58. LaRosa, G. J., Thomas, K. M., Kaufmann, M. E., Mark, R., White, M., Taylor, L., Gray, G., Witt, D., and Navarro, J. (1992) Amino terminus of the interleukin-8 receptor is a major determinant of receptor subtype specificity, *J. Biol. Chem. 267*, 25402-25406.

59. Katancik, J. A., Sharma, A., and de Nardin, E. (2000) Interleukin 8, neutrophil-activating peptide-2 and GRO-alpha bind to and elicit cell activation via specific and different amino acid residues of CXCR2, *Cytokine 12*, 1480-1488.

60. Han, K. H., Green, S. R., Tangirala, R. K., Tanaka, S., and Quehenberger, O. (1999) Role of the first extracellular loop in the functional activation of CCR2. The first extracellular loop contains distinct domains necessary for both agonist binding and transmembrane signaling, *J. Biol. Chem. 274*, 32055-32062.

61. Hebert, C. A., Chuntharapai, A., Smith, M., Colby, T., Kim, J., and Horuk, R. (1993) Partial functional mapping of the human interleukin-8 type A receptor. Identification of a major ligand binding domain, *J. Biol. Chem. 268*, 18549-18553.

62. Hebert, C. A., Vitangcol, R. V., and Baker, J. B. (1991) Scanning mutagenesis of interleukin-8 identifies a cluster of residues required for receptor binding, *J. Biol. Chem. 266*, 18989-18994.

63. Gong, J. H., Uguccioni, M., Dewald, B., Baggiolini, M., and Clark-Lewis, I. (1996) RANTES and MCP-3 antagonists bind multiple chemokine receptors, *J. Biol. Chem. 271*, 10521-10527.

64. Hammond, M. E., Shyamala, V., Siani, M. A., Gallegos, C. A., Feucht, P. H., Abbott, J., Lapointe, G. R., Moghadam, M., Khoja, H., Zakel, J., and Tekamp-Olson, P. (1996) Receptor recognition and specificity of interleukin-8 is determined by residues that cluster near a surface-accessible hydrophobic pocket, *J. Biol. Chem. 271*, 8228-8235.

65. Clark-Lewis, I., Dewald, B., Geiser, T., Moser, B., and Baggiolini, M. (1993) Platelet factor 4 binds to interleukin 8 receptors and activates neutrophils when its N terminus is modified with Glu-Leu-Arg, *Proc. Natl. Acad. Sci. U. S. A. 90*, 3574-3577.

66. Clark-Lewis, I., Dewald, B., Loetscher, M., Moser, B., and Baggiolini, M. (1994) Structural requirements for interleukin-8 function identified by design of analogs and CXC chemokine hybrids, *J. Biol. Chem. 269*, 16075-16081.

67. Clark-Lewis, I., Kim, K. S., Rajarathnam, K., Gong, J. H., Dewald, B., Moser, B., Baggiolini, M., and Sykes, B. D. (1995) Structure-activity relationships of chemokines, *J. Leukoc. Biol. 57*, 703-711.

68. Clark-Lewis, I., Schumacher, C., Baggiolini, M., and Moser, B. (1991) Structure-activity relationships of interleukin-8 determined using chemically synthesized analogs. Critical role of NH2-terminal residues and evidence for uncoupling of neutrophil chemotaxis, exocytosis, and receptor binding activities, *J. Biol. Chem. 266*, 23128-23134.

69. Campanella, G. S., Lee, E. M., Sun, J., and Luster, A. D. (2003) CXCR3 and heparin binding sites of the chemokine IP-10 (CXCL10), *J. Biol. Chem. 278*, 17066-17074.

70. Chung, I. Y., Kim, Y. H., Choi, M. K., Noh, Y. J., Park, C. S., Kwon, D. Y., Lee, D. Y., Lee, Y. S., Chang, H. S., and Kim, K. S. (2004) Eotaxin and monocyte chemotactic protein-3 use different modes of action, *Biochem. Biophys. Res. Commun. 314*, 646-653.

71. Brelot, A., Heveker, N., Montes, M., and Alizon, M. (2000) Identification of residues of CXCR4 critical for human immunodeficiency virus coreceptor and chemokine receptor activities, *J. Biol. Chem. 275*, 23736-23744.

72. Bondue, A., Jao, S. C., Blanpain, C., Parmentier, M., and LiWang, P. J. (2002) Characterization of the role of the N-loop of MIP-1 beta in CCR5 binding, *Biochemistry 41*, 13548-13555.

73. Blanpain, C., Doranz, B. J., Bondue, A., Govaerts, C., De Leener, A., Vassart, G., Doms, R. W., Proudfoot, A., and Parmentier, M. (2003) The core domain of chemokines binds CCR5 extracellular domains while their amino terminus interacts with the transmembrane helix bundle, *J. Biol. Chem. 278*, 5179-5187.

74. Baly, D. L., Horuk, R., Yansura, D. G., Simmons, L. C., Fairbrother, W. J., Kotts, C., Wirth, C. M., Gillece-Castro, B. L., Toy, K., Hesselgesser, J., and Allison, D. E. (1998) A His19 to Ala mutant of melanoma growth-stimulating activity is a partial antagonist of the CXCR2 receptor, *J. Immunol. 161*, 4944-4949.

75. Ahuja, S. K., and Murphy, P. M. (1996) The CXC chemokines growth-regulated oncogene (GRO) alpha, GRObeta, GROgamma, neutrophil-activating peptide-2, and epithelial cell-derived neutrophil-activating peptide-78 are potent agonists for the type B, but not the type A, human interleukin-8 receptor, *J. Biol. Chem. 271*, 20545-20550.

76. Lowman, H. B., Slagle, P. H., DeForge, L. E., Wirth, C. M., Gillece-Castro, B. L., Bourell, J. H., and Fairbrother, W. J. (1996) Exchanging interleukin-8 and melanoma growth-stimulating activity receptor binding specificities, *J. Biol. Chem. 271*, 14344-14352.

77. Jones, S. A., Wolf, M., Qin, S., Mackay, C. R., and Baggiolini, M. (1996) Different functions for the interleukin 8 receptors (IL-8R) of human neutrophil leukocytes: NADPH oxidase and phospholipase D are activated through IL-8R1 but not IL-8R2, *Proc. Natl. Acad. Sci. U.S.A. 93*, 6682-6686.

78. Murphy, P. M. (1997) Neutrophil receptors for interleukin-8 and related CXC chemokines, *Semin. Hematol. 34*, 311-318.

79. Hesselgesser, J., Chitnis, C. E., Miller, L. H., Yansura, D. G., Simmons, L. C., Fairbrother, W. J., Kotts, C., Wirth, C., Gillece-Castro, B. L., and Horuk, R. (1995) A mutant of melanoma growth stimulating activity does not activate neutrophils but blocks erythrocyte invasion by malaria, *J. Biol. Chem. 270*, 11472-11476.

80. Suetomi, K., Lu, Z., Heck, T., Wood, T. G., Prusak, D. J., Dunn, K. J., and Navarro, J. (1999) Differential mechanisms of recognition and activation of interleukin-8 receptor subtypes, *J. Biol. Chem. 274*, 11768-11772.

81. Proudfoot, A. E., Power, C. A., Hoogewerf, A. J., Montjovent, M. O., Borlat, F., Offord, R. E., and Wells, T. N. (1996) Extension of recombinant human RANTES by the retention of the initiating methionine produces a potent antagonist, *J. Biol. Chem. 271*, 2599-2603.

82. Chuntharapai, A., and Kim, K. J. (1995) Regulation of the expression of IL-8 receptor A/B by IL-8: possible functions of each receptor, *J. Immunol. 155*, 2587-2594.

83. Richardson, R. M., Marjoram, R. J., Barak, L. S., and Snyderman, R. (2003) Role of the cytoplasmic tails of CXCR1 and CXCR2 in mediating leukocyte migration, activation, and regulation, *J. Immunol. 170*, 2904-2911.

84. Prado, G. N., Suzuki, H., Wilkinson, N., Cousins, B., and Navarro, J. (1996) Role of the C terminus of the interleukin 8 receptor in signal transduction and internalization, *J. Biol. Chem. 271*, 19186-19190.

85. Prado, G. N., Suetomi, K., Shumate, D., Maxwell, C., Ravindran, A., Rajarathnam, K., and Navarro, J. (2007) Chemokine signaling specificity: essential role for the N-terminal domain of chemokine receptors, *Biochemistry 46*, 8961-8968.

86. Suzuki, H., Prado, G. N., Wilkinson, N., and Navarro, J. (1994) The N terminus of interleukin-8 (IL-8) receptor confers high affinity binding to human IL-8, *J. Biol. Chem. 269*, 18263-18266.

87. Ahuja, S. K., Lee, J. C., and Murphy, P. M. (1996) CXC chemokines bind to unique sets of selectivity determinants that can function independently and are broadly distributed on multiple domains of human interleukin-8 receptor B. Determinants of high affinity binding and receptor activation are distinct, *J. Biol. Chem. 271*, 225-232.

88. Gayle, R. B., 3rd, Sleath, P. R., Srinivason, S., Birks, C. W., Weerawarna, K. S., Cerretti, D. P., Kozlosky, C. J., Nelson, N., Vanden Bos, T., and Beckmann, M. P. (1993) Importance of the amino terminus of the interleukin-8 receptor in ligand interactions, *J. Biol. Chem. 268*, 7283-7289.

89. Leong, S. R., Kabakoff, R. C., and Hebert, C. A. (1994) Complete mutagenesis of the extracellular domain of interleukin-8 (IL-8) type A receptor identifies charged residues mediating IL-8 binding and signal transduction, *J. Biol. Chem. 269*, 19343-19348.

90. Attwood M.R., Borkakoti N., Bottomley G.A., Conway E.A., Cowan I., Fallowfield A.G., Handa B.K., Jones P.S., Keech E., Kirtland S.J., Williams G., and F.X., W. (1996) Identification and characterisation of an inhibitor of interleukin-8: a receptor based approach, *Bioorg. Med. Chem. Lett. 6*, 1869-1974.

91. Rajagopalan, L., and Rajarathnam, K. (2004) Ligand selectivity and affinity of chemokine receptor CXCR1. Role of N-terminal domain, *J. Biol. Chem. 279*, 30000-30008.

92. Rajagopalan, L., Rosgen, J., Bolen, D. W., and Rajarathnam, K. (2005) Novel use of an osmolyte to dissect multiple thermodynamic linkages in a chemokine ligand-receptor system, *Biochemistry 44*, 12932-12939.

93. Clubb, R. T., Omichinski, J. G., Clore, G. M., and Gronenborn, A. M. (1994) Mapping the binding surface of interleukin-8 complexes with an N-terminal fragment of the type 1 human interleukin-8 receptor, *FEBS Lett. 338*, 93-97.

94. Duma, L., Haussinger, D., Rogowski, M., Lusso, P., and Grzesiek, S. (2007) Recognition of RANTES by extracellular parts of the CCR5 receptor, *J. Mol. Biol. 365*, 1063-1075.

95. Fernando, H., Chin, C., Rosgen, J., and Rajarathnam, K. (2004) Dimer dissociation is essential for interleukin-8 (IL-8) binding to CXCR1 receptor, *J. Biol. Chem. 279*, 36175-36178.

96. DeLano, W. L. (2002) The PyMOL Molecular Graphics System DeLano Scientific, San Carlos, CA, USA.

97. Burrows, S. D., Doyle, M. L., Murphy, K. P., Franklin, S. G., White, J. R., Brooks, I., McNulty, D. E., Scott, M. O., Knutson, J. R., Porter, D., and et al. (1994) Determination of the monomer-dimer equilibrium of interleukin-8 reveals it is a monomer at physiological concentrations, *Biochemistry 33*, 12741-12745.

98. Wishart, D. S., Bigam, C. G., Yao, J., Abildgaard, F., Dyson, H. J., Oldfield, E., Markley, J. L., and Sykes, B. D. (1995) 1H, 13C and 15N chemical shift referencing in biomolecular NMR, *J. Biomol. NMR 6*, 135-140.

99. Delaglio, F., Grzesiek, S., Vuister, G. W., Zhu, G., Pfeifer, J., and Bax, A. (1995) NMRPipe: a multidimensional spectral processing system based on UNIX pipes, *J. Biomol. NMR 6*, 277-293.

100. Johnson, B. A., and Blevins, R. A. (1994) NMR View: A computer program for the visualization and analysis of NMR data, *J. Biol. NMR 4*, 603-614.

101. Farrow, N. A., Muhandiram, R., Singer, A. U., Pascal, S. M., Kay, C. M., Gish, G., Shoelson, S. E., Pawson, T., Forman-Kay, J. D., and Kay, L. E. (1994) Backbone dynamics of a free and phosphopeptide-complexed Src homology 2 domain studied by 15N NMR relaxation, *Biochemistry 33*, 5984-6003.

102. Spyracopoulos, L. (2006) A suite of Mathematica notebooks for the analysis of protein main chain 15N NMR relaxation data, *J. Biomol. NMR 36*, 215-224.

103. Lian, L. and Roberts, G.C.K. (1993) Effects of chemical exchange on NMR spectra. In NMR of macromolecules. A practical approach (Roberts, G.C.K., Ed) pp 153–182, Oxford University Press, Oxford, UK.

104. Qin, J., Vinogradova, O., and Gronenborn, A. M. (2001) Protein-protein interactions probed by nuclear magnetic resonance spectroscopy, *Methods Enzymol. 339*, 377-389.

105. Reuben, J., and Fiat, D. (1969) Nuclear magnetic resonance studies of solutions of the rare-earth ions and their complexes. IV. Concentration and temperature dependence of the oxygen-17 transverse relaxation in aqueous solutions, *J. Chem. Phys. 51*, 10.

106. Rajarathnam, K., Sykes, B. D., Dewald, B., Baggiolini, M., and Clark-Lewis, I. (1999) Disulfide bridges in interleukin-8 probed using non-natural disulfide analogues: dissociation of roles in structure from function, *Biochemistry 38*, 7653-7658.

107. Kuschert, G. S., Hoogewerf, A. J., Proudfoot, A. E., Chung, C. W., Cooke, R. M., Hubbard, R. E., Wells, T. N., and Sanderson, P. N. (1998) Identification of a glycosaminoglycan binding surface on human interleukin-8, *Biochemistry 37*, 11193-11201.

108. Grasberger, B. L., Gronenborn, A. M., and Clore, G. M. (1993) Analysis of the backbone dynamics of interleukin-8 by 15N relaxation measurements, *J. Mol. Biol. 230*, 364-372.

109. Fernando, H., Nagle, G. T., and Rajarathnam, K. (2007) Thermodynamic characterization of interleukin-8 monomer binding to CXCR1 receptor N-terminal domain, *FEBS J. 274*, 241-251.

110. Fernando, H., Chin, C., Rosgen, J., and Rajarathnam, K. (2004) Dimer dissociation is essential for interleukin-8 (IL-8) binding to CXCR1 receptor, *J. Biol. Chem. 279*, 36175-36178.

111. Shoemaker, B. A., Portman, J. J., and Wolynes, P. G. (2000) Speeding molecular recognition by using the folding funnel: the fly-casting mechanism, *Proc. Natl. Acad. Sci. U.S.A* 97, 8868-8873.

112. Veldkamp, C. T., Seibert, C., Peterson, F. C., Sakmar, T. P., and Volkman, B. F. (2006) Recognition of a CXCR4 sulfotyrosine by the chemokine stromal cell-derived factor-1alpha (SDF-1alpha/CXCL12), *J. Mol. Biol. 359*, 1400-1409.

113. Das, S. T., Rajagopalan, L., Guerrero-Plata, A., Sai, J., Richmond, A., Garofalo, R. P., and Rajarathnam, K. Monomeric and dimeric CXCL8 are both essential for in vivo neutrophil recruitment, *PLoS One* 5, e11754.

114. Jin, H., Shen, X., Baggett, B. R., Kong, X., and LiWang, P. J. (2007) The human CC chemokine MIP-1beta dimer is not competent to bind to the CCR5 receptor, *J. Biol. Chem. 282*, 27976-27983.

115. Proudfoot, A. E., Handel, T. M., Johnson, Z., Lau, E. K., LiWang, P., Clark-Lewis, I., Borlat, F., Wells, T. N., and Kosco-Vilbois, M. H. (2003) Glycosaminoglycan binding and oligomerization are essential for the in vivo activity of certain chemokines, *Proc. Natl. Acad. Sci. U. S. A. 100*, 1885-1890.

116. Willard, L., Ranjan, A., Zhang, H., Monzavi, H., Boyko, R. F., Sykes, B. D., and Wishart, D. S. (2003) VADAR: a web server for quantitative evaluation of protein structure quality, *Nucleic Acids Res. 31*, 3316-3319.

117. Jones, S. A., Dewald, B., Clark-Lewis, I., and Baggiolini, M. (1997) Chemokine antagonists that discriminate between interleukin-8 receptors. Selective blockers of CXCR2, *J. Biol. Chem. 272*, 16166-16169.

118. Lee, J., Horuk, R., Rice, G. C., Bennett, G. L., Camerato, T., and Wood, W. I. (1992) Characterization of two high affinity human interleukin-8 receptors, *J. Biol. Chem. 267*, 16283-16287.

119. Muhandiram, D. R., and Kay, L.E. (1994) Gradient-enhanced triple-resonance three dimensional NMR experiments with improved sensitivity, *J. Mag. Reson.,* Series B *103*, 203-216.

120. Murphy, J. W., Yuan, H., Kong, Y., Xiong, Y., and Lolis, E. J. (2009) Heterologous quaternary structure of CXCL12 and its relationship to the CC chemokine family, *Proteins 78*, 1331-1337.

121. Meunier, S., Bernassau, J. M., Guillemot, J. C., Ferrara, P., and Darbon, H. (1997) Determination of the three-dimensional structure of CC chemokine monocyte chemoattractant protein 3 by 1H two-dimensional NMR spectroscopy, *Biochemistry 36*, 4412-4422.

122. McConnell, H. M. (1958) Reaction rates by nuclear magnetic resonance, *J. Chem. Phys.* 28, 430-431.

123. Wiseman, T., Williston, S., Brandts, J. F., and Lin, L. N. (1989) Rapid measurement of binding constants and heats of binding using a new titration calorimeter, *Anal. Biochem. 179*, 131-137.

124. Pardi, A., Wagner, G., and Wuthrich, K. (1983) Protein conformation and proton nuclear-magnetic-resonance chemical shifts, *Eur. J. Biochem. 137*, 445-454.

125. Wishart, D. S., Sykes, B. D., and Richards, F. M. (1991) Relationship between nuclear magnetic resonance chemical shift and protein secondary structure, *J. Mol. Biol. 222*, 311-333.

126. de Dios, A. C., Pearson, J. G., and Oldfield, E. (1993) Secondary and tertiary structural effects on protein NMR chemical shifts: an ab initio approach, *Science* 260, 1491-1496.

127. Clayden, N. J., Williams, R.J.P. (1982) Peptide group shifts, *J. Magn. Reson. 49*, 383-396.

128. Rajarathnam, K., Clark-Lewis, I., and Sykes, B. D. (1994) 1H NMR studies of interleukin 8 analogs: characterization of the domains essential for function, *Biochemistry 33*, 6623-6630.

129. Shoup, D., Lipari, G., and Szabo, A. (1981) Diffusion-controlled bimolecular reaction rates. The effect of rotational diffusion and orientation constraints, *Biophys. J. 36*, 697-714.

130. Suel, G. M., Lockless, S. W., Wall, M. A., and Ranganathan, R. (2003) Evolutionarily conserved networks of residues mediate allosteric communication in proteins, *Nat. Struct. Biol. 10*, 59-69.

131. Lockless, S. W., and Ranganathan, R. (1999) Evolutionarily conserved pathways of energetic connectivity in protein families, *Science 286*, 295-299.

132. Xie, K. (2001) Interleukin-8 and human cancer biology, *Cytokine Growth Factor Rev. 12*, 375-391.

133. Harada, A., Sekido, N., Akahoshi, T., Wada, T., Mukaida, N., and Matsushima, K. (1994) Essential involvement of interleukin-8 (IL-8) in acute inflammation, *J. Leukoc. Biol. 56*, 559-564.

134. Boisvert, W. A., Curtiss, L. K., and Terkeltaub, R. A. (2000) Interleukin-8 and its receptor CXCR2 in atherosclerosis, *Immunol. Res. 21*, 129-137.

135. Karin, M. (2005) Inflammation and cancer: the long reach of Ras, *Nat. Med. 11*, 20-21.

136. Saunders, J., and Tarby, C. M. (1999) Opportunities for novel therapeutic agents acting at chemokine receptors, *Drug. Discov. Today. 4*, 80-92.

137. Hruby, V.J., al-Obeidi, F., and Kazmierski, W. (1990) Emerging approaches in the molecular design of receptor-selective peptide ligands: conformational, topographical and dynamic considerations, *Biochem. J. 268*, 249-262.

138. Hruby, V.J., and Smith, C. W. (1987) Structure-activity relationships of neurohypophyseal peptides, in *The Peptides: analysis, synthesis, biology*. (Smith, C. W., Ed.), pp 77-197, Academic Press, New York, NY.

139. Lokesh, G. L., Rachamallu, A., Kumar, G. D., and Natarajan, A. (2006) High-throughput fluorescence polarization assay to identify small molecule inhibitors of BRCT domains of breast cancer gene 1, *Anal. Biochem. 352*, 135-141.

140. Freire, E. (2009) A thermodynamic approach to the affinity optimization of drug candidates, *Chem. Biol. Drug. Des. 74*, 468-472.

141. Ladbury, J. E., Klebe, G., and Freire, E. (2009) Adding calorimetric data to decision making in lead discovery: a hot tip, *Nat. Rev. Drug. Discov. 9*, 23-27.

142. Zang, X., Yu, Z., and Chu, Y. H. (1998) Tight-binding streptavidin ligands from a cyclic peptide library, *Bioorg. Med. Chem. Lett. 8*, 2327-2332.

143. Cummins, S. F., Nichols, A. E., Rajarathnam, K., and Nagle, G. T. (2004) A conserved heptapeptide sequence in the waterborne attractin pheromone stimulates mate attraction in Aplysia, *Peptides 25*, 185-189.

144. Proudfoot, A. E., Power, C. A., and Schwarz, M. K. (2010) Anti-chemokine small molecule drugs: a promising future?, *Expert Opin. Investig. Drugs 19*, 345-355.

145. Bradley, M. E., Bond, M. E., Manini, J., Brown, Z., and Charlton, S. J. (2009) SB265610 is an allosteric, inverse agonist at the human CXCR2 receptor, *Br. J. Pharmacol. 158*, 328-338.

146. Bertini, R., Allegretti, M., Bizzarri, C., Moriconi, A., Locati, M., Zampella, G., Cervellera, M. N., Di Cioccio, V., Cesta, M. C., Galliera, E., Martinez, F. O., Di Bitondo, R., Troiani, G., Sabbatini, V., D'Anniballe, G., Anacardio, R., Cutrin, J. C., Cavalieri, B., Mainiero, F., Strippoli, R., Villa, P., Di Girolamo, M., Martin, F., Gentile, M., Santoni, A., Corda, D., Poli, G., Mantovani, A., Ghezzi, P., and Colotta, F. (2004) Noncompetitive allosteric inhibitors of the inflammatory chemokine receptors CXCR1 and CXCR2: prevention of reperfusion injury, *Proc. Natl. Acad. Sci. U. S. A. 101*, 11791-11796.

147. Moriconi, A., Cesta, M. C., Cervellera, M. N., Aramini, A., Coniglio, S., Colagioia, S., Beccari, A. R., Bizzarri, C., Cavicchia, M. R., Locati, M., Galliera, E., Di Benedetto, P., Vigilante, P., Bertini, R., and Allegretti, M. (2007) Design of noncompetitive interleukin-8 inhibitors acting on CXCR1 and CXCR2, *J. Med. Chem. 50*, 3984-4002.

148. White, J. R., Lee, J. M., Young, P. R., Hertzberg, R. P., Jurewicz, A. J., Chaikin, M. A., Widdowson, K., Foley, J. J., Martin, L. D., Griswold, D. E., and Sarau, H. M. (1998) Identification of a potent, selective non-peptide CXCR2 antagonist that inhibits interleukin-8-induced neutrophil migration, *J. Biol. Chem. 273*, 10095-10098.

149. Gonsiorek, W., Fan, X., Hesk, D., Fossetta, J., Qiu, H., Jakway, J., Billah, M., Dwyer, M., Chao, J., Deno, G., Taveras, A., Lundell, D. J., and Hipkin, R. W. (2007) Pharmacological characterization of Sch527123, a potent allosteric CXCR1/CXCR2 antagonist, *J. Pharmacol. Exp. Ther. 322*, 477-485.

150. Fitzgerald, M. F., and Fox, J. C. (2007) Emerging trends in the therapy of COPD: novel anti-inflammatory agents in clinical development, *Drug. Discov. Today 12*, 479-486.

151. Attwood M.R., Conway E.A., Dunsdon, R. M., Greening, J. R., Handa B.K., Jones P.S., Jordan, S. C., Keech E., and F.X., W. (1997) Peptide based inhibitors of interleukin-8: structural simplification and enhanced potency, *Bioorg. Med. Chem. Lett. 7*, 429-432.

152. Fujii, N., Nakashima, H., and Tamamura, H. (2003) The therapeutic potential of CXCR4 antagonists in the treatment of HIV, *Expert Opin. Investig. Drugs 12*, 185-195.

153. Fujii, N., Oishi, S., Hiramatsu, K., Araki, T., Ueda, S., Tamamura, H., Otaka, A., Kusano, S., Terakubo, S., Nakashima, H., Broach, J. A., Trent, J. O., Wang, Z. X., and Peiper, S. C. (2003) Molecular-size reduction of a potent CXCR4-chemokine antagonist using orthogonal combination of conformation- and sequence-based libraries, *Angew. Chem. Int. Ed. Engl. 42*, 3251-3253.

154. Tamamura, H., Hori, A., Kanzaki, N., Hiramatsu, K., Mizumoto, M., Nakashima, H., Yamamoto, N., Otaka, A., and Fujii, N. (2003) T140 analogs as CXCR4 antagonists identified as anti-metastatic agents in the treatment of breast cancer, *FEBS Lett. 550*, 79-83.

VITA

Aishwarya Ravindran was born in Chennai, India, on November 21st 1982. She graduated from Alagappa College of Technology, Anna University, with a Bachelor of Technology Degree in Industrial Biotechnology in 2004, and joined the Ph.D program at the University of Texas Medical Branch in August of the same year. In 2005, she began her doctoral research in the lab of Dr. Krishna Rajarathnam in the Department of Biochemistry and Molecular Biology (Molecular Biophysics Educational Track).

While at UTMB, Aishwarya received the American Heart Association pre-doctoral fellowship in 2008. In the same year, she was also awarded the Graduate School of Biomedical Sciences incentive fellowship for achieving external funding from the American Heart Association, and the Barbara Bowman award for academic and research excellence. She was nominated to the Who's Who in American Universities and Colleges in 2010.

Aishwarya presented posters at the Gordon Research Conference and at the Gordon Keanen Research Seminar in 2010. She has also presented posters at the 21st Annual Gibbs Conference on Bio-thermodynamics at Carbondale, Illinois in 2007 and at the John S. Dunn, Sr. Gulf Coast Consortium for Magnetic Resonance Conference, Houston, Texas in 2009. She has presented her research at the Annual Structural Biology Symposium at UTMB every year from 2004-2009, where she received the best poster award in 2006, and also received the best poster award for her research presented at the 14th Annual Sealy Center for Molecular Science Forum in 2006.

Aishwarya served on several departmental committees and organizations including the Biological Chemistry Student Organization from 2004-2010. She was one of the founding members of the Biophysics Journal Club at the Department of Biochemistry and Molecular Biology in 2007 and was the chair of the Biochemistry Journal Club in 2009. She served as a judge at the Galveston County Science Fair held at Texas A&M University, Galveston in 2008.

Aishwarya can be contacted at 210 Market Street, #G-202, Galveston, Texas 77550.

EDUCATION

B.Tech, April 2004, Alagappa College of Technology, Anna University, Chennai, India

PUBLICATIONS

A. Articles in Peer-Reviewed Journals:

Ravindran, A., Joseph, P.R., Rajarathnam, K. Structural Basis for Differential Binding of the Interleukin-8 Monomer and Dimer to the CXCR1 N-Domain: Role of Coupled Interactions and Dynamics. *Biochemistry,* 48(37): 8795-8805, 2009.

Prado G.N., Suetomi K., Shumate D., Maxwell C., **Ravindran A.,** Rajarathnam K., Navarro J. Chemokine Signaling Specificity: Essential Role for the N-Terminal Domain of Chemokine Receptors. *Biochemistry*, 46(41): 8961-8967, 2007.

B. Abstracts in Proceedings of Conferences/Symposia:

1. Novel coupling interactions mediate chemokine receptor activation -- A critical role for a solvent exposed hydrophobe. **Aishwarya Ravindran,** Prem Raj Joseph, and Krishna Rajarathnam. John S. Dunn, Sr. Gulf Coast Consortium for Magnetic Resonance, University of Texas Health Science Center, Houston, TX, July 2010.

2. Novel coupling interactions mediate chemokine receptor activation -- A critical role for a solvent exposed hydrophobe. **Aishwarya Ravindran,** Prem Raj Joseph, and Krishna Rajarathnam. Gordon Research Conference, Biomolecular Interactions and Methods. Galveston, TX, Jan 2010.

3. Novel coupling interactions mediate chemokine receptor activation -- A critical role for a solvent exposed hydrophobe. **Aishwarya Ravindran,** Prem Raj Joseph, and Krishna Rajarathnam. Gordon Keanen Research Seminar, Biomolecular Interactions and Methods: Protein Interactions and Dynamics. Galveston, TX, Jan 2010.

4. Structural Basis of Binding of IL-8 Monomer and Dimer to CXCR1 N-domain. **Aishwarya Ravindran,** Prem Raj Joseph, and Krishna Rajarathnam. 14th Annual Structural Biology Symposium, UTMB, Galveston, TX, March 2009.

5. The Structural Basis of Chemokine-Receptor Interaction. **Aishwarya Ravindran,** Prem Raj Joseph, and Krishna Rajarathnam. John S. Dunn, Sr. Gulf Coast Consortium for Magnetic Resonance, University of Texas Health Science Center, Houston, TX, February 2009.

6. Exploring the role of N-loop Lys-15 for Interleukin-8 structure and *in vivo* function. Rachita Navara, Prem Raj Joseph, **Aishwarya Ravindran,** Pavani Gangavarapu, Roberto Garofalo, and Krishna Rajarathnam. Summer Undergraduate Research Program poster presentation, UTMB, Galveston, TX, August 2008.

7. The Structural Basis of Chemokine-Receptor Interaction. **Aishwarya Ravindran,** Prem Raj Joseph, and Krishna Rajarathnam. 13th Annual Structural Biology Symposium, UTMB, Galveston, TX, May 2008.

8. Structural Basis of Chemokine Function. **Aishwarya Ravindran,** Prem Raj Joseph, and Krishna Rajarathnam. 21st Annual Gibbs Conference on Bio-thermodynamics, Carbondale, IL, USA, September 2007.

9. Structural Basis of Chemokine Function. **Aishwarya Ravindran,** Prem Raj Joseph, and Krishna Rajarathnam. 12th Annual Structural Biology Symposium, UTMB, Galveston, TX, May 2007.

10. The Role of the 30s 'GP' Motif in Interleukin-8 Stability, Structure, Function and In vivo Physiology. Mesias Pedroza, **Aishwarya Ravindran**, Pavani Gangavarapu, Sai Hari Gandham, Prem Raj Joseph, Gregg Nagle, Greg Prado, Roberto Garofalo and Krishna Rajarathnam. Summer Undergraduate Research Program poster presentation, UTMB, Galveston, TX, August 2006.

11. Probing Disulfide Function in Folded Proteins Using Non-natural Amino Acids. **Aishwarya Ravindran**, Anurag Mishra, and Krishna Rajarathnam. 14th Annual Science Forum, Sealy Center for Molecular Science and Sealy Center for Cancer Cell Biology, UTMB, Galveston, June 2006, and 11th Annual Structural Biology Symposium, UTMB, Galveston, TX, May 2006.

12. Bioinformatics Study for the Tomato Protein NP24 from the Pathogenesis-Related 5 Family. **Aishwarya Ravindran,** Ovidiu Ivanciuc, and Werner Braun. 10th Annual Structural Biology Symposium, UTMB, Galveston, TX, May 2005.